MECHANISMS OF PIN1 REGULATION OF IRAK-M STABILITY IN TLR/IL-1R SIGNALING AND STRUCTURE DETERMINATION OF IRAK-M DEATH DOMAIN

A Dissertation

Presented to the Faculty of the Graduate School

of Cornell University

In Partial Fulfillment of the Requirements for the Degree of

Doctor of Philosophy

by

Jeahoo Kwon

August 2018

MECHANISMS OF PIN1 REGULATION OF IRAK-M STABILITY IN TLR/IL-1R SIGNALING AND STRUCTURE DETERMINATION OF IRAK-M DEATH DOMAIN

Jeahoo Kwon, Ph. D.

Cornell University 2018

Asthma is a chronic inflammatory sickness of the airways caused by environmental and genetic factors. The mechanisms of activation of the innate immunity signaling pathways that cause asthma are not fully understood yet. This study investigated the novel targets for the development of new asthma therapeutics. Innate immunity provides the first line of defense against bacterial and viral pathogens. Toll-like receptors (TLRs) act as sentinels to detect specific pathogen-associated molecular patterns (PAMPs). TLR-initiated signaling cascades trigger inflammatory, allergic and non-allergic responses via NF-kappaB signaling. Loss of proper innate immunity regulation leads to inflammatory diseases such as asthma. IRAK-M is a known negative regulator of TLR signaling and is known to assemble into the activated TLR signaling complex to attenuate downstream signaling. Prolyl peptide bonds, such as in the phosphorylated Ser/Thr-Pro (pS/T-P) motifs recognized by Pin1, can exist in two distinct isomer conformations, cis and trans, that exchange on a slow time scale (exchange time constant of several minutes). Pin1 can accelerate the isomerization rate of pS/T-P motifs by orders of magnitude. The NMR experiments reported here show that Pin1 directly interacts with and isomerizes the phosphoS110-P111 peptide bond

in a phosphopeptide corresponding to the IRAK-M sequence 103-124 (pIRAK-M), and also acts on the corresponding peptide harboring the phosphomimetic mutation S110E. Assembly of IRAK-M into the TLR signaling complex is mediated by its N-terminal death domain. Oligomerization is a hallmark of Death Domains (DD). The IRAKM-DD has eluded structure determination due to aggregation. Here, we report the 1H, 13C and 15N backbone and side chain resonance assignments for a double-mutant IRAK-M Death Domain (R56D, Y61E) that is a highly soluble monomer well suited for NMR studies. Furthermore, we solved IRAK-M Death Domain structure and simulated docking prediction.

BIOGRAPHICAL SKETCH

Jeahoo Kwon was born on January 11, 1982 in Seoul Korea as the youngest child. He was the only son of the family, and he was taken care of by all of his family like all Asian families.

Jeahoo was the class leader of the Math Olympiad class during Middle School, and he became the class leader of the research Olympiad team during high school. Jeahoo Kwon won the 1st APEC Science research Olympiad Korea. He was also interested in dancing, and he did dancing club activities.

Jeahoo Kwon served Korean Military service for two years as an environmental management engineer. He studied English in his free time, and he planned to study abroad.

Jeahoo Kwon went to University of Wisconsin, Madison, College of Agriculture and Life Sciences, and studied Biochemistry with a Physics minor. He started lab working at Silvia Cavagnero Lab, where Jeahoo experienced NMR for the first time. Jeahoo got into the charm of NMR, and he decided to study NMR for his Ph.D. He received his bachelor's degree, and graduated with distinction.

Jeahoo Kwon went to graduate school at Cornell University and joined Linda Nicholson Lab. Jeahoo has been trained in NMR theory and practice by his professor, Linda K. Nicholson. He studied protein dynamics and protein structures using NMR and X-ray crystallography. He also learned humanism from his professor. He learned that scientists can have a warm heart.

ACKNOWLEDGMENTS

I would first like to thank my Professor Linda K. Nicholson for all of the support and guidance she provided for me during my graduate school life. Linda took care of me as her family, so I could feel like in my home country. Linda has provided me extensive personal and professional guidance and taught me a great deal about both scientific research and life in general. Without her patience and counsel, I would never have been able to see it through to completion. Linda is not only my academic parent, but also my other parent.

I would also like to thank my parents for their support and trust. You are always there for me. Mother, I always love you. My sisters and nephews always make me happy.

I am grateful to all of those with whom I have had the pleasure to work during this project and other related projects. Each of the members of my Special Committee, Robert Oswald and Yuxin Mao, has provided me professional guidance and support for a lot of scientific material and instruments for my projects. Kun Ping Lu and Morris Nechama collaborated with me for this project and we had great success. Woonghee Lee has helped me with a lot of guidance for Ponderosa software.

I would like to thank Biophysics folks. They always treated me as friends and gave me a sense of belonging to the group, so I was not lonely during my graduate life.

TABLE OF CONTENTS

Chapter 1

Background and Overview

Background

Allergic Asthma

Allergic asthma is an inflammatory disorder characterized by pulmonary infiltration of type 2 T helper cells [1, 2] in response to airborne allergens, house dust mites (HDM), viruses or pollen [3], that causes swelling and narrowing of the airways in the lungs. However, asthma signaling pathways are still not fully understood and better treatments are constantly under development. Asthma is caused by cytokine (IL-4, IL-5, IL-9, and IL-13) and chemokine secretion from T-helper type 2 (Th2) cells in lung tissue [4-8]. These cytokines are necessary for adaptive T_H2 immunity development. The production of type 2 cytokines is regulated by upstream signaling pathways, including those initiated by the Toll-like receptor/interleukin-1 receptor (TLR/IL-1R) superfamily [9, 10] . The activation of such TLRs by airborne allergens often induces T_H2 response [11] via mediators such as interleukin 33 (IL-33), a ligand for IL-1R [12-14]. IL-33 comes mainly from epithelial cells that form the first line of defense against inhaled allergens and microorganisms in the lung. IL-33 is secreted to act as both a chemo attractant and an immune modulator to activate cells of both the innate and adaptive arms of immunity upon stimulation, or as a result of tissue damage. The production of cytokines and chemokines is regulated by transcription factors, such as NF-*k*B, AP-1, GATA and STAT, and these transcription factors' activities are elevated in asthma. Also, IL-33 levels are elevated compared to healthy individuals or wild-type mice [15]. How these IL-33 signaling pathways are regulated, especially after engaging a TLR/IL-1R, is not fully understood.

Toll-Like Receptor/interleukin-1 receptor (TLR/IL-1R) Signal pathway in asthma

Toll-Like Receptors (TLRs) recognize specific molecular markers that are present in microbial components, such as viral double-stranded RNA or bacterial lipopolysaccharides, and serve as a first line of defense against pathogens [16]. Interleukin-1 Receptors (IL-1R) provide a second phase of defense in response to TLR-induced signaling [17, 18]. TLR/IL-1R signaling regulates transcription factor NF-*k*B, which activates gene expression to secrete cytokines. TLR/IL1-R family members share structural and functional properties. TLR/IL1-R family members activate the same MyD88-dependent pathway to induce an inflammation response [10, 17].

Recognition of pathogens by TLR/IL1-R triggers an association with myeloid differentiation primary-response protein 88 (MyD88), which recruits IL-1R-associated kinase 4 (IRAK4). IRAK4 recruits IRAK1 to induce the phosphorylation of IRAK1 kinase domain (IRAK1-KD). Phosphorylated IRAK1-KD auto-phosphorylates IRAK1-UD leading to recruitment of TRAF6 and to dissociation from IRAK4. The model that IRAK-M prevents the formation of IRAK4-IRAK1 or IRAK1-TRAF6 by forming a heterodimer with IRAK-1 and binding both MyD88 and TRAF6 was proposed [19, 20]. IRAK1-TRAF6 complex combines with transforming-growth factor-β-activated kinase (TAK1). TAK1 activation is induced by its ubiquitination by TRAF6. TAK1 phosphorylates the IkB kinase (IKK) which phosphorylates inhibitor of κB (IκB). NF-κB forms a complex with IκB. When IKK phosphorylates two serine residues located in an IκB regulatory domain, IκB is ubiquitinated and NF-κB is released [10]. NF-κB activates expression of cytokine genes. Der2, a major HDM allergen, shares structural homology with MD-2, which is an LPS-binding component of TLR4 that increases TLR4 signaling. The inhaled HDM allergens activate TLR4 and induce secretion of various cytokines,

including IL-33, IL-25, and GM-CSF, by epithelial cells [14, 21, 22]. HDM also induces a Th2 cell response by IL-33 mediated promotion of Th2 cell development and stimulation of dendritic cells (DCs). The Th2 cell cytokine response promotes the development of allergic inflammation. TLR/IL1-R signaling is not only involved in innate immunity but also leads to the development of antigen adaptive immunity.

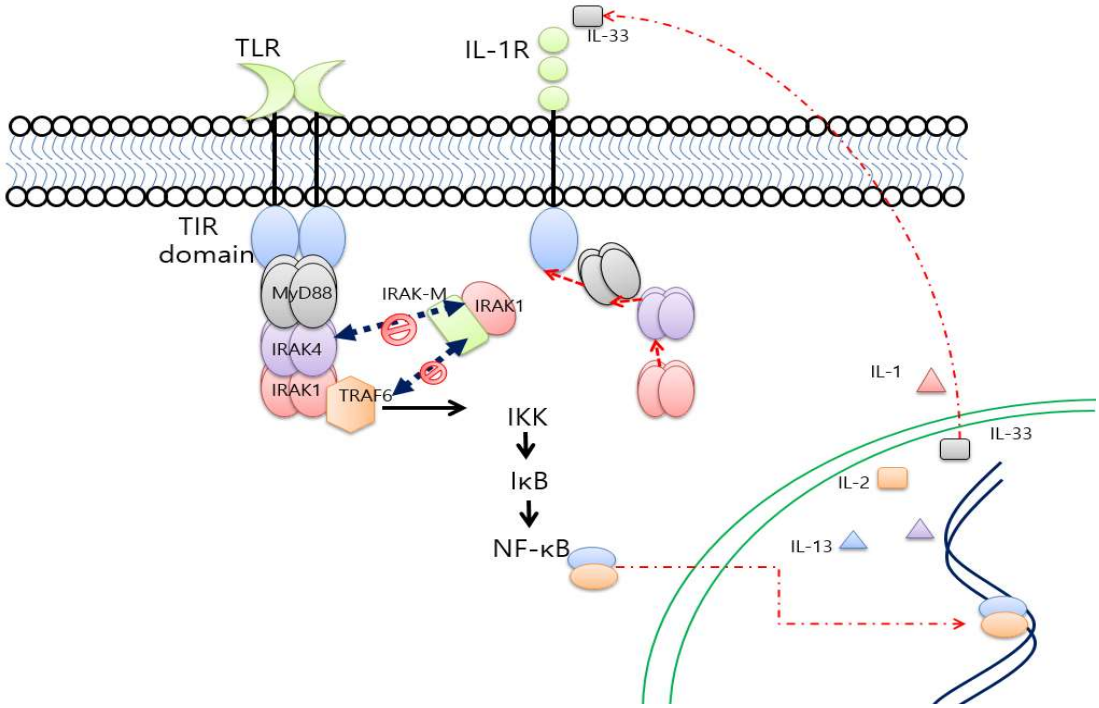

Figure 1.1. TLR/1L-1R signal pathway in asthma

Myddosome complex

Toll-Like Receptors (TLRs) transfer the signals to MyD88 and IRAK family through a toll-IL-1 receptor (TIL) after TLRs detect microbial components. The crystal structure of the death domains [23] complex of the MyD88-IRAK4-IRAK2 was solved [24]. Myddosome consists of six of MyD88 DD, four of IRAK4 DD, and four of IRAK2 DD as a left-handed helical formation (Figure. 1.2). The DDs of IRAK2, IRAK4, and MyD88 are similar in structure.

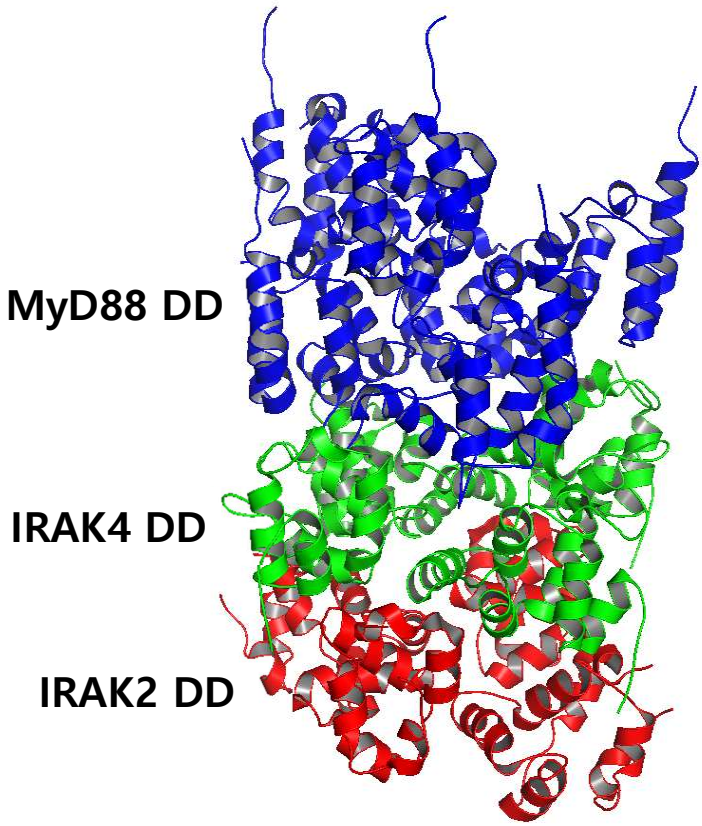

Figure 1.2. Myddosome complex

IRAK family

The interleukin-1 receptor-associated kinase (IRAK) family members are important signaling mediators of the TLR/IL-1R signaling pathways. In the vertebrate genome, there are 4 members of the IRAK family: IRAK1, IRAK2, IRAK-M, and IRAK4 [25]. All IRAKs have an N-terminal death domain [23] and a kinase domain (KD). IRAK1 and IRAK4 have active Ser/Thr kinases, but IRAK-M and IRAK-2 do not have active kinases. IRAK1 and IRAK4 have a critical Asp residue (IRAK1 D340, IRAK4 D311) in the kinase domain. However, IRAK2 has an Asn residue (IRAK2 N335), and IRAK-M has a Ser residue (IRAKM S293) instead of

aspartate at this key position in their kinase domain [26]. IRAK-M and IRAK2 are known negative regulators of TLR/IL-1R signaling, which is accomplished by binding the MyD88 adaptor complex [19, 20]. All IRAKs have the linker or the undefined domain (IRAK1) between the death domain and the kinase domain. IRAK4 does not have a C-terminal domain.

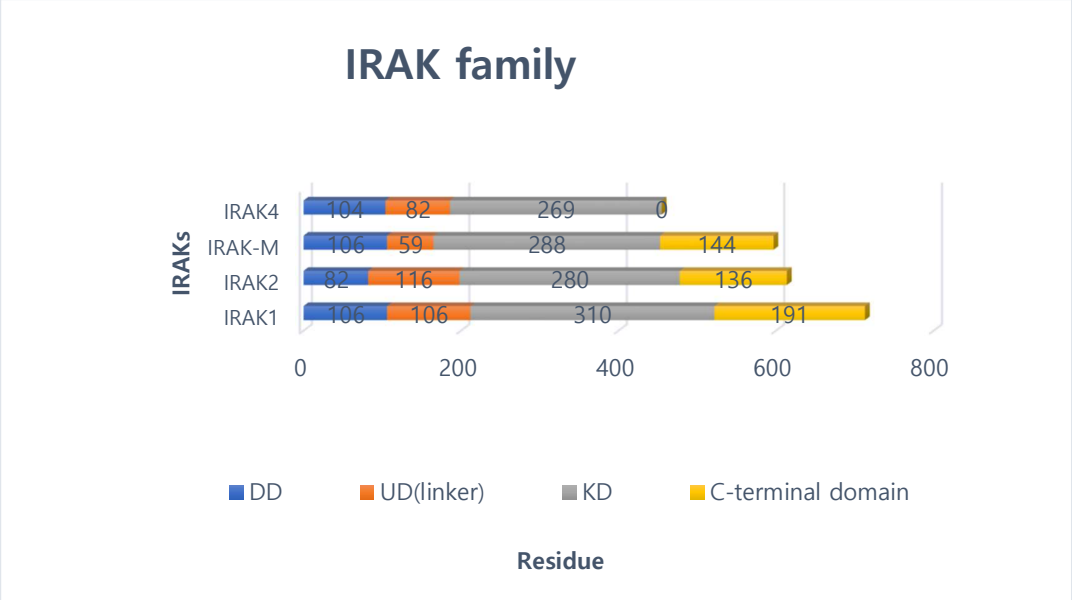

Figure 1.3. The domains of IRAK family

Death Domain

The death domain [23] is significantly important in IRAK family binding [24, 27]. The DDs of the IRAK family have common amino acid residues which especially have hydrophobic side chains such as leucine, isoleucine, and tryptophan (Figure 1.4). In addition, IRAK family DDs have commonly charged amino acid residues such as aspartic acid and glutamic acid as negatively charged, and arginine as positively charged (Figure 1.4). The DD of IRAK family has 30 to 39% of similarity (Figure 1.5). The DD of IRAK2, IRAK4, and MyD88 has similar structures based on Myddosome crystal structure. The alignment of DDs and phylogenetic tree are generated by Clustal Omega (EMBL-EBI, http://www.ebi.ac.uk/Tools/msa/clustalo/)

```
IRAK4       ------MNKP--ITPSTYVRCLN---VGLIRKLSDFIDPQEGWKKLAVAIKKPSGDDRYN
IRAKM       MAGNCG--ARGALSAHTLLFDLPPALLGELCAVLDSCDGALGWRGLAERLSSSW------
IRAK1       MAGGPGPGEPAAPGAQHFLYEVPPWVMCRFYKVMDALEP-ADWCQFAALIVRDQ------
IRAK2       --------------MACYIYQLPSWVLDDLCRNMDALSE-WDWMEFASYVITDL------
                             :  :    :  :    *  .   .*  :*  :

IRAK4       QFHIRRFEAL-LQTGKSPTSELLFDWGTTNCTVGDLVDLLIQNEFFAPASLLLPDAVPKT
IRAKM       -LDVRHIEKY-VDQGKSGTRELLWSWAQKNKTIGDLLQVLQEMGHRRAIHLITNYGAVLS
IRAK1       -TELRLCERS-----GQRTASVLWPWINRNARVADLVHILTHLQLLRARDIITAWHPPAP
IRAK2       -TQLRKIKSMERVQGVSITRELLWWWGMRQATVQQLVDLLCRLELYRAAQIILNWKPAPE
              .:*  :        . * .:*: *   :  : :*:.:* .        ::

IRAK4       AN----------
IRAKM       PSE--KSYQEGG
IRAK1       LPS---------
IRAK2       IRCPIPAFPDSV
```

Figure 1.4. The alignment of the death domain of the IRAK family

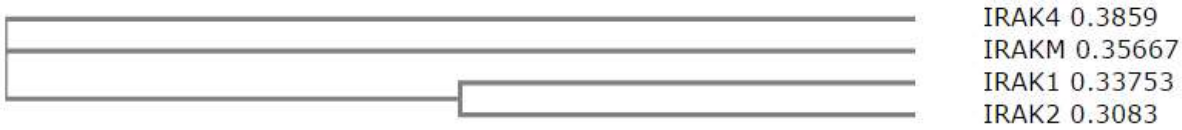

Figure 1.5. Phylogenetic Tree of the death domain of the IRAK family

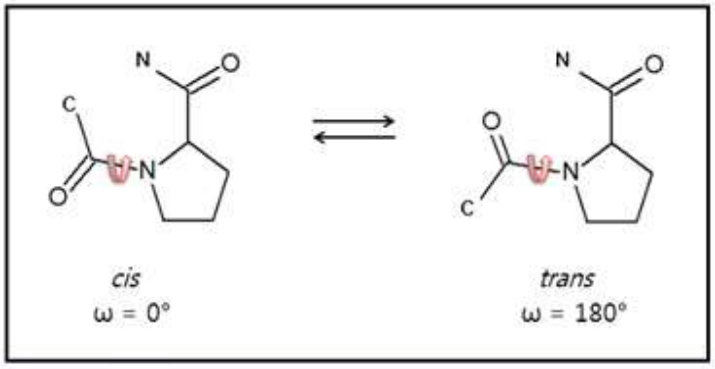

Figure 1.6. *cis/trans* isomers of Pin1 substrates.

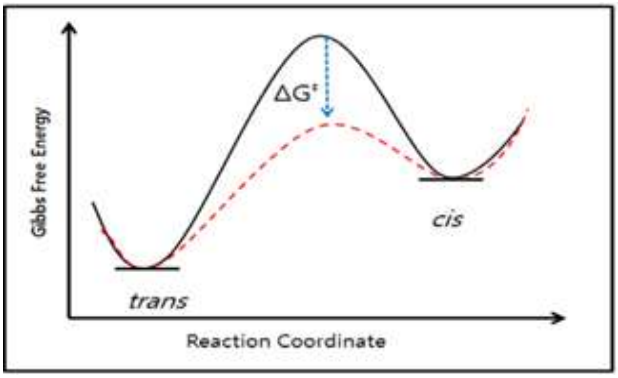

Figure 1.7. Pin1 reduces energy barrier of *cis/trans* converstion.

Pin1 plays important roles in innate immunity

Peptidyl-prolyl *cis/trans* isomerase 1 (Pin1) is the only known phosphorylation-specific peptidyl- prolyl isomerase in humans. Proline is characterized by its unique ability to exist in two conformations: *cis* and *trans* (Figure 1.6). Proline *cis/trans* isomerization is often important as the rate-determining step in protein folding [28]. Pin1 catalyzes isomerization of phosphorylated S/T-P motifs by reducing the energy barrier of *cis/trans* conversion [29] (Figure 1.7). Pin1 has two domains: an N-terminal WW domain and a C-terminal peptidyl-prolyl isomerase (PPIase) domain. The group IV WW domain found in Pin1 binds to phosphorylated S/T-Pro motifs, and PPIase domain isomerizes pS/T-Pro sites [30]. Pin1 can regulate protein function in cell signaling by controlling protein conformational exchanges upon phosphorylation [31, 32] . A Pin1 knockout (Pin1-/-) inhibits HDM-induced pro-inflammatory cytokine production, indicating a central role of Pin1 in innate immunity signaling. Pin1 is activated by treating cells with IL-33, which activates IL-1R signaling in Th2 cells that induce asthma [14, 33]. Pin1 knockout (Pin1-/-) abolishes IRAK1 activation as well as cytokine production in a mouse asthma model [34].

Interleukin-33 treatment activates Pin1, and Pin 1 has an important role in asthma

IL-33 levels are elevated in asthma. Our collaborators have shown that IL-33 stimulation activates Pin1 activity and induces asthma [35] . A Pin1-/- showed significant suppression of Th2 cell cytokine production and asthma even after IL-33 induction. This data is similar with that obtained by inhibiting IL-33 in mouse asthma models [36, 37]. Inhibition of IL-33 results in asthma suppression as was observed in the Pin1-/- mouse model [35].

IRAK-M regulates Toll-like receptor signaling.

IRAK-M is a known negative regulator of Toll-like receptor signaling [19]. There are three ways to repress Toll-like receptor signaling. First, IRAK-M associates with IRAK1 to prevent IRAK1 dissociation from Mydossome complexes and to prevent the formation of IRAK1-TRAF6 complexes [16, 20, 38]. Second, it has been recently found that IRAK-M induces inhibitory molecules through TLR7 as part of a second wave of signaling in response to endocytosed pathogen [38]. Third, IRAK-M has been shown to inhibit the IRAK2-mediated TLR signaling pathway that stabilizes specific mRNAs to promote cytokine and chemokine production [17]. Hence, by either blocking or promoting signaling, IRAK-M plays key roles in negative regulation of TLR signaling.

Although its major function appears to be repressive, activation of NF-kB by IRAK-M when both IRAK1 and IRAK2 were eliminated has also been reported [35, 39]. In support of specific activation roles of IRAK-M, through collaboration we have identified IRAK-M as a novel Pin1 target critical for IL-33 signaling in type 2 (TH2) allergic response associated with asthma [35]. Briefly, Pin1 is activated in IL-33-induced airway inflammation. Notably, IRAK-M is phosphorylated at its S115-P site by IRAK1 upon IL-33 treatment, which induces asthma, and

phosphorylated IRAK-M is immune-precipitated by Pin1 antibody [35]. Pin1 binding and isomerization of the pS115-P motif increases IRAK-M nuclear translocation and protein stability that correlates with increased expression of a set of pro-inflammatroy cytokines that induce inflammation. These results were correlated with molecular features of asthma in humans by analyzing samples obtained from asthmatic patients challenged with Derp1 (a major allergen of house dust mites), where Pin1 activation and IRAK-M levels were increased, and expression of the IRAK-M downstream pro-inflammatroy cytokines were increased [35].

IRAK-M consists of three domains and a linker: death domain [23], linker, kinase domain (UD), and C-terminal domain. pSer110-Pro111 is a potential target site for Pin1 and also for TRAF6 (tumour-necrosis-factor receptor-associated factor 6**)**. TRAF6 binds to PxExx(Ar/Ac) motifs and the S110-PSEKSY116 motif in lRAK-M linker meets the requirements for a canonical TRAF6 binding motif [40]. IRAK-M is expressed in monocytes and macrophages in TLR/IL-1 signaling [26] and is also expressed in lung epithelial cells [23].

Overview

Quantification of the interaction between phosphorylated IRAK-M and Pin1

Pin1, which consists of both a WW domain and a PPIase Domain, induces an acceleration of the isomerization of pS-P motifs in IRAK-M [3]. Our collaborator's previous data shows that Pin1 binds to IRAK-M tightly as it immuno-precipitates with Pin1. Over expressed Pin1 also stabilizes IRAK-M and locates IRAK-M to the nucleus [35]. Pin1 is a pleiotropic enzyme, which has multiple effects and interacts with multiple proteins. The interaction between Pin1 and IRAK-M can be direct or indirect. Immunoprecipitation data are consistent with a model that Pin1 directly interacts with IRAK-M *in vivo* [35]. Here we tested the model

that Pin1 directly interacts with IRAK-M *in vitro* by using purified recombinant Pin1 and synthetic phosphopeptides, and excluding any other proteins. The dissociation constant K_D between a phosphopeptide representing IRAK-M residues X-X phosphorylated at S110 (pIRAK-M) and Pin1 were determined by NMR titration using ^{1}H ^{-15}N HSQC spectra. The K_D between Pin1 and the corresponding peptide with phosphomimetic mutation S110E was also determined. The isomerization rate of pS110-P111 in IRAK-M and mutation S110E-P111 in these IRAK-M peptides were determined by NMR ROESY experiments. The resulting data, presented in Chapter 2, demonstrates a direct *in vitro* interaction between Pin1 and the IRAK-M sequence containing pS110-P111 that we show (in Chapter 4) is solvent-accessible. These results support a model in which Pin1 interacts directly with IRAK-M phosphorylated at S110 *in vivo*, and the retention of Pin1 isomerization of the S110E mutant explains the functional effects of this mutant in the mouse asthma model [35].

^{1}H, ^{13}C, ^{15}N backbone and side-chain resonance assignment of human R56D, Y61E variant of the IRAK-M death domain

IRAK-M consists of three domains and a linker: death domain [23], linker, kinase domain (KD), and C-terminal domain. The association between IRAKs occur through the death domain [7]. Even though the role of IRAK-M in Toll-like receptor signaling is significant, the mechanism of IRAK-M Death Domain is still veiled. The IRAK-M death domain is not soluble in E.coli and rapidly aggregates, precluding the detection of strong NMR signal for each residue. Hypothesizing that the observed aggregation was due to the expected oligomerization of the death domain, we imparted electrostatic repulsion by mutating suspected oligomer interface residues to negatively charged amino acids, producing the double mutant R56D, Y61E. This strategy yielded soluble monomeric IRAK-M death domain. Uniformly 15N-labeled IRAK-M

DD (R59D,Y61E) yielded a well dispersed 15N-1H HSQC spectrum, and 13C, 15N-labeled protein was subsequently produced. For the first step to unveil the mechanism of the IRAK-M death domain, the chemical shifts of IRAK-M death domain were assigned. In Chapter 3, I present the backbone and sidechain assignments of a 124- residue consist of IRAK-M [1-119] and 5 extra residues at the N-terminal, and identify the secondary structure of the IRAK-M [1-119] that is consists of 6 α-helices.

Structure determination of human R56D, Y61E variant of the IRAK-M death domain

Asthma is a chronic inflammatory sickness of the airways caused by environmental and genetic factors. The mechanisms of activation of the innate immunity signaling pathways that causes asthma are not fully understood yet. This study investigated the novel targets for the development of new asthma therapeutics, with a specific focus on IRAKM that is the negative regulator within the context of Toll-Like Receptors(TLRs) signaling. Toll-Like Receptors (TLRs) recognizes specific molecular markers that are present in microbial components, such as viral double-stranded RNA or bacterial lipopolysaccharides, and serve as a first line of defense against pathogens. Toll-Like Receptors (TLRs) transfer the signals to MyD88 and IRAK family through a toll-IL-1 receptor (TIL) after TLRs detect microbial components. Assembly of IRAK-M into the TLR signaling complex is mediated by its N-terminal death domain. Oligomerization is a hallmark of Death Domains [23]. The IRAKM-DD has eluded structure determination due to aggregation. Here, we solved structure of a double-mutant IRAK-M Death Domain (R56D, Y61E) that is a highly soluble monomer well suited for NMR studies. Furthermore, we simulated possible docking model between IRAK-M DD and IRAK families multi-structures.

References

1. Bosnjak, B., et al., *Treatment of allergic asthma: modulation of Th2 cells and their responses.* Respir Res, 2011. **12**: p. 114.
2. McGuirk, P., S.C. Higgins, and K.H. Mills, *The role of regulatory T cells in respiratory infections and allergy and asthma.* Curr Allergy Asthma Rep, 2010. **10**(1): p. 21-8.
3. Galli, S.J., M. Tsai, and A.M. Piliponsky, *The development of allergic inflammation.* Nature, 2008. **454**(7203): p. 445-54.
4. Adcock, I.M. and G. Caramori, *Cross-talk between pro-inflammatory transcription factors and glucocorticoids.* Immunol Cell Biol, 2001. **79**(4): p. 376-84.
5. Barnes, P.J., *Immunology of asthma and chronic obstructive pulmonary disease.* Nat Rev Immunol, 2008. **8**(3): p. 183-92.
6. Canonica, G.W., *Treating asthma as an inflammatory disease.* Chest, 2006. **130**(1 Suppl): p. 21S-28S.
7. Karin, M. and F.R. Greten, *NF-kappaB: linking inflammation and immunity to cancer development and progression.* Nat Rev Immunol, 2005. **5**(10): p. 749-59.
8. Shaulian, E. and M. Karin, *AP-1 as a regulator of cell life and death.* Nat Cell Biol, 2002. **4**(5): p. E131-6.
9. Lin, Y.T., A. Verma, and C.P. Hodgkinson, *Toll-like receptors and human disease: lessons from single nucleotide polymorphisms.* Curr Genomics, 2012. **13**(8): p. 633-45.
10. O'Neill, L.A., *The interleukin-1 receptor/Toll-like receptor superfamily: 10 years of progress.* Immunol Rev, 2008. **226**: p. 10-8.

11. Dong, L., et al., *Different doses of lipopolysaccharides regulate the lung inflammation of asthmatic mice via TLR4 pathway in alveolar macrophages.* J Asthma, 2009. **46**(3): p. 229-33.

12. Guo, Z., et al., *IL-33 promotes airway remodeling and is a marker of asthma disease severity.* J Asthma, 2014. **51**(8): p. 863-9.

13. Iikura, M., et al., *IL-33 can promote survival, adhesion and cytokine production in human mast cells.* Lab Invest, 2007. **87**(10): p. 971-8.

14. Schmitz, J., et al., *IL-33, an interleukin-1-like cytokine that signals via the IL-1 receptor-related protein ST2 and induces T helper type 2-associated cytokines.* Immunity, 2005. **23**(5): p. 479-90.

15. Prefontaine, D., et al., *Increased expression of IL-33 in severe asthma: evidence of expression by airway smooth muscle cells.* J Immunol, 2009. **183**(8): p. 5094-103.

16. Delneste, Y., C. Beauvillain, and P. Jeannin, *[Innate immunity: structure and function of TLRs].* Med Sci (Paris), 2007. **23**(1): p. 67-73.

17. Akira, S. and K. Takeda, *Toll-like receptor signalling.* Nat Rev Immunol, 2004. **4**(7): p. 499-511.

18. Gay, N.J. and F.J. Keith, *Drosophila Toll and IL-1 receptor.* Nature, 1991. **351**(6325): p. 355-6.

19. Kobayashi, K., et al., *IRAK-M is a negative regulator of Toll-like receptor signaling.* Cell, 2002. **110**(2): p. 191-202.

20. Wang, J., et al., *Negative regulation of Toll-like receptor signaling pathway.* Microbes Infect, 2009. **11**(3): p. 321-7.

21. Hammad, H., et al., *House dust mite allergen induces asthma via Toll-like receptor 4 triggering of airway structural cells.* Nat Med, 2009. **15**(4): p. 410-6.

22. Trompette, A., et al., *Allergenicity resulting from functional mimicry of a Toll-like receptor complex protein.* Nature, 2009. **457**(7229): p. 585-8.

23. Balaci, L., et al., *IRAK-M is involved in the pathogenesis of early-onset persistent asthma.* Am J Hum Genet, 2007. **80**(6): p. 1103-14.

24. Lin, S.C., Y.C. Lo, and H. Wu, *Helical assembly in the MyD88-IRAK4-IRAK2 complex in TLR/IL-1R signalling.* Nature, 2010. **465**(7300): p. 885-90.

25. Gosu, V., et al., *Molecular evolution and structural features of IRAK family members.* PLoS One, 2012. **7**(11): p. e49771.

26. Fukao, T. and S. Koyasu, *PI3K and negative regulation of TLR signaling.* Trends Immunol, 2003. **24**(7): p. 358-63.

27. Feinstein, E., et al., *The death domain: a module shared by proteins with diverse cellular functions.* Trends Biochem Sci, 1995. **20**(9): p. 342-4.

28. Wedemeyer, W.J., E. Welker, and H.A. Scheraga, *Proline cis-trans isomerization and protein folding.* Biochemistry, 2002. **41**(50): p. 14637-44.

29. Fischer, G. and T. Aumuller, *Regulation of peptide bond cis/trans isomerization by enzyme catalysis and its implication in physiological processes.* Rev Physiol Biochem Pharmacol, 2003. **148**: p. 105-50.

30. Verdecia, M.A., et al., *Structural basis for phosphoserine-proline recognition by group IV WW domains.* Nat Struct Biol, 2000. **7**(8): p. 639-43.

31. Lu, K.P., et al., *Prolyl cis-trans isomerization as a molecular timer.* Nat Chem Biol, 2007. **3**(10): p. 619-29.

32. Lu, K.P. and X.Z. Zhou, *The prolyl isomerase PIN1: a pivotal new twist in phosphorylation signalling and disease.* Nat Rev Mol Cell Biol, 2007. **8**(11): p. 904-16.

33. Funakoshi-Tago, M., et al., *TRAF6 is a critical signal transducer in IL-33 signaling pathway.* Cell Signal, 2008. **20**(9): p. 1679-86.

34. Tun-Kyi, A., et al., *Essential role for the prolyl isomerase Pin1 in Toll-like receptor signaling and type I interferon-mediated immunity.* Nat Immunol, 2011. **12**(8): p. 733-41.

35. Nechama, M., et al., *The IL-33-PIN1-IRAK-M axis is critical for type 2 immunity in IL-33-induced allergic airway inflammation.* Nat Commun, 2018. **9**(1): p. 1603.

36. Hayakawa, H., et al., *Soluble ST2 blocks interleukin-33 signaling in allergic airway inflammation.* J Biol Chem, 2007. **282**(36): p. 26369-80.

37. Kondo, Y., et al., *Administration of IL-33 induces airway hyperresponsiveness and goblet cell hyperplasia in the lungs in the absence of adaptive immune system.* Int Immunol, 2008. **20**(6): p. 791-800.

38. Zhou, H., et al., *IRAK-M mediates Toll-like receptor/IL-1R-induced NFkappaB activation and cytokine production.* EMBO J, 2013. **32**(4): p. 583-96.

39. Su, J., et al., *Differential regulation and role of interleukin-1 receptor associated kinase-M in innate immunity signaling.* Cell Signal, 2007. **19**(7): p. 1596-601.

40. Ye, H., et al., *Distinct molecular mechanism for initiating TRAF6 signalling.* Nature, 2002. **418**(6896): p. 443-7.

Chapter 2

Pin1 catalyzes cis/trans isomerization of the pS110-Pro motif in IRAK-M

Parts of this chapter are published in Nechama, Kwon et al. 2018 (Nechama, M., et al. The IL-33-PIN1-IRAK-M axis is critical for type 2 immunity in IL-33-induced allergic airway inflammation. Nat Commun 9(1): 1603 (2018))

Abstract

Asthma is a chronic inflammatory sickness of the airways caused by environmental and genetic factors. The mechanisms of activation of the innate immunity signaling pathways that cause asthma are not fully understood yet. This study investigated novel targets for the development of new asthma therapeutics, with a specific focus on the peptidyl-prolyl isomerase enzyme Pin1 and a key substrate in innate immunity signaling, IRAK-M. Prolyl peptide bonds, such as in the phosphorylated Ser/Thr-Pro (pS/T-P) motifs recognized by Pin1, can exist in two distinct isomer conformations, *cis* and *trans*, that exchange on a slow time scale (exchange time constant of several minutes). Pin1 can accelerate the isomerization rate of pS/T-P motifs by several orders of magnitude. The NMR experiments reported here show that Pin1 directly interacts with and isomerizes the phosphoS110-P111 peptide bond in a phosphopeptide corresponding to the IRAK-M sequence 103-124 (pIRAK-M), and also acts on the corresponding peptide harboring the phosphomimetic mutation S110E. This study determined the dissociation constant, K_D, for binding of Pin1 to each of the two peptides by titrating ^{15}N-labeled Pin1 WW domain with unlabeled peptide and quantifying bound and free populations using ^{1}H ^{-15}N HSQC spectra. Moreover, the Pin1-catalyzed *cis-trans* isomerization rates of

pS110-P111 and S110E-P111 in these IRAK-M peptides were determined using ROESY experiments. These results, together with collaborative biological experiments, implicate the Pin1/IRAKM pS110-P111 interaction as critical for dendritic cell activation, type 2 immunity and IL-33 induced airway inflammation. Collectively, these findings offer new therapeutic targets for allergic asthma.

Introduction

The dual domain enzyme Pin1, which consists of a WW domain and a PPIase domain, is the only known phosphorylation-specific peptidyl-prolyl isomerase in humans (1, 2). Pin1 regulates protein function in cell signaling by accelerating the interchange between *cis* and *trans* conformations of specific pS/T-P motifs (1, 2). While the PPIase domain catalyzes isomerization of substrates, the WW domain is a binding module that typically interacts more strongly with the targeted substrates (1, 2). Interactions between Pin1 and several of its substrates are predominantly mediated by the WW domain, with significantly lower affinity attributed to the PPIase domain as expected for a classical enzyme (3).

Our collaborative work with Kun Ping Lu (BIDMC, Harvard Medical School) has shown that Pin1 positively regulates the TLR/IL-1R signaling pathway in asthma and is a potential therapeutic target in the treatment of immune diseases (4). More recently, the influence of Pin1 on IL-33 induced immune signaling was found to involve a functional interaction between Pin1 and IRAK-M. Our collaborator's data shows IRAK-M immuno-precipitates with Pin1, that over expression of Pin1 stabilizes IRAK-M and locates IRAK-M to the nucleus in dendritic cell line DC2.4 (mouse model) when stimulated with IL-33, and that the S110E mutation in IRAK-M retains the Pin1-dependent stabilization and localization effects thereby implicating the

phosphoS110-P111 site (5). The P111A mutation totally abolished IRAKM phosphorylation and Pin1 interaction, which further suggests that proline-directed phosphorylation of this site is needed for Pin1 interaction (5). Since Pin1 is a pleiotropic enzyme, with multiple effects mediated by interactions with multiple proteins, it is critical to establish whether the observed Pin1-dependent effects are due to direct interaction between Pin1 and the phosphoSer110-P111 site in IRAK-M. Moreover, while immunoprecipitation data are consistent with a model that Pin1 directly interacts with IRAK-M *in vivo* (5), this does not definitively prove a direct interaction since a multiprotein complex could be involved.

The *in vitro* experiments reported here test for a direct interaction between the isolated putative partners, excluding any other proteins. The dissociation constant K_D between a phosphorylated IRAK-M peptide (IRAK-M residues 103-124 with Ser110 phosphorylated, pIRAK-M) and the Pin1 WW domain were determined by NMR titration using the ^{1}H ^{-15}N HSQC spectrum as a readout. The K_D between Pin1 and phosphomimetic mutation IRAK-M S110E in the same peptide were also determined. The isomerization rate of pS110-P111 and mutation S110E-P111 in these IRAK-M peptides were determined by NMR ROESY experiments.

Materials and Methods

The ^{15}N- labeled Pin1 WW domain (Pin1 residues 1-50) was expressed and purified as described (6). The Pin1 WW domain was expressed in *E. coli* (BL21(DE3)) using M9 minimal media containing ^{15}N-NH_4Cl (Cambridge Isotope Laboratories, Inc.). Cells were induced at OD_{600} of 0.6 ~ 0.8 by adding 1mM final concentration of Isopropyl β-D-1-thiogalactopyranoside (IPTG) at 37°C and harvested at OD_{600} of 2.0. The Pin1 gene was inserted into a pET28 vector with

Kanamycin resistance as a fusion protein with an N-terminal His_6-tag. Pin1 was expressed in LB culture. The cells were induced at OD_{600} of 0.6~0.8 by adding 1mM of a final concentration of IPTG at 16°C for 20 hours. Synthetic peptides pSer110 (comprised of IRAKM residues 103-124 with Ser110 phosphorylated, TNYGAVL(**pS)**PSEKSYQEGGFPNI), and IRAKM Ser110E (IRAKM residues 103-124 with the Ser110E substitution), were purchased from Tufts University, Core Facility, Boston, MA.

Nuclear magnetic resonance (NMR) experiments were performed on a Varian Inova 600-MHz spectrometer at 25 °C. NMR spectra were processed and analyzed using NMRPipe and Sparky software (7, 8). The composite chemical shift change in the 2D ^{1}H ^{-15}N HSQC was monitored during NMR titration experiments and was fit to the standard bimolecular binding equation as described (equation 1) (6). The Solver function in Excel (Microsoft) was used to fit the data to the standard bimolecular binding equation (Equation 1):

$$[WW:IRAKM] = \frac{[WWo] + [IRAKMo] + K_D + \sqrt{([WWo] + [IRAKMo] + K_D)^2 - 4[WWo][IRAKMo]}}{2} \quad \textbf{Equation 1}$$

In the above equation for a two-state binding equilibrium (free and bound) between protein and ligand, K_D is the dissociation constant, $[WW_o]$ refers to the total concentration of WW domain in sample, $[IRAKM_o]$ refers to the total concentration of synthetic IRAK-M peptide, and [WW:IRAK-M] refers to the concentration of protein:peptide complex.

To quantify the binding affinity between the Pin1 WW domain and peptides, the ^{15}N labeled Pin1 WW domain was titrated with the each of the synthetic peptides, pSer110 and IRAKM Ser110E. A reverse titration method was used, where the ^{15}N labeled protein was mixed with high concentration synthetic peptide for the first sample. Subsequent samples were a serial dilution of this sample with one part derived from the previous sample and one part from a stock solution of the ^{15}N labeled Pin1 WW domain at the same concentration as the ^{15}N labeled Pin1

WW domain in the first sample. This resulted in a titration where the concentration of the ^{15}N Pin1 WW domain was constant, and the concentration of synthetic peptide decreased by a factor of ½ in each successive sample. For each of the pSer110 and IRAKM Ser110E peptides, a ^{1}H - ^{15}N HSQC of each titration point was acquired on a Varian Inova 600-MHz spectrometer at 25 °C, and the resulting composite chemical shift changes, $\Delta\omega$, were quantified using Equation 2:

$$\Delta\omega = \sqrt{(\delta_H - \delta_H^{free})^2 + (0.154 \times (\delta_N - \delta_N^{free}))^2} \qquad \textbf{Equation 2}$$

In Equation 2, δ_i is the chemical shift of dimension *i*, and δ^{free} is the chemical shift of the free state (6). The composite chemical shift change as a function of titrated ligand was used to obtain the concentration of bound complex, [WW:IRAKM], at each titration point using Equation 3:

$$\Delta\omega = \frac{[WW{:}IRAKM] \times (\delta^{bound} - \delta^{free})}{[WW^{tot}]} \qquad \textbf{Equation 3}$$

The K_D value was subsequently fit using Equation 1.

For the quantification of Pin1 isomerization of peptides pSer110 and IRAKM Ser110E, homonuclear 2D rotating-frame overhauser effect spectroscopy (ROESY) NMR experiments were performed. For Pin1 catalysis of pSer110, 13.8μM of Pin1 was added to 4.44mM of pSer110, and ROESY experiments were acquired with 0ms, 4ms, 8ms, 20ms, 40ms, 60ms, 80ms, 100ms, and 150ms mixing times. For Pin1 catalysis of IRAKM Ser110E, 20 μM of Pin1 was added to 4.18mM of IRAKM Ser110E, and ROESY experiments were acquired with 0ms, 16ms, 20ms, 40ms, 60ms, 80ms, 100ms, and 150ms mixing times. For the appropriate controls,

each of pSer110 and IRAKM Ser110E was detected by ROESY without Pin1. The ratios *trans* to *cis* were measured by Total Correlation Spectroscopy (TOCSY) for both pS110 and IRAKM Ser110E. The intensity ratios of cross peaks to diagonal peaks for *cis* and *trans* conformation in the ROESY spectra were fit using the equations 4 (9)

$$I_{cc}(t_m) = \frac{I_c(0)\{-(\lambda_2 - a_{11})e^{-\lambda_1 t_m} + (\lambda_1 - a_{11})e^{-\lambda_2 t_m}\}}{\lambda_1 - \lambda_2}$$

$$I_{tt}(t_m) = \frac{I_t(0)\{-(\lambda_2 - a_{22})e^{-\lambda_1 t_m} + (\lambda_1 - a_{22})e^{-\lambda_2 t_m}\}}{\lambda_1 - \lambda_2}$$

$$I_{ct}(t_m) = \frac{I_c(0)\{a_{21}e^{-\lambda_1 t_m} - a_{21}e^{-\lambda_2 t_m}\}}{\lambda_1 - \lambda_2} \qquad \textbf{Equations 4}$$

$$I_{tc}(t_m) = \frac{I_t(0)\{a_{12}e^{-\lambda_1 t_m} - a_{12}e^{-\lambda_2 t_m}\}}{\lambda_1 - \lambda_2}$$

$$\lambda_{1,2} = 1/2\{(a_{11} + a_{22}) \pm \sqrt{(a_{11} - a_{22})^2 + 4k_{ct}^{cat}k_{tc}^{cat}}\}$$

$$a_{11} = k_{ct}^{cat} + R_{2,c}, a_{22} = k_{tc}^{cat} + R_{2,t}, a_{12} = -k_{tc}^{cat}, a_{21} = -k_{ct}^{cat}$$

In the above equations, $R_{2,c}$ and $R_{2,t}$ are the transverse relaxation rates of magnetization in *cis* and *trans* isomer states, k_{ct}^{cat} and k_{tc}^{cat} represent the exchange rates between *cis* and *trans*, and $I_c(0)$ and $I_t(0)$ are the transverse magnetization of the *cis* and *trans* isomer states at the beginning of the mixing time t_m. R2, transverse relaxation rates, were measure by fitting to a single exponential equation, I(t)=I(0)Exp(-t*R2), where I is an intensity of trans/cis peaks (9). We fit the data to equations 4 rather than the simplified equation that assumes trans and cis populations are equal, because the populations of *cis* and *trans* are significantly different in both pSer110 and IRAKM Ser110E peptides.

Results

Pin1 directly interacts with phospho-Ser110 and Ser110E IRAKM peptides *in vitro*

To determine whether Pin1 can directly interact with the phosphorylated serine 110 (pSer110) site in IRAKM and with the Ser110E mutant of this motif, two-dimensional nuclear magnetic resonance spectroscopy (NMR) was employed. For detection of binding, the WW domain of Pin1, which facilitates binding to Pin1 substrates, was uniformly labeled with ^{15}N, providing the ability to use NMR to detect residue-specific changes in the chemical environment that result from the addition of unlabeled IRAKM peptide. The covalently bonded nitrogen and amide proton (NH) of each residue in the ^{15}N-labeled Pin1 WW domain yields a peak in the two-dimensional ^{1}H-^{15}N Heteronuclear Single Quantum Coherence (HSQC) spectrum (Figure 2.1 a). The coordinates of each peak, given by the chemical shift in each of the nitrogen and proton dimensions, are sensitive to the chemical environment of the NH group and thereby serve as sensors to detect ligand binding. The kinetics of ligand binding can be in either fast or slow exchange, inducing peaks to move with increasing ligand concentration or causing the appearance of new peaks, respectively. The induced chemical shift perturbation ($\Delta\delta$) of the ^{15}N-labeled Pin1 WW domain observed during titration with the IRAKM peptides can be quantitatively analyzed to yield binding affinity (6).

The binding of the ^{15}N-labeled Pin1 WW domain to the phosphorylated IRAKM (pSer110) and IRAKM Ser110E peptides was monitored using the ^{1}H-^{15}N HSQC experiment. For titrations using each peptide, the positions of several peaks in the spectrum of ^{15}N Pin1 WW domain change with increasing peptide concentration, moving toward their respective positions in the spectrum of the saturated complex (Figure 2.1 b-e). This peak movement with the addition of ligand demonstrated fast exchange kinetics and allowed the corresponding dissociation

constant (K_D) for each peptide to be determined from the induced chemical shift perturbation as described in Materials and Methods (6). The composite chemical shift titration curves were well fit using the simple two-state binding model (Figure 2.2). The resulting dissociation constant (K_D) between the Pin1 WW domain and pSer110 was 60.7μM±11.5μM (mean ± s.d.), and K_D between the Pin1 WW domain with IRAKM Ser110E was 1.51mM ± 0.22mM (mean ± s.d.).

Isomerization by Pin1

Pin1, which consists of both a WW domain and a Peptidyl-prolyl-*cis-trans*-isomerase domain (PPIase), accelerates the isomerization of specific phosphorylated S/T-P motifs. In cellular experiments performed by the Lu lab, Pin1-K63A, a catalysis deficient Pin1 mutant could not stabilize IRAKM, which suggests that isomerization may be necessary for IRAKM stabilization (5). Moreover, the IRAK-M(S110E) mutant showed enhanced Pin1-dependent stabilization, suggesting that Pin1 might also catalyze the E-P peptide bond in IRAK-M(S110E). To determine whether Pin1 catalyzes isomerization of the pIRAKM and IRAKM Ser110E peptides, homonuclear 2D rotating-frame overhauser effect spectroscopy (ROESY) NMR experiments were performed. The intensities of exchange cross peaks and diagonal peaks for the two isomer states, *cis* and *trans*, are changed depending on the exchange rates (k_{tc}, k_{ct}), and on the ROESY mixing time (t_m).

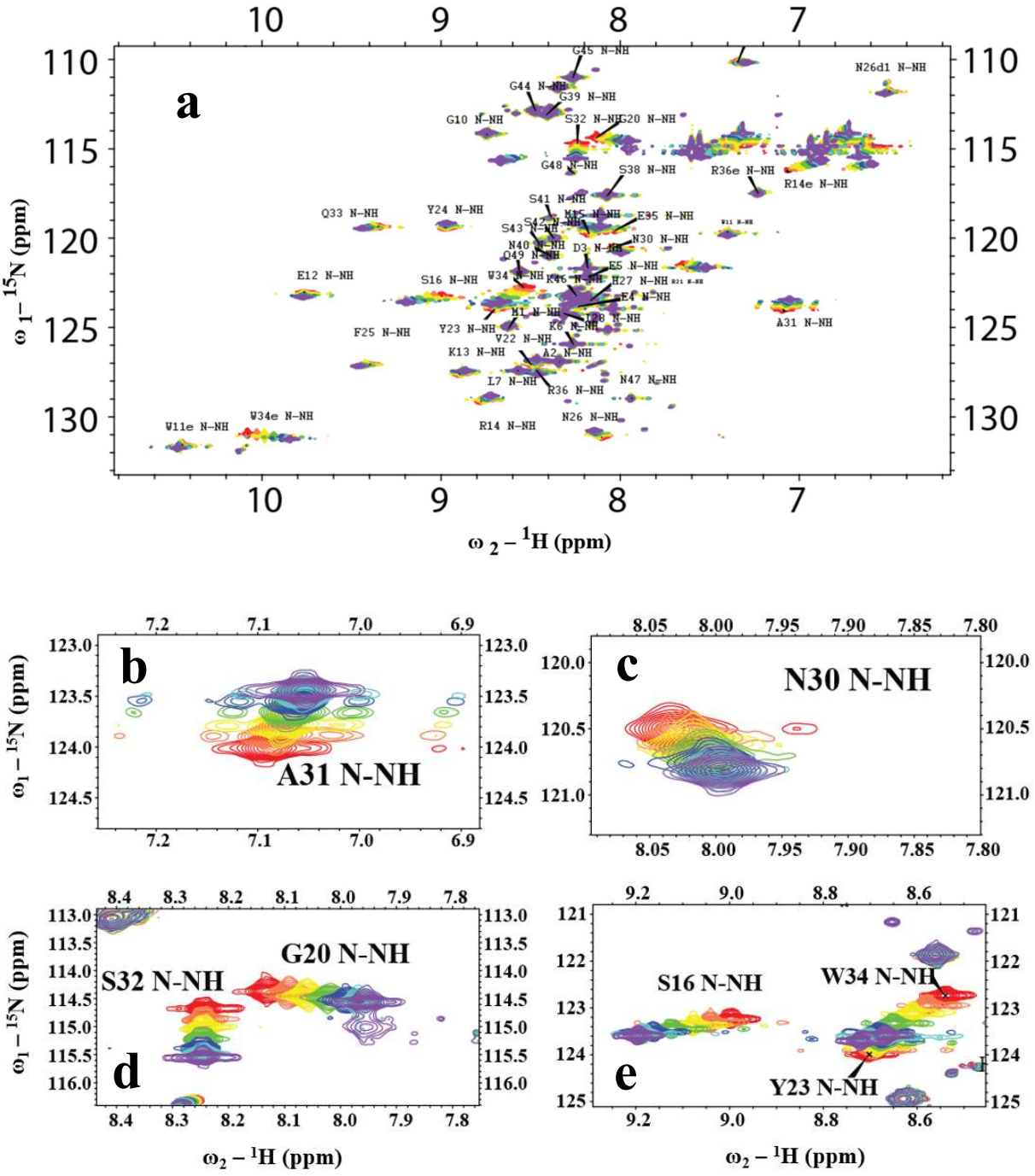

Figure 2.1. IRAKM-pSer110 binds to Pin1. (a) The full ^{1}H-^{15}N HSQC spectrum of WW domain titration with the IRAKM-pSer110 peptide with apo labeling. (b-e) Chemical shift perturbations in extracted regions of the ^{1}H-^{15}N HSQC spectrum of ^{15}N-labeled Pin1 WW domain resulting from titration with the IRAKM-pSer110 peptide. Overlaid spectra of apo (5)

and increasing amounts of ligand (rainbow of colors, with purple as highest ligand concentration).

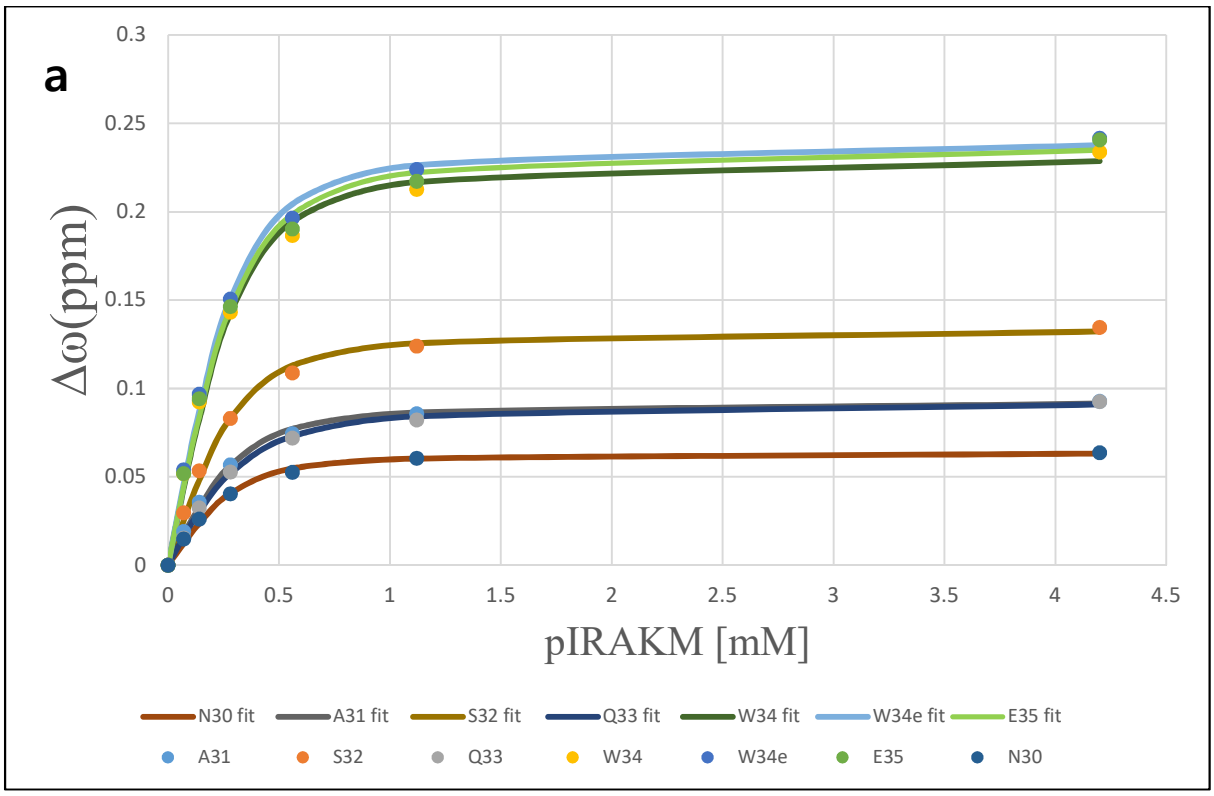

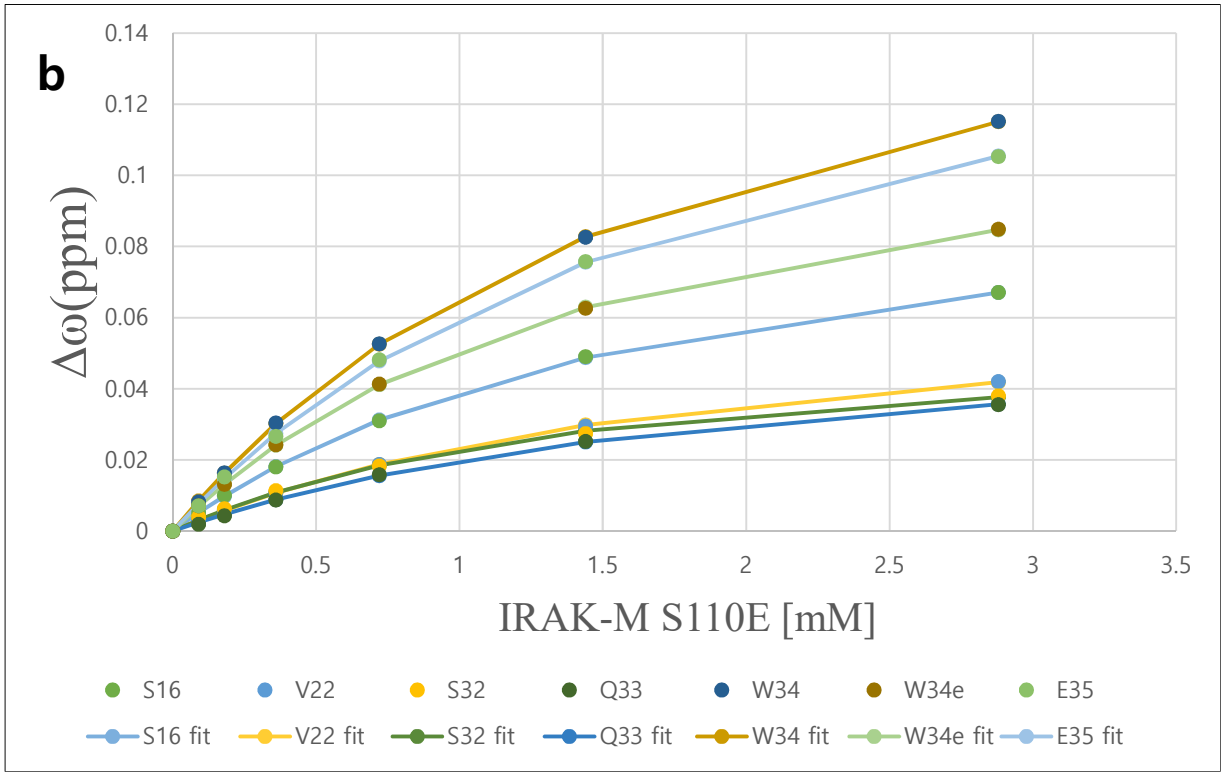

Figure 2.2. Plot of composite chemical shift change (Δω) (Equation 2) (6) as a function of a) pIRAKM concentration or b) IRAK-M S110E concentration for a selection of ^{15}N-WW domain residues. Filled circles represent experimental values, and solid lines denote best-fit two-state binding model curves for the indicated residues

When Pin1 is present, exchange cross-peaks between *cis* and *trans* isomers appeared in ROESY spectra of both pIRAKM (phosphorylated Ser-Pro) and IRAKM Ser110E (Glu-Pro) peptides (Figure 2.3). Conversely, in the absence of Pin1, exchange cross-peaks between *cis* and *trans* isomers of the peptide bond were missing for both pIRAKM and IRAKM Ser110E peptides (Figure 2.3). These results show that Pin1 catalyzes the *cis-trans* isomerization of phosphorylated Ser-Pro motif, and phosphomimetic mutation Glu-Pro as well. These results support a direct Pin1 interaction with pIRAK-M and IRAK-M Ser110E, and provide insights into

possible mechanisms by which Pin1 might affect IRAKM stabilization *in-vivo*.

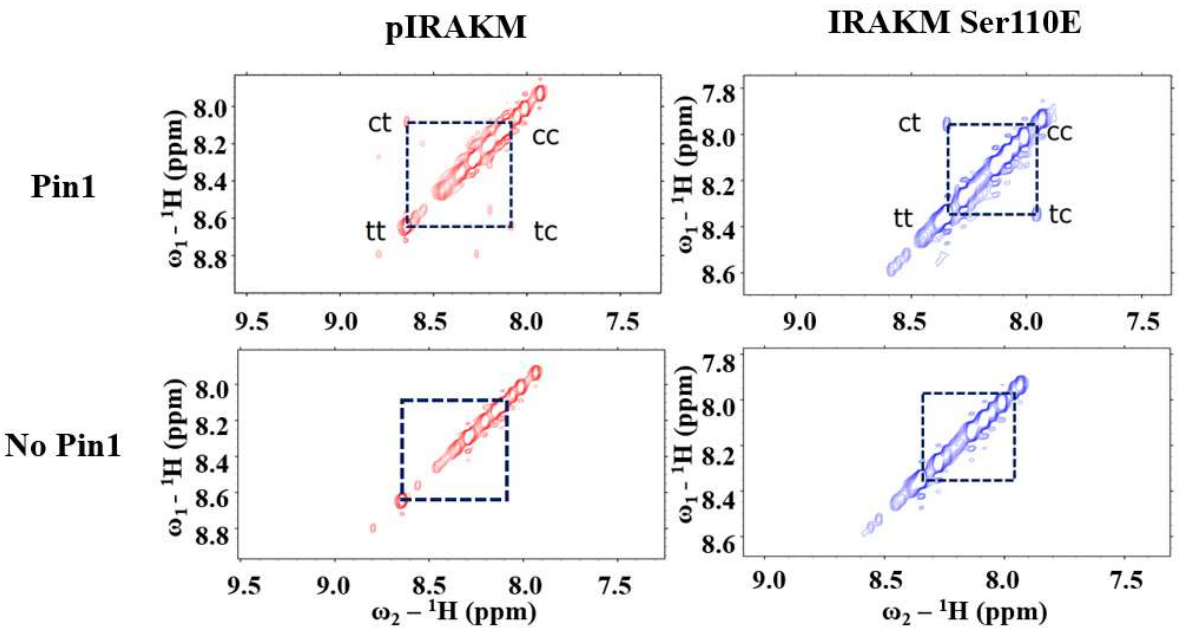

Figure 2.3. Homonuclear two-dimensional ^{1}H-^{1}H rotating frame Overhauser effect correlation spectroscopy spectra of phosphorylated IRAKM peptide or IRAKM S110E peptide in the presence of Pin1 or absence of Pin1. Diagonal (labeled **cc** or **tt**) and cross peaks (labeled **ct** and **tc**) for the amide proton of Ser110 (or E110) are connected by dashed lines. In the presence of Pin1, cross peaks between *cis* and *trans* appear for both phosphorylated IRAKM peptide and IRAKM-S110E peptide. In the absence of Pin1, no cross peaks were observed.

Acquisition of ROESY spectra at a series of mixing times allowed quantification of the Pin1-catalyzed isomerization rate for both pIRAK-M and IRAK-M Ser110E peptides, as described in Materials and Methods. The intensities of the diagonal peaks decreased and exchange peaks increased with increasing t_m (10) (Figure 2.4). Fitting of these curves to Equations 4 (above) yielded isomerization rates of 28.98 s^{-1} for pSer110 and 0.84 s^{-1} for

Ser110E(Table 2.1).

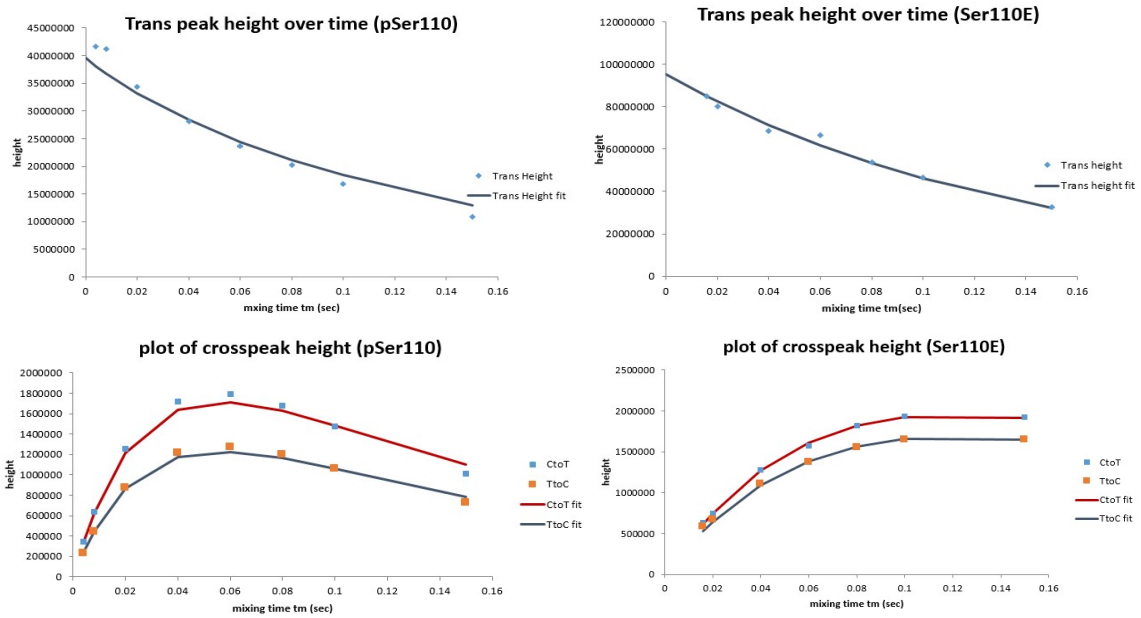

Figure 2.4. The intensities of exchange and diagonal peaks in ROESY spectra for pSer110 and IRAKM Ser110E depend on the ROESY experiment mixing time (t_m).

Table 2.1. Isomerization rates of pSer110 and IRAKM Ser110E by Pin1

	pSer110	Ser110E
Concentration	4.4 mM	4.18mM
Pin1	13.8 μM	20 μM
trans/cis	10.7	6.87
R2 (s^{-1}) <Trans, Cis>	6.8, 7.5	7.2, 8.6
k_{ex} (s^{-1})	28.98	0.84
k_{tc} (s^{-1})	2.48	0.11
k_{ct} (s^{-1})	26.50	0.73

Discussion

These NMR results indicate that Pin1 not only binds to but also catalyzes cis/trans isomerization of the pS110-Pro motif in IRAKM. Of additional great interest are the findings that Pin1 interacts with IRAKM Ser110E, the analogous phosphomimetic synthetic peptide, and catalyzes cis/trans isomerization of the Glu-Pro peptide bond in this peptide . The dissociation constant K_D between Pin1 and phosphorylated IRAKM peptide is a smaller value (stronger affinity) than K_D between Pin1 and IRAKM S110E peptide, but Pin1 still interacts with the Glu-Pro site. In addition, the isomerization rate of the pS110-Pro motif is faster than the isomerization of the Glu-Pro by Pin1. However, the isomerization rate of Glu-Pro by Pin1 is much faster than without Pin1. Previous studies regarding the specificity of Pin1 for phosphoSer/Thr-Pro versus Glu-Pro showed that Glu-Pro is around 10- to 20-fold weaker that phosphoSer/Thr-Pro in Pin1 PPIase assays, but that this level of activity is sufficient to be used

as a substrate for Pin1 PPIase assays (11-13). These results suggest that the IRAKM S110E mutant might function as a constitutive Pin1 substrate in cells.

To pursue the hypothesis that IRAKM S110E might serve as a constitutively active Pin1 substrate in cells and function similar to IRAKM phosphorylated at S110, our collaborators stably expressed either wild type IRAKM or IRAKM S110E in the DC2.4 mouse dendritic cell line (5). The Glu mutation mimics phosphorylation by placement of a negative charge, but is in a "permanent" negatively charged state, rather than a reversible one. Because stimulation of DC2.4 cells with IL-33 induces IRAKM phosphorylation at S110 and activation of Pin1, the effects of IL-33 treatment on wild type and S110E IRAKM stability and subcellular localization were compared. While the Pin1-IRAKM interaction was evident only after IL-33 stimulation, for IRAK-M S110E a much weaker PIN1 interaction was evident even before IL-33 stimulation. Interestingly, S110E IRAKM showed higher nuclear localization that wild type IRAKM, indicating that IRAK-M nuclear localization seems to be dependent on S110 phosphorylation and on PIN1. Finally, while wild type IRAKM is rapidly degraded via the proteasome, the phosphomimetic mutation S110E rendered IRAK-M completely resistant to degradation in mouse embryonic fibroblasts (MEFs), indicating that the permanent negative state of IRAKM evades proteasomal degradation. These results suggest that pSP IRAKM is protective against degradation, while SP IRAKM is susceptible to degradation. Moreover, the dependence of this protection on Pin1 implies that the interaction of pSP IRAKM or EP IRAKM with Pin1 protects IRAKM from proteasomal degradation, while SP IRAKM that is unable to interact with Pin1 is degraded. Overall, these cell biology experiments support the hypothesis that IRAKM S110E serves as a constitutive Pin1 substrate in mouse cells.

Our NMR results demonstrate that Pin1 binds to and catalyzes cis/trans isomerization of

the pS110-Pro motif and its E110-Pro phosphomimetic mutant in IRAKM. These results suggest that Pin1 interacts with pSP IRAKM directly *in vivo* as well, and that this interaction might play a central role in innate immunity. Indeed, through collaboration we have shown that IRAK-M has a distinctive function upon IL-33 stimulation where it serves as a significant mediator for IL-33 signaling in DCs in a manner dependent on IRAKM phosphorylation at S110 and on Pin1 (5). These synergistic NMR and biological studies have shown that the IL-33-PIN1-IRAK-M is an axis critical for dendritic cell activation, type 2 immunity and IL-33 induced airway inflammation, and offer new therapeutic targets for allergic asthma (5).

Reference

1. Lu KP, Finn G, Lee TH, Nicholson LK. Prolyl cis-trans isomerization as a molecular timer. Nat Chem Biol. 2007;3(10):619-29.

2. Lu KP, Zhou XZ. The prolyl isomerase PIN1: a pivotal new twist in phosphorylation signalling and disease. Nat Rev Mol Cell Biol. 2007;8(11):904-16.

3. Verdecia MA, Bowman ME, Lu KP, Hunter T, Noel JP. Structural basis for phosphoserine-proline recognition by group IV WW domains. Nat Struct Biol. 2000;7(8):639-43.

4. Tun-Kyi A, Finn G, Greenwood A, Nowak M, Lee TH, Asara JM, et al. Essential role for the prolyl isomerase Pin1 in Toll-like receptor signaling and type I interferon-mediated immunity. Nat Immunol. 2011;12(8):733-41.

5. Nechama M, Kwon J, Wei S, Kyi AT, Welner RS, Ben-Dov IZ, et al. The IL-33-PIN1-IRAK-M axis is critical for type 2 immunity in IL-33-induced allergic airway inflammation. Nat Commun. 2018;9(1):1603.

6. Soumya De AIG, Monique J. Rogals , Evgenii L. Kovrigin, Kun Ping Lu, and Linda K. Nicholson Complete Thermodynamic and Kinetic Characterization of the Isomer-Specific Interaction between Pin1-WW Domain and the Amyloid Precursor Protein Cytoplasmic Tail Phosphorylated at Thr668. Biochemistry. 2012;51(43):8583–96.

7. Delaglio F, Grzesiek S, Vuister GW, Zhu G, Pfeifer J, Bax A. NMRPipe: a multidimensional spectral processing system based on UNIX pipes. J Biomol NMR. 1995;6(3):277-93.

8. Kneller TDGaDG. SPARKY 3. University of California, San Francisco.

9. Farrow NA, Zhang O, Forman-Kay JD, Kay LE. A heteronuclear correlation experiment for simultaneous determination of 15N longitudinal decay and chemical exchange rates of systems in slow equilibrium. J Biomol NMR. 1994;4(5):727-34.

10. Pastorino L, Sun A, Lu PJ, Zhou XZ, Balastik M, Finn G, et al. The prolyl isomerase Pin1 regulates amyloid precursor protein processing and amyloid-beta production. Nature. 2006;440(7083):528-34.

11. Kops O, Eckerskorn C, Hottenrott S, Fischer G, Mi H, Tropschug M. Ssp1, a site-specific parvulin homolog from Neurospora crassa active in protein folding. J Biol Chem. 1998;273(48):31971-6.

12. Uchida T, Takamiya M, Takahashi M, Miyashita H, Ikeda H, Terada T, et al. Pin1 and Par14 peptidyl prolyl isomerase inhibitors block cell proliferation. Chem Biol. 2003;10(1):15-24.

13. Yaffe MB, Schutkowski M, Shen M, Zhou XZ, Stukenberg PT, Rahfeld JU, et al. Sequence-specific and phosphorylation-dependent proline isomerization: a potential mitotic regulatory mechanism. Science. 1997;278(5345):1957-60.

Chapter 3

^{1}H, ^{13}C, ^{15}N backbone and sidechain resonance assignments of human R56D, Y61E variant of the IRAK-M death domain

Abstract

Innate immunity provides the first line of defense against bacterial and viral pathogens. Toll-like receptors (TLRs) act as sentinels to detect specific pathogen-associated molecular patterns. TLR stimulation launches signaling cascades that induce type I interferons (IFNs), inhibitory factors and pro-inflammatory cytokines, thereby initiating and regulating innate and adaptive immunity. Loss of proper innate immunity regulation leads to inflammation-related diseases such as asthma. IRAK-M is a known negative regulator of TLR/IL-1R signaling, and is thought to assemble into activated TLR/IL-1R signaling complexes to regulate downstream signaling. The IRAK-M N-terminal death domain (IRAK-M DD) mediates interactions with components of these signaling complexes, yet the specific interaction interfaces have not been experimentally determined. The wild type IRAK-M DD has eluded structure determination due to aggregation of the recombinantly expressed domain. Here, we report the ^{1}H, ^{13}C and ^{15}N backbone and sidechain resonance assignments for a soluble monomeric double-mutant IRAK-M DD (R56D, Y61E) that is well suited for NMR studies. These NMR resonance assignments will enable structural and dynamics studies to investigate the detailed mechanisms by which the IRAK-M DD associates with activated TLR/IL-1R signaling complexes to regulate innate immunity signaling.

Keywords Death domain · IRAK-M · Toll-like receptor · Asthma · Heteronuclear NMR

Biological context

Allergic asthma is the most frequently occurring type of asthma, and is triggered by TLR-mediated detection of signals from extracellular pathogens [1]. TLRs positioned at the surface of epithelial cells and dendritic cells (DCs) detect airborne allergens such as microorganisms, house dust mites, and viral proteins, and upregulate innate immunity signaling cascades through the expression of cytokines that induce inflammation [2, 3]. When production of cytokines is not properly regulated, the resulting inflammation causes contraction of muscles around the airways [4]. TLRs initiate signaling cascades through MyD88 and IL-1R-associated kinase (IRAK) family members that trigger inflammation via NF-κB signaling [5]. There are four members of the IRAK family, namely IRAK1, IRAK2, IRAK-M and IRAK4 [6, 7].

TLR activation leads to receptor dimerization and possibly to higher order receptor clustering, and to the subsequent assembly of a multi-protein signaling complex known as the Myddosome [8]. The x-ray crystal structure of the Myddosome suggests that this signaling complex anchors to the cytoplasmic TIR domains of activated receptors via four MyD88 subunits, and extends into the cytosol through assembly of four IRAK4 subunits onto the MyD88 tetramer, followed by assembly of four IRAK1 or IRAK2 (IRAK1/2) subunits onto the IRAK4 tetramer [9]. The MyD88, IRAK4 and IRAK1/2 homotetramer layers are formed by the death domain of each subunit, generating a hetero-oligomeric death domain scaffold terminated by a tetramer of IRAK1 or IRAK2 death domains [9].

IRAK family members consist of an N-terminal death domain (DD), a linker, a Ser/Thr kinase domain (KD), and an intrinsically disordered C-terminal domain. Associations between different IRAK family members are mediated by intermolecular interactions between their respective DDs [9]. The IRAK family member IRAK-M is a known negative regulator of Toll-like receptor signaling and is essential for normal function of the innate immune system [10]. IRAK-M also is a positive mediator of IL-33 induced inflammation [11]. Consequently, IRAK-M has important implications for asthma. While the IRAK-M DD is implicated in these functions, the detailed mechanisms of these effects are not yet elucidated. It has been proposed that IRAK-M is recruited via its DD to the Myddosome complex to directly block downstream signaling [9]. Alternatively, it has been recently found that IRAK-M induces inhibitory molecules through TLR7 as part of a second wave of signaling in response to endocytosed pathogen [12]. Even though the role of IRAK-M and its DD in Toll-like receptor signaling is well established, the structural mechanisms by which IRAK-M DD regulates TLR signaling are only beginning to be illuminated.

In pursuit of the NMR structure of the IRAK-M DD, we found that the recombinantly expressed domain is not soluble and rapidly aggregates. Based on the hypothesis that aggregation was due to higher order oligomerization, we designed mutations to impart electrostatic repulsion between predicted subunit interfaces, yielding a double mutant (R56D, Y61E) with high solubility as a monomer. As a first step toward structure-function studies of this domain, we present here the backbone and sidechain chemical shift assignments of a 124-residue protein construct in which residues 1-5 represent non-native amino acids resulting from insertion cloning (italicized in Figure 3.1A), and residues 6-124 correspond to native IRAK-M residues 1-119 with mutations R56D and Y61E (Figure 3.1A).

Methods and experiments

Protein expression and purification

The human IRAK-M (IRAK3, NCBI: NM_007199.2)[1-119] gene was inserted into the pMAL-c2X vector with maltose binding protein (MBP) as an N-terminal fusion partner, separated by a Factor XA cleavage site. A vector harboring the R56D and Y61D mutations was made from this vector using a single primer (forward primer, with mutations underlined: 5' AGC AGC TGG CTG GAT GTT GAT CAT ATT GAA AAG GAT GTA GAC CAA GGT AAA AGT G 3') and the BIO RAD-iProof High-Fidelity DNA Polymerase. The resulting expression plasmid, pMAL-c2X, encodes the MBP-IRAK-M[1-119:R56D,Y61D] fusion protein, with a Factor XA cut site between MBP and IRAK-M[1-119:R56D,Y61D]. Further mutagenesis of this vector to change Y61D to Y61E was similarly achieved using a single primer (forward primer, D61E, with mutation underlined: 5' GTT GAT CAT ATT GAA AAG GAG GTA GAC CAA GGT AAA AGT GG 3') and the BIO RAD-iProof High-Fidelity DNA Polymerase to generate expression plasmid pMAL-c2X encoding the MBP-IRAK-M[1-119:R56D,Y61E] fusion protein with a Factor XA cut site between MBP and IRAK-M[1-119:R56D,Y61E]. The MBP-IRAK-M[1-119:R56D,Y61E] vector with Ampicillin resistance was transformed into BL21-Gold(DE3) cells (Agilent Technologies) and screened by Carbenicillin LB-agar plate. A single colony was inoculated to 10ml LB (Luria broth) culture and incubated at 37°C for 8 hours. Cells were collected by gentle centrifugation at 2000g, cells were transferred to 100ml of M9 minimal media with 1g/L of $^{15}NH_4Cl$ as the sole nitrogen source and 4g/L of ^{13}C glucose as a sole carbon source, and incubated at 37°C for 16 hours. The dense cells were transferred to two flasks each containing 1L M9 minimal media (same as 100ml starter culture), and were induced at 0.8 OD_{600} by adding 1mM of final concentration of IPTG at 37°C for 6 hours.

Cells were harvested by centrifugation at 3500g. The cell pellet was dissolved in 40ml of wash buffer (20mM Tris, 200mM NaCl, 1mM EDTA, and 0.2mM TCEP, pH 7.4) with 40mg of lysozyme (Amresco) and 100µl of PI cocktail (Thermo Fisher Scientific, EDTA-free), and incubated 30min on ice. The dissolved cells were sonicated on ice, alternating 1 second sonication and 1 second pause for 1min, for four 1min cycles. Cell debris was removed by centrifugation, the supernatant was incubated with 5 mL of Amylose Resin (New England BioLabs), pre-equilibrated with wash buffer, for 5hours at 4°C. The column was washed with 4 bed volumes of wash buffer, and the fusion protein was eluted with 2 bed volumes of elution buffer (10mM of Maltose added to wash buffer). Eluted fusion protein was dialyzed into Factor Xa cleavage buffer (20 mM Tris-HCl, 100 mM NaCl, 2 mM CaCl2, pH = 8.0). Factor Xa Protease (New England BioLabs) was added (100ul of 1ug/ul to 20ml of fusion protein) and the solution was gently rocked at room temperature for overnight. The cleaved proteins were concentrated to 2ml and loaded onto a size exclusion FPLC column (GE Superdex^{TM} 75 prep grade), and run with FPLC buffer (10mM Tris, 20mM NaCl, and 0.2mM TCEP, pH 8.0). Eluted fractions of IRAKM[1-119:R56D,Y61E] were collected, pooled and concentrated. The pH was adjusted to 6.7 using 0.1M HCl, and total concentration of 5mM of TCEP and 5mM of NaN3 was added. IRAK-M[1-119:R56D,Y61E] concentration was measured by UV absorption at 280 nm (extinction coefficient = 25105 cm-1 M-1), and final concentration was 800µM in 300µL.

NMR spectroscopy

All NMR spectra were recorded at 25°C on a Varian Inova 600MHz spectrometer equipped with a $^{1}H/^{13}C/^{15}N$ triple resonance probe with Z-axis gradient. A uniformly ^{15}N-labeled IRAK-M[1-119:R56D,Y61E] sample was used to collect 2D ^{15}N-^{1}H HSQC spectra and 3D ^{1}H-

^{15}N NOESY and ^{1}H-^{15}N TOCSY spectra. A uniformly ^{13}C/^{15}N-labeled sample was used to collect 2D ^{1}H-^{15}N HSQC spectra and 3D HNCA, HN(CO)CA, HNCO, HN(CA)CO, CBCANH, CBCA(CO)NH, H(CCO)NH, C(CO)NH, HCCH-TOCSY, ^{1}H-^{13}C aliphatic NOESY, and ^{1}H-^{13}C aromatic NOESY spectra. Backbone assignments were obtained from ^{1}H-^{15}N HSQC, ^{1}H-^{15}N NOESY, ^{1}H-^{15}N TOCSY, HNCA, HN(CO)CA, HNCO, HN(CA)CO, CBCANH, CBCA(CO)NH, H(CCO)NH, C(CO)NH, and HCCH-TOCSY spectra. Aromatic ring resonances were assigned using the 2D ^{1}H-^{15}N NOESY, 3D ^{1}H-^{13}C aliphatic NOESY, and 3D ^{1}H-^{13}C aromatic NOESY spectra. Carbonyl resonances were assigned using a HNCO spectrum. Assignments were determined using PINE [13] imbedded in NMRFAM-SPARKY [14-16], followed by human adjustments.

Assignments and secondary structure

Backbone assignments are complete except for S55, numbered according to protein construct (Figure 3.1A, red numbering). The assigned ^{15}N-^{1}H-HSQC spectrum (Figure 3.1B) also uses the numbering scheme of the full construct. Backbone assignments are 97% complete, and sidechain assignments 85% complete. 87% of overall assignments are complete. These backbone and sidechain chemical shift assignments have been deposited in the BioMagResBank (http://www.bmrb.wisc.edu/) with accession number 30237. PECAN embedded in PINE provided secondary structure predictions based on the NMR chemical shift assignments for the IRAK-M DD sequence [17]. IRAK-M[1-119:R56D,Y61E] is predicted to consist of 6 α-helices and connecting loops (Figure 3.2), in good agreement with other known death domain structures such as IRAK2 DD and IRAK4 DD [9]. In future work these chemical shift assignments will be used to study the mechanisms by which IRAK-M carries out its varied regulatory roles in

innate immunity signaling.

Acknowledgements

We express sincere appreciation for Woonghee Lee's assistance with running NMRFAM software. This work was supported by the National Science Foundation grant MCB-1615350 (LKN) and by the National Institutes of Health grant 1R01-HL111430 (KPL).

A

```
          1         10         20         30         40         50         60
          |   10    |    20    |    30    |    40    |    50    |    60    |
SEFGS MAGNCGARGA LSAHTLLFDL PPALLGELCA VLDSCDGALG WRGLAERLSS SWLDVDHIEK

          70         80         90        100        110        119
      70  |    80    |    90    |   100    |   100    |   100    |
EVDQGKSGTR ELLWSWAQKN KTIGDLLQVL QEMGHRRAIH LITNYGAVLS PSEKSYQEG
```

B

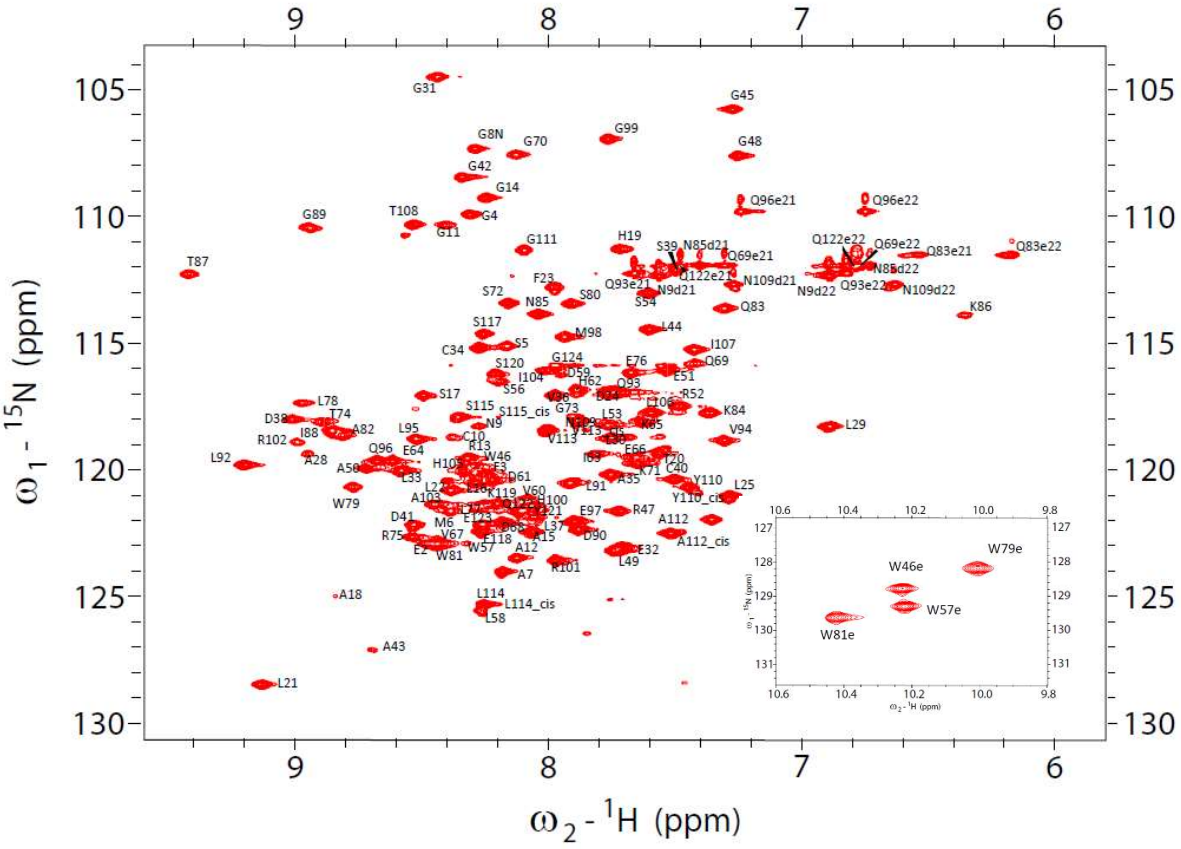

Figure 3.1 a. Primary sequence of IRAKM[1-119:R56D,Y61E], with numbering corresponding to native IRAK-M (black) and protein construct numbering (red). b. ^{1}H-^{15}N HSQC spectrum of ^{13}C/^{15}N-IRAKM[1-119:R56D,Y61E], with peak assignments labeled according to protein construct numbering (consistent with numbering of BioMagResBank accession number 30237). The inset shows the tryptophan indole region of the spectrum.

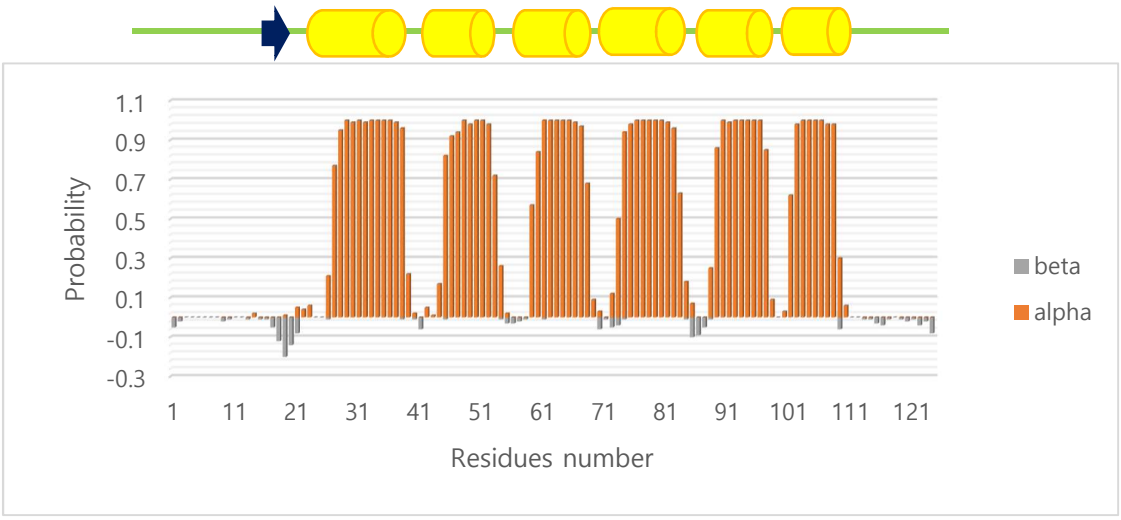

Figure 3.2 Secondary structure prediction for IRAK-M[1-119:R56D,Y61E] by PECAN [17] in PINE [13], based on chemical shift and amino acid sequence for predicting low energy conformation. Positive probability indicates α-helix and negative probability indicates β-strand.

References

1. Barnes, P.J., *Immunology of asthma and chronic obstructive pulmonary disease.* Nat Rev Immunol, 2008. **8**(3): p. 183-92.
2. Akira, S., S. Uematsu, and O. Takeuchi, *Pathogen recognition and innate immunity.* Cell, 2006. **124**(4): p. 783-801.
3. Galli, S.J., M. Tsai, and A.M. Piliponsky, *The development of allergic inflammation.* Nature, 2008. **454**(7203): p. 445-54.
4. Trompette, A., et al., *Allergenicity resulting from functional mimicry of a Toll-like receptor complex protein.* Nature, 2009. **457**(7229): p. 585-8.
5. Kawai, T. and S. Akira, *Signaling to NF-kappaB by Toll-like receptors.* Trends Mol Med, 2007. **13**(11): p. 460-9.
6. Cao, Z., W.J. Henzel, and X. Gao, *IRAK: a kinase associated with the interleukin-1 receptor.* Science, 1996. **271**(5252): p. 1128-31.
7. Li, S., et al., *IRAK-4: a novel member of the IRAK family with the properties of an IRAK-kinase.* Proc Natl Acad Sci U S A, 2002. **99**(8): p. 5567-72.
8. Gay, N.J., et al., *Assembly and localization of Toll-like receptor signalling complexes.* Nat Rev Immunol, 2014. **14**(8): p. 546-58.
9. Lin, S.C., Y.C. Lo, and H. Wu, *Helical assembly in the MyD88-IRAK4-IRAK2 complex in TLR/IL-1R signalling.* Nature, 2010. **465**(7300): p. 885-90.
10. Kobayashi, K., et al., *IRAK-M is a negative regulator of Toll-like receptor signaling.* Cell, 2002. **110**(2): p. 191-202.
11. Nechama, M., et al., *The IL-33-PIN1-IRAK-M axis is critical for type 2 immunity in IL-33-induced allergic airway inflammation.* Nature Communications, 2018. **9**(1): p. 1603.

12. Zhou, H., et al., *IRAK-M mediates Toll-like receptor/IL-1R-induced NFkappaB activation and cytokine production.* EMBO J, 2013. **32**(4): p. 583-96.

13. Bahrami, A., et al., *Probabilistic interaction network of evidence algorithm and its application to complete labeling of peak lists from protein NMR spectroscopy.* PLoS Comput Biol, 2009. **5**(3): p. e1000307.

14. Lee, W., et al., *Integrative NMR for biomolecular research.* J Biomol NMR, 2016. **64**(4): p. 307-32.

15. Lee, W., M. Tonelli, and J.L. Markley, *NMRFAM-SPARKY: enhanced software for biomolecular NMR spectroscopy.* Bioinformatics, 2015. **31**(8): p. 1325-7.

16. Lee, W., et al., *PINE-SPARKY: graphical interface for evaluating automated probabilistic peak assignments in protein NMR spectroscopy.* Bioinformatics, 2009. **25**(16): p. 2085-7.

17. Eghbalnia, H.R., et al., *Protein energetic conformational analysis from NMR chemical shifts (PECAN) and its use in determining secondary structural elements.* J Biomol NMR, 2005. **32**(1): p. 71-81.

Chapter Four

IRAKM death domain structure determination and insights from simulations of docking to the Myddosome

Abstract

Asthma is a chronic inflammatory sickness of the airways caused by environmental and genetic factors. The mechanisms of activation of innate immunity signaling pathways that cause asthma are not fully understood yet. This study investigated novel targets for the development of new asthma therapeutics, with a specific focus on IRAKM that is a negative regulator within the context of Toll-Like Receptor (TLR) signaling. Toll-Like Receptors recognize specific molecular markers that are present in microbial components, and transfer these signals through their intracellular TIR domains to MyD88 and IRAK family members that assemble into an activated signaling complex inside the cell. Assembly of IRAK-M into the TLR signaling complex is mediated by its N-terminal death domain (DD). Oligomerization is a hallmark of DDs. The wild-type IRAKM-DD has eluded structure determination due to aggregation. Here, we solved the solution NMR structure of a double-mutant IRAKM-DD (R56D, Y61E) that is a highly soluble monomer well suited for NMR studies. This experimentally determined structure was used in simulations to investigate possible docking of IRAK-M DD into the activated TLR signaling complex as well as with multiple IRAK family members and oligomers. Based on these docking studies, a mechanistic model is proposed for IRAKM regulation of IRAK1-mediated TLR signaling.

Introduction

Innate immunity is an essential first line of defense against invasion by pathogens [1]. This rapid, built-in immune response is initiated by stimulation of Toll-like receptors (TLRs), a family of inherited transmembrane proteins that act as sentinels to detect the presence of viral, bacterial and fungal pathogens [2]. TLRs recognize molecular signals distinct to pathogens, such as flagellin, double-stranded RNA, and lipopolysaccharides [3-5]. TLR stimulation launches signaling cascades that induce type I interferons (IFNs), inhibitory factors and pro-inflammatory cytokines, thereby initiating and regulating innate and adaptive immunity (REFS). Pro-inflammatory cytokines include interleukin-1β (IL-1β), IL-18 and IL-33, whose cognate receptors are members of the interleukin-1 receptor (IL-1R) family [6]. Stimulation of IL-1Rs further amplifies the immune response and induces inflammation, highlighting the need for tight regulation of not only IL-1R signaling, but also of the initiating TLR signaling pathways [7].

The TLR and IL-1R families are part of the IL-1R/TLR superfamily, classified on the basis of possession of a Toll/IL-1 receptor (TIR) domain responsible for their downstream intracellular signaling [6, 8]. Intracellular signaling by TLRs (except TLR3) and by the specific IL-1Rs stimulated by IL-1β, IL-18 or IL-33 involves a shared set of proteins that are recruited to the TIR domains of the activated receptors to form a multiprotein signaling complex known as the Myddosome (Figure 4.1) [9]. These shared components include the adaptor protein MyD88, which based on possession of its own TIR domain is classified in the IL-1R/TLR superfamily [6, 9]. MyD88 also possesses a death domain (DD), which is a modular α–helical oligomerization domain essential for formation of activated signaling complexes that mediate downstream signaling [10-12]. Shared components of this class of intracellular signaling also include the interleukin-1-receptor associated kinase (IRAK) family of proteins, which in the vertebrate

genome include 4 members: IRAK1, IRAK2, IRAK-M, and IRAK4 [4-8, 13]. IRAK family members are important mediators of the TLR/IL-1R signaling pathways. Each IRAK family member contains two folded domains (a death domain and a serine/threonine kinase domain) separated by a linker region unique to each member, and a C-terminal region. The kinase domains of all but IRAKM (whose kinase domain is inactive) participate in phosphorylation-mediated signaling events [14-18].

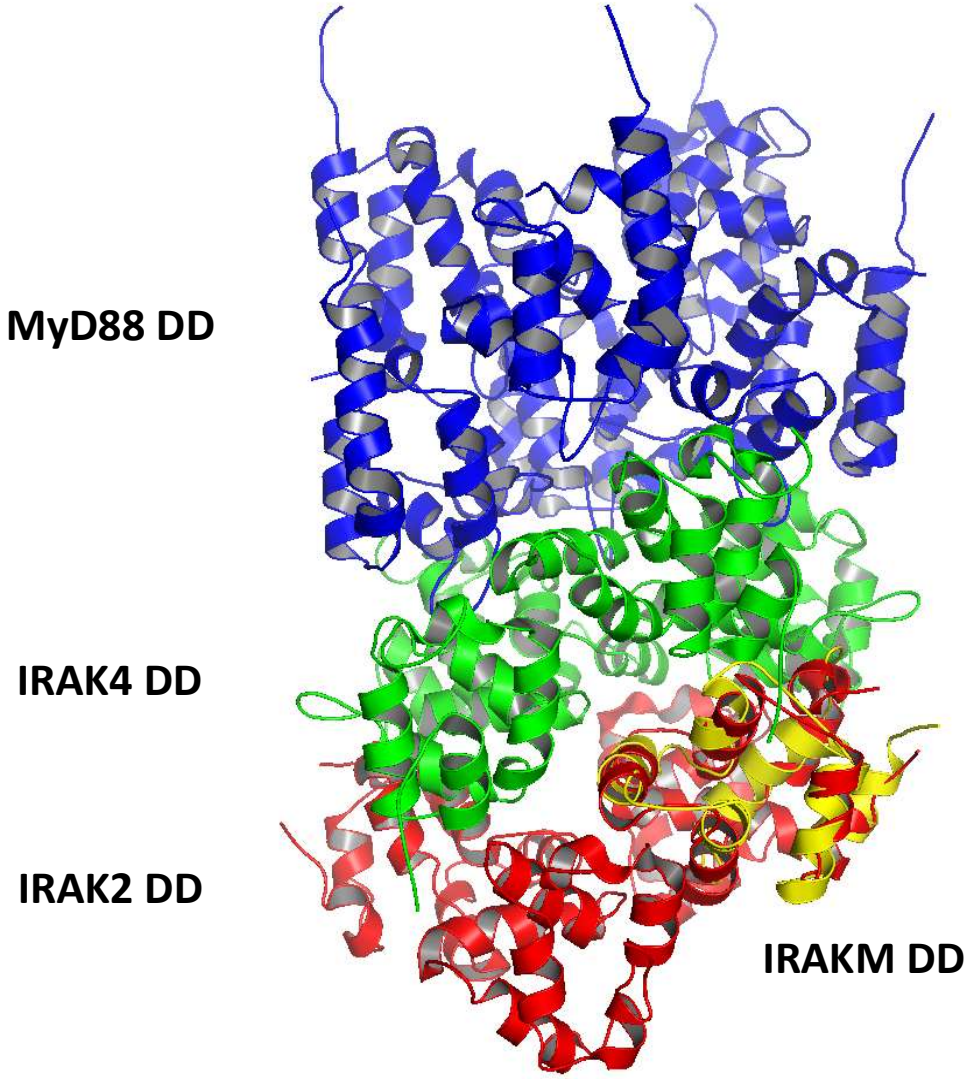

Figure 4.1. Crystal structure of Myddosome complex with aligned IRAKM DD

IRAK-M is a known negative regulator of Toll-like receptor signaling [9, 10]. Expressed in lung epithelial cells [13] and in monocytes and macrophages [11], IRAK-M represses TLR signaling in three ways (Figure 4.2). First, IRAK-M associates with IRAK1 to prevent IRAK1 dissociation from Mydossome complexes and to prevent the formation of downstream IRAK1-TRAF6 signaling complexes [1, 5]. In support of this negative regulatory model, Kobayashi (2002) showed that IRAK1-TRAF6 complex formation was inhibited by IRAK-M expression in the 293T cell model [4]. Second, it has been recently found that IRAK-M induces inhibitory molecules through TLR7 as part of a MEKK3-mediated second wave of signaling in response to endocytosed pathogen [12]. Previous modeling studies have proposed that IRAK-M interacts with MyD88-IRAK4 to mediate the MEKK3 dependent pathway, where IRAK-M serves as an intermediate signaling component to transmit signaling upon TLR activation [12]. These modeling studies also suggested that IRAK-M specifically interacts with IRAK-2, but not with IRAK-1, and suppresses IRAK-2 mediated translation of cytokines and chemokines [12]. Third, IRAK-M has been shown to inhibit the IRAK2-mediated TLR signaling pathway that stabilizes specific mRNAs to promote cytokine and chemokine production [3]. Hence, by either blocking or promoting signaling, IRAK-M plays key roles in negative regulation of TLR signaling.

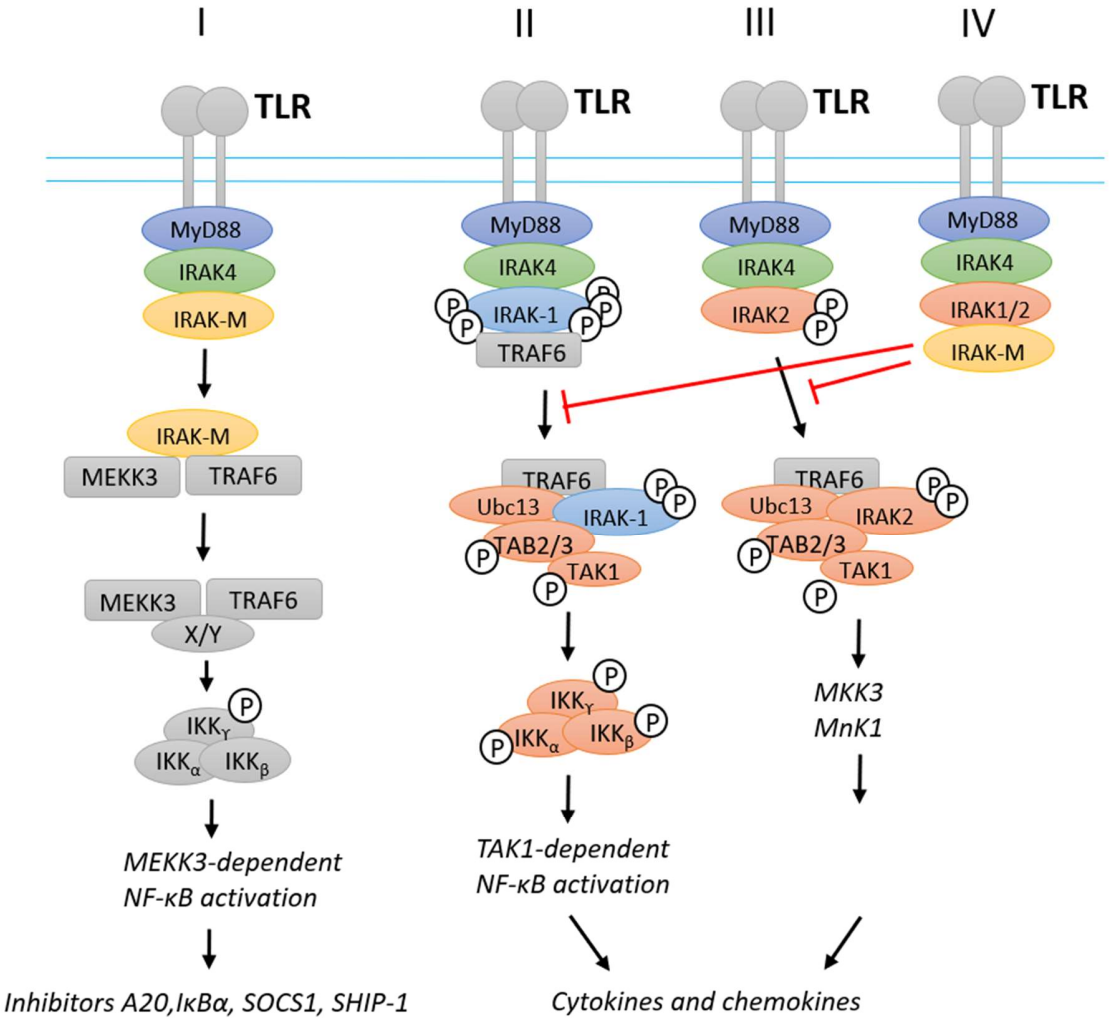

Figure 4.2. Literature-based model for the regulatory role of IRAK-M in TLR signaling (adapted from Figure.8 on, Hao Zhou et al, EMBO, (2013)). Double blue lines represent the plasma membrane, black arrows indicate promotion of or flow to the indicated state or consequence, and red lines terminated with a "T" indicate inhibition of the indicated step or process. Encircled "P" indicates phosphorylated site(s). Standard UniProt abbreviations are used for all proteins. "X/Y" denotes intermediate involved molecules.

Although its major function appears to be repressive, activation of NF-kB by IRAK-M when both IRAK1 and IRAK2 were eliminated has also been reported [14, 15]. Overexpression of IRAK-M in HEK293 cells activates NF-kB, and this effect is dependent on the IRAK-M N-terminal DD [31]. In support of specific activation roles of IRAK-M, through collaboration we have identified IRAK-M as a novel Pin1 target critical for IL-33 signaling in type 2 (TH2) allergic response associated with asthma. Briefly, Pin1 is activated in IL-33-induced airway inflammation. Notably, IRAK-M is phosphorylated at its S115-P site by IRAK1 upon IL-33 treatment, which induces asthma, and phosphorylated IRAK-M is immune-precipitated by Pin1 antibody [15]. Pin1 binding and isomerization of the pS115-P motif increases IRAK-M nuclear translocation and protein stability that correlates with increased expression of a set of pro-inflammatroy cytokines that induce inflammation. In addition, treatment of mouse models with ATRA (a Pin1 inhibitor) or genetic ablation of Pin1 or IRAK-M reduce TH2 polarization, dendritic cell (DC) activation and overall lung inflammation upon IL-33 challenge. These results were correlated with molecular features of asthma in humans by analyzing samples obtained from asthmatic patients challenged with Derp1 (a major allergen of house dust mites), where Pin1 activation and IRAK-M levels were increased, and expression of the IRAK-M downstream pro-inflammatroy cytokines were increased [15].

The death domains of IRAK family members are central players in mediating signaling and regulatory interactions, which is exemplefied by the Myddosome structure [9]. These domains are rich in hydrophobic amino acid side chains such as leucine, isoleucine, and tryptophan, and in charged amino acid residues such as negatively charged aspartic acid and glutamic acid, and positively charged arginine (Chapter one. Figure 1.4). The DDs of IRAK family members have 30 to 39% pairwise similarity (Chapter one. Figure 1.5). The crystal

structure of the Myddosome complex, composed of six MyD88 DD, four IRAK4 DD, and four IRAK2 DD assembled into a left-handed helical oligomer (Figure 4.1), revealed packing interactions involved in hetero- and homo-subunit interactions [8]. Notably, although the DDs of MyD88, IRAK4, and IRAK2 have highly similar structures in this complex, the variation in DD surface residues between the different proteins enables the sequential and specific assembly of the complex. Importantly, the structure of the IRAK-M DD had not yet been reported.

In this study, we investigated the structure and interactions of the IRAK-M DD by NMR spectroscopy and docking simulations, respectively. Since we found that the wild-type IRAKM-DD is of very limited solubility, mutagenesis was applied to identify a double mutant (R56E,Y61D) that adopts the same fold as wild type, is highly soluble, and is highly amenable to solution NMR analysis. The high-resolution NMR structure of IRAKM-DD(R56E,Y61D) was determined, confirming the expected DD fold and providing important information regarding surface-exposed residues. This structure was used to construct a model of wild type IRAK-M DD that was then used to simulate interactions of this domain with the DDs of other IRAK family members, individually and in the context of the Myddosome structure. The elucidated IRAKM-DD structure, together with the docking results, suggest a mechanism by which IRAM-M could negatively regulate IRAK1-mediated pro-inflammatory signaling, and by which Pin1 could regulate this process.

Materials and Methods

Plasmid Construction

To construct the expression vector for IRAKM-DD, the pMAL-c2X parent vector with Ampicillin resistance was used. The pMAL-c2X vector contains the tac promoter and lacI, enabling protein expression level to be controlled by IPTG concentration. This vector codes for the Maltose Binding Protein (MBP), and allows for insertion of a desired gene that will be expressed as a fusion partner C-terminal to MBP. The restriction site NdeI is 5' to the MBP gene. Restriction sites SacI, EcoRI, BamHI, XbaI, SalI, OstI and HindII are located 3' to the MBP gene. Plasmids used are described in detail in Appendix 1.

The IRAKM DD gene was PCR-amplified from clone hIRAKM (IRAK3, NCBI: NM_007199.2) using the forward primer with BamHI, 5' act gat gga tcc atg gcg ggg aac tgt ggg gcc cgc ggc gcg 3', and the backward primer with HindIII, 5' gac agt aag ctt tca acc ttc ctg ata act ctt ctc tga agg 3'. The BamHI and HindIII restriction sites were used to cut the PCR insert and pMAL-c2X plasmid, and the resulting PCR product and vector pMAL-c2X were ligated using sticky ends to yield the pMAL-c2X_IRAKM[1-119] plasmid that expresses MBP fused to IRAKM residues 1–119.

The R56D and Y61D mutations in IRAKM were achieved using the pMAL-c2X_IRAKM[1-119] vector. PCR amplification and mutagenesis were performed using BIO RAD-iProof High-Fidelity DNA Polymerase with forward primer 5' agc agc tgg ctg gat gtt gat cat att gaa aag gat gta gac caa ggt aaa agt g 3'and backward primer 5' c act ttt acc ttg gtc tac atc ctt ttc aat atg atc aac atc cag cca gct gct 3' to generate the expression plasmid pMAL-c2X _IRAKM[1-119:R56D,Y61D].

The R56D and Y61E mutations were achieved using the pMAL-c2X-IRAKM[1-

119:R56D,Y61D] vector, with a single primer (forward primer, D61E, with mutation underlined: 5’ GTT GAT CAT ATT GAA AAG GAG GTA GAC CAA GGT AAA AGT GG 3’). Mutagenesis was performed using BIO-RAD-iProof High-Fidelity DNA Polymerase with 15 seconds annealing at 65°C and 2 minutes 30 seconds extension at 72°C for 30 cycles. The resulting expression plasmid, pMAL-c2X-IRAKM[1-119:R56D,Y61E], encodes the MBP-IRAKM[1-119:R56D,Y61E] fusion protein, with a Factor XA cut site between MBP and IRAKM[1-119:R56D,Y61E].

Protein expression and purification

The pMAL-c2X-IRAKM[1-119:R56D,Y61E] vector with Ampicillin resistance was transformed into BL21-Gold(DE3) cells (Agilent Technologies) and screened by Carbenicillin LB-agar plate. A single colony was inoculated to 10ml LB (Luria broth) culture and incubated at 37°C for 8 hours. Cells were collected by centrifugation at 2000g as gentle condition, and cells were transferred to 100ml of M9 minimal media with 1g/L of 15NH4Cl as the sole nitrogen source and 4g/L of 13C glucose as a sole carbon source and incubated at 37°C for 16 hours. The dense cells were transferred to two of 1L M9 minimal media same as a 100ml starter culture and were induced at 0.8 OD600 by adding 1mM of a final concentration of IPTG at 37°C for 6 hours.

Cells were harvested by centrifugation at 3500g. The cell pellet was dissolved in 40ml of wash buffer (20mM Tris, 200mM NaCl, 1mM EDTA, and 0.2mM TCEP, pH 7.4) with 40mg of lysozyme (amresco) and 100µl of PI cocktail (Thermo,EDTA-free), and incubated 30min on the ice. The dissolved cells were sonicated on ice, 1 second sonication and 1 second pause for 1min, four cycles. Cell debris was removed by centrifugation, the supernatant was incubated with 5 mL of Amylose Resin (BioLabs), pre-equilibrated with wash buffer, for 5hours at 4°C. The column was washed with 4 bed volumes of wash buffer, and the fusion protein was eluted with 2 bed

volumes of elution buffer (10mM of Maltose added to wash buffer). Eluted fusion protein was dialyzed into Factor Xa cleavage buffer (20 mM Tris-HCl, 100 mM NaCl, 2 mM CaCl2, pH = 8.0). Factor Xa Protease (NEW ENGLAND BioLabs) was added (100ul of 1ug/ul to 20ml of the fusion protein) and the solution was gently rocked at room temperature for overnight. The cleaved proteins were concentrated to 2ml and loaded onto a size exclusion FPLC column (GE SuperdexTM 75 pg), and run with FPLC buffer (10mM Tris, 20mM NaCl, and 0.2mM TCEP, pH 8.0). Eluted fractions of IRAKM[1-119:R56D,Y61E] were collected, pooled and concentrated. The pH was adjusted to 6.67 using 0.1M HCl, and the total concentration of 5mM of TCEP and 5mM of NaN3 was added. IRAKM[1-119:R56D,Y61E] concentration was measured by UV absorption at 280 nm (extinction coefficient = 25105 cm-1 M-1), and final concentration was 800µM in 300µL.

NMR spectroscopy

All NMR spectra were recorded at 25°C on a Varian Inova 600MHz spectrometer equipped with a 1H/13C/15N triple resonance probe with Z-axis gradient. For structure determination, two and three dimensional NMR spectra were acquired as described in Chapter 3, using the experimental parameters summarized in Table 4.1.

Table 4.1. NMR parameters

	NT(H)	Ni(C)	Ni(N)	SW(H)	SW(C)	SW(N)	OBS(H)	OBS(C)	OBS(N)	CAR(H)	CAR(C)	CAR(N)
NHSQC	2048	-	512	8000	-	2000	599.357	-	60.739	4.773	-	118.733
CHSQC	2048	512	-	8000	21102.69	-	599.357	150.713	-	4.773	70.026	-
HNCA	2048	128	128	8000	4522	2000	599.357	150.716	60.739	4.773	56.128	118.733
HNCACO	2048	128	128	8000	3770.1	2000	599.357	150.716	60.739	4.773	174.122	118.733
HNCO	2048	128	128	8000	3770.1	2000	599.357	150.733	60.739	4.773	174.122	118.733
HNCOCA	2048	128	128	8000	4522	2000	599.357	150.716	60.739	4.773	56.128	118.733
CCONH	2048	256	64	8000	12057.14	2000	599.357	150.714	60.739	4.773	46.128	118.733
CBCACONH	2048	128	128	8000	12058.68	2000	599.357	150.714	60.739	4.773	46.128	118.733
CBCANH	2048	128	128	8000	12057.14	2000	599.357	150.714	60.739	4.773	46.128	118.733
HCCHTOCSY	2048	128	256(H)	8000	12059.09	8000(H)	599.357	150.714	599.357(H)	4.773	43.127	4.773(H)
CNOESY_Aliph	2048	128	256(H)	8000	12059.09	8000(H)	599.357	150.714	599.357(H)	4.773	43.127	4.773(H)
CNOESY_AROM	2048	128	128(H)	8000	12059.09	8000(H)	599.357	150.714	99.357(H)	4.773	124	4.773(H)
CCHTOCSY	2048	128	128	8000	12059.09	12058.42 (C)	599.357	150.709	150.709(C)	4.773	35.128	35.128(C)

SW - Spectral Width (Hz), **OBS -** Observe Freq (MHz)**, CAR** - Center Position (PPM)

Solving protein structure by NMR

The chemical shifts that were determined as described in Chapter 3 (BioMagResBank-http://www.bmrb.wisc.edu/, accession number 26941), along with 3D 1H-15N NOESY, 3D 1H-13C aliphatic NOESY, and 3D 1H-13C aromatic NOESY were used for solving the IRAKM[1-119:R56D,Y61E] structure. We submitted the chemical shifts and three sets of raw NOESY spectra in '.ucsf' format to Ponderosa Client. Ponderosa Client is an online tool for submitting input to the Ponderosa Server (http://ponderosa.nmrfam.wisc.edu/), an automated NOE assignment and structure determination tool. Once Ponderosa Server completes the calculations, Ponderosa produces and sends a zip file that contains NOE information with initial structures. The files from Ponderosa server were analyzed using Ponderosa Analyzer to validate and refine the structure. The Blacklist/Whitelist were built by checking the structure (Pymol) and NOE peaks (NMR spectra) and resubmitting the data several times to Ponderosa Client (Figure 4.3). Blacklist and Whitelist are graphical weighting factors of inter-residue contacts. Before every resubmission of the data for refinement, the limits for distance and angle constraints were carefully removed or reset (Figure 4.4). The structure determination process requires the following steps for submitting data to Ponderosa Client: 1) Ponderosa refinement, 2) Ponderosa-X refinement, 3) Constraints only-X, 4-a) Constraints only-X for final step with implicit solvation, and 4-b) Constraints only-X for final step with explicit solvation. Ponderosa refinement (step 1) uses CYANA automation, and the rest of the steps use XPLOR-NIH [20-23].

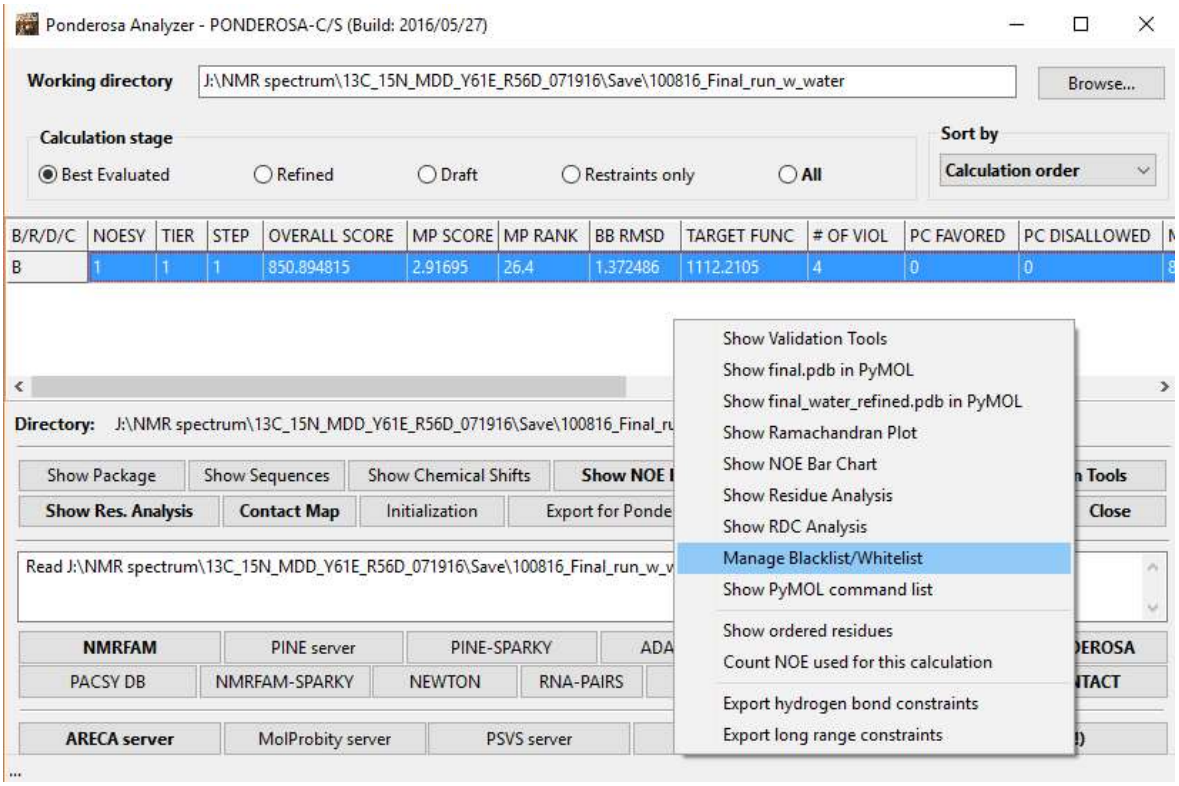

Figure 4.3. Ponderosa Analyzer

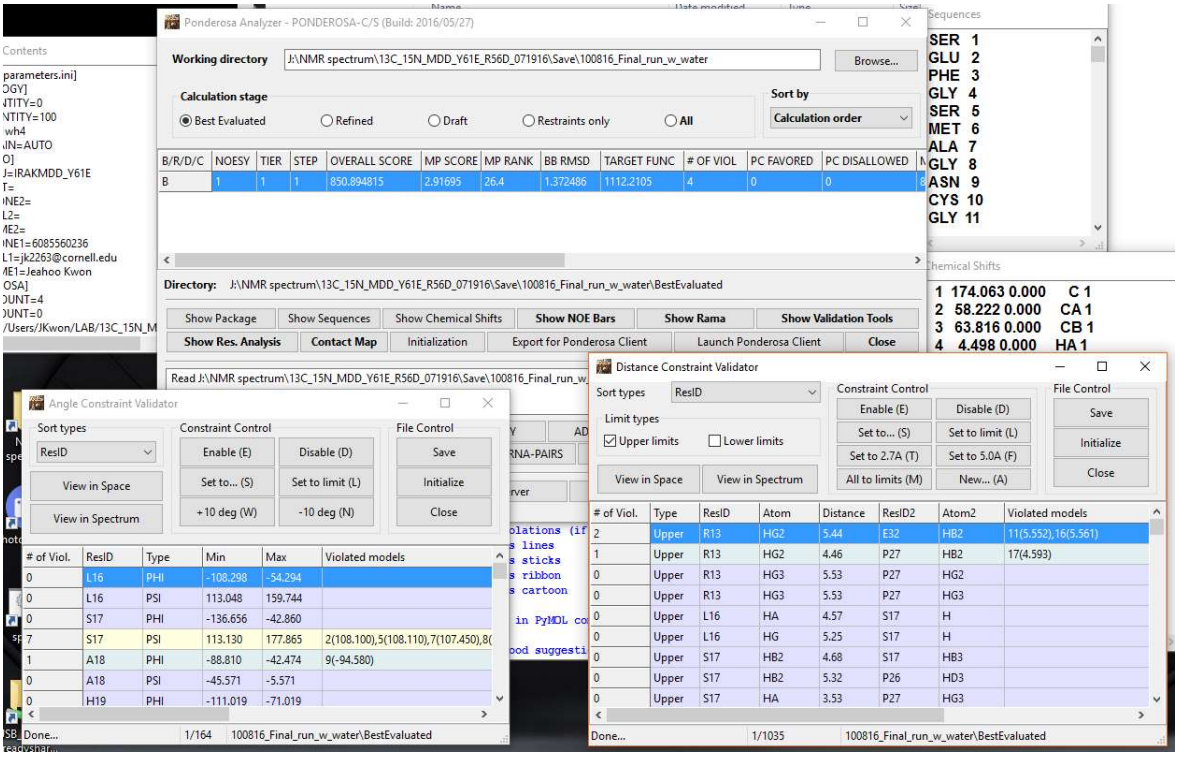

Figure 4.4. Ponderosa analyzer validator tools.

Protein docking simulations

Docking simulations were performed using the protein docking prediction server ClusPro (https://cluspro.bu.edu/home.php). ClusPro can simulate protein docking of oligomer forms, which was essential for the studies performed here 40-41 [24-27]. ClusPro employs PIPER, an FFT-based docking program that uses a pairwise interaction potential as part of its scoring function that combined Eatt (attraction), Erep (repulsive), Eelec (electrostatic energy), and EDARS (Decoys As the Reference State) [30].

$$E = 0.40E_{rep} + -0.40E_{att} + 600E_{elec} + 1.00E_{DARS}$$

For docking of IRAK-M DD into a Myddosome containing IRAK1, SwissModel was

used to build a homology model of the IRAK-1 DD using IRAK2 DD subunits L, M and N in the 3MOP structure as templates, and three copies of the resulting homology model were aligned with the L, M and N IRAK2 subunits in the Myddosome complex (3MOP) to generate a Myddosome model with three IRAK-1 DD subunits and an empty space at the K subunit position. IRAK-M was docked with this modified oligomer (composed of six MyD88, four IRAK4 and three IRAK1 DD subunits) using ClusPro. For docking of IRAK-M DD into a Myddosome containing IRAK2, the K subunit of IRAK2 was removed from the Myddosome structure, and docking of IRAK-M DD to this complex (composed of six MyD88, four IRAK4 and three IRAK2 DD subunits) was simulated using ClusPro.

Root mean square deviation (RMSD) calculations.

The PDB files that were evaluated structural differences were opened in SwissPdbView. The structures were aligned with dominated regions using <Fit> column. Each structural differences were calculated using <Calculated RMS> at <Fit> column. Average RMSD were calculated for each molecule $\sum_{i=1}^{n} RMS(i)/_{n}$ and Mean global RMSD were calculated $\sum_{i=1}^{n} Average\ RMSD(i)/_{n}$

Results

NMR study of wild type IRAKM-DD is limited.

The wild type (WT) IRAKM-DD was expressed with maltose binding protein (MBP) as a solubility-enhancement tag [31]. When cleaved from MBP, IRAKM-DD rapidly precipitated in all buffer conditions explored. While the larger 42 kDa MBP does not give rise to observed peaks in the standard 15N-1H HSQC spectrum, a smaller fusion partner can be selectively detected by NMR if tethered to MBP by a sufficiently long linker that allows independent rotational diffusion [Reference MBP-ubiquitin paper]. Indeed, the 15N-1H HSQC spectrum of 180 uM 15N-labeled MBP-IRAKMDD (59 kDa) shows a well-dispersed set of peaks indicative of a folded protein of approximately 100 residues that are not observed in the corresponding spectrum of 15N-labeled MBP alone (Figure 4.5, overlay of 183 uM fusion, MBP alone). Concentration of MBP-IRAKMDD to 480 uM significantly broadened peaks in the 15N-1H HSQC spectrum but sequential dilution (330, 230 150, 91 uM) progressively narrowed the peaks, suggesting reversible oligomerization. Due to the insolubility of cleaved IRAKM-DD and the low fusion protein concentration required for obtaining high quality NMR data, mutagenesis was pursued to inhibit oligomerization and enhance solubility of the IRAKM-DD monomer.

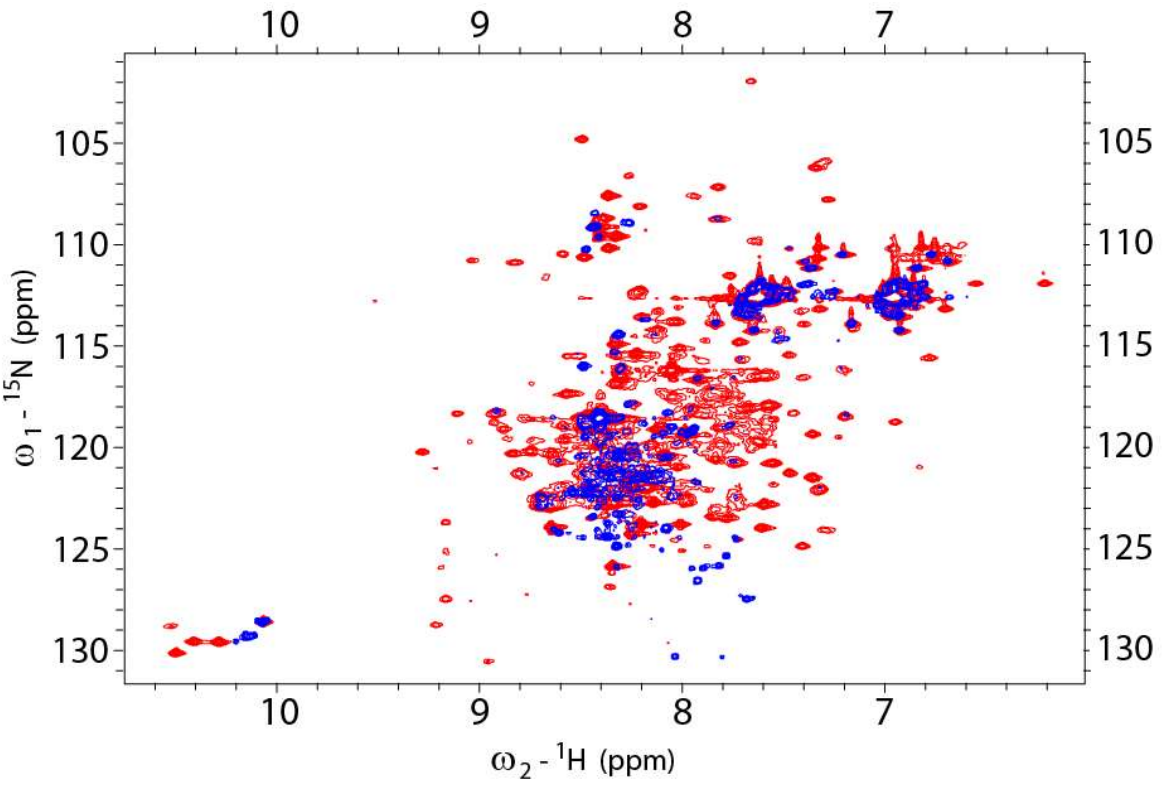

Figure 4.5. The overlay the 15N-1H HSQC spectrum of 180 uM 15N-labeled MBP-IRAKMDD (Red) and 136uM MBP alone (Blue).

Double mutant IRAKM-DD(R56D,Y61E) is highly amenable to NMR studies.

To visualize potential interface residues in the IRAK-M death domain that could be altered to inhibit oligomerization, a homology model was constructed based on the IRAK-2 death domain in the multiprotein oligomeric Myddosome structure [10]. Substitution of each of the four IRAK-2 subunits in the Myddosome structure with an IRAKM-DD homology model suggested a key intermolecular salt bridge involving R56 and a potential aromatic network involving Y61. To inhibit these putative interactions through electrostatic repulsion, the R56D and Y61E mutations were incorporated into the MBP-IRAKM[1–119] expression vector,

yielding a soluble fusion protein. Cleavage of this MBP- IRAKM[1–119:R56D,Y61E] fusion protein yielded soluble IRAKM[1–119:R56D,Y61E] monomer, ascertained by size exclusion chromatography. The 1H-15N HSQC spectrum of 15N-IRAK-M[1–119:R56D,Y61E] shows well-dispersed peaks, indicating that the domain is folded (Figure 4.6). Notably, this spectrum overlays peak-for-peak (with only a few exceptions) with the MBP-wild-type IRAKM-DD spectrum (Figure 4.7), suggesting that the double mutant retains the native WT fold. The backbone (97%) and sidechain (85%) assignments were determined for IRAKM[1–119:R56D,Y61E] and are deposited at the BioMagResBank (http://www.bmrb.wisc.edu/, accession number 26941). This folded monomeric IRAKM[1–119:R56D,Y61E] mutant was used for high resolution structure determination.

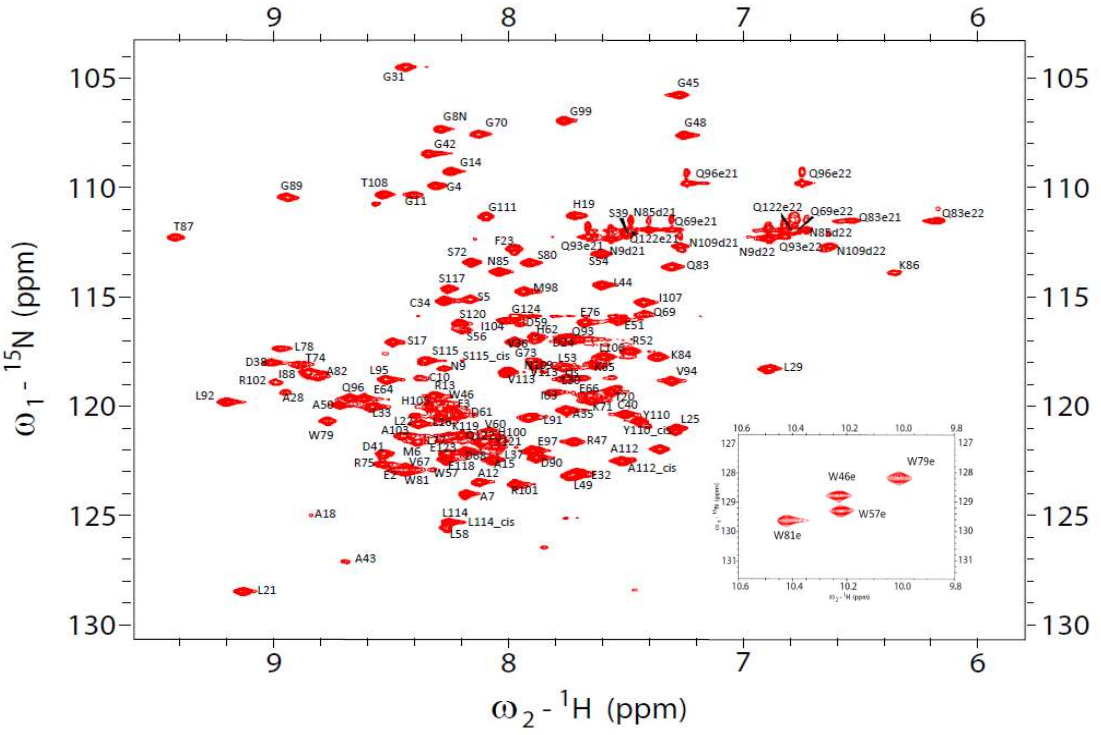

Figure 4.6. 2D ^{1}H-^{15}N HSQC spectrum of uniformly 13C/15N labeled IRAKM[1-119:R56D,Y61E]

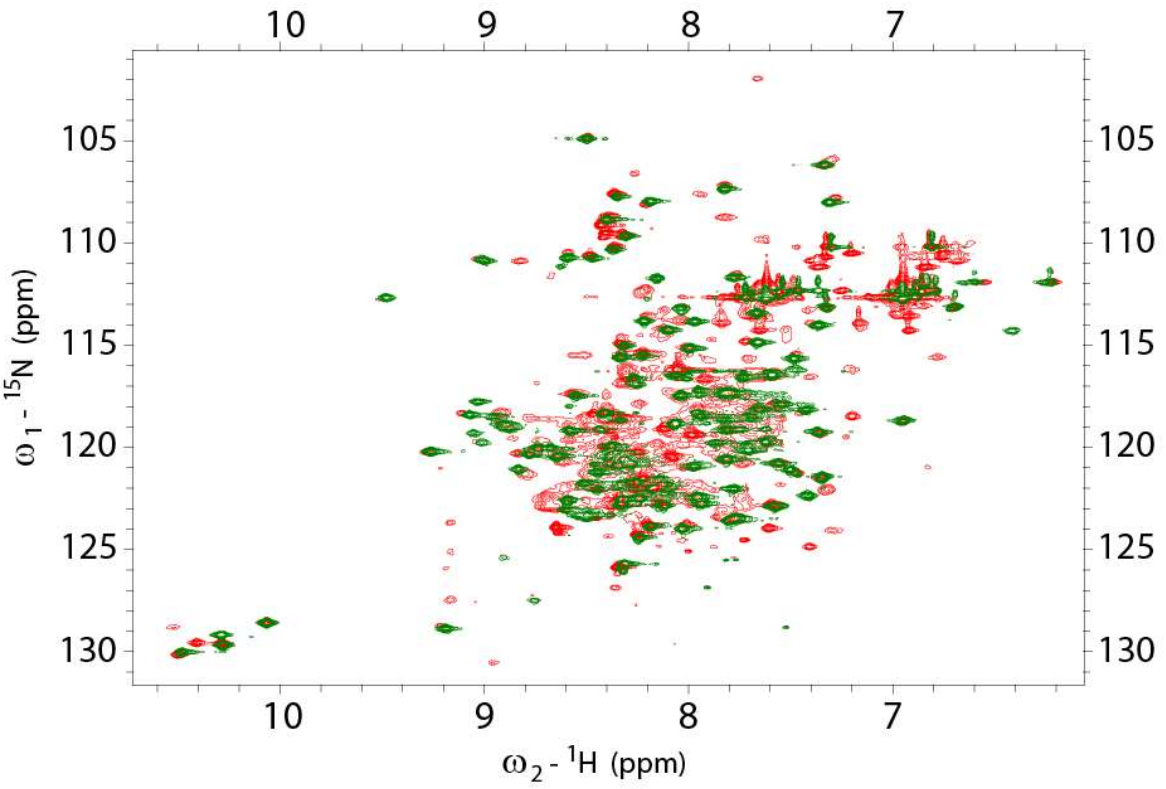

Figure 4.7. The overlay the 15N-1H HSQC spectrum of 180 uM 15N-labeled MBP-IRAKMDD (Red) and 13C/15N labeled IRAKM[1-119:R56D,Y61E] (Green).

NMR structure of the IRAKM death domain.

The application of standard 15N-separated and 13C-separated three-dimensional NOESY experiments, along with chemical shift constraints, enabled the high-resolution NMR structure of IRAKM[1-119:R56D,Y61E] to be determined. The structure adopts the canonical DD fold, demonstrating that the R56D and Y61E mutations do not disrupt the native fold. This structure consists of six α-helices: α1 (P27 – S39), α2 (W46 – L53), α3 (D59 – V67), α4 (T74 – S80), α5 (I88 – M98) and α6 (R101 – N109) (Figure 4.8a). These results are also well matched with the canonical death domain fold and with predictions from PECAN (Protein energetic

conformational analysis from NMR chemical shifts) based on theNMR chemical shift assignments (Chapter 3), with the exception of the end of the fourth alpha-helix where PECAN predicts that helix 4 ends at residue K84 (Chapter 3 and [BioMagResBank-http://www.bmrb.wisc.edu/, with accession number 26941]). The resulting ensemble of lowest energy structures have a well defined α-helical core (residues 19-52, 61-110) with a backbone RMSD of 0.19 Å. The overall structure quality was slightly better than the average NMR structure in terms of clash score (11) and sidechain outliers (9%), and slightly worse in terms of Ramachandran outliers (3%).

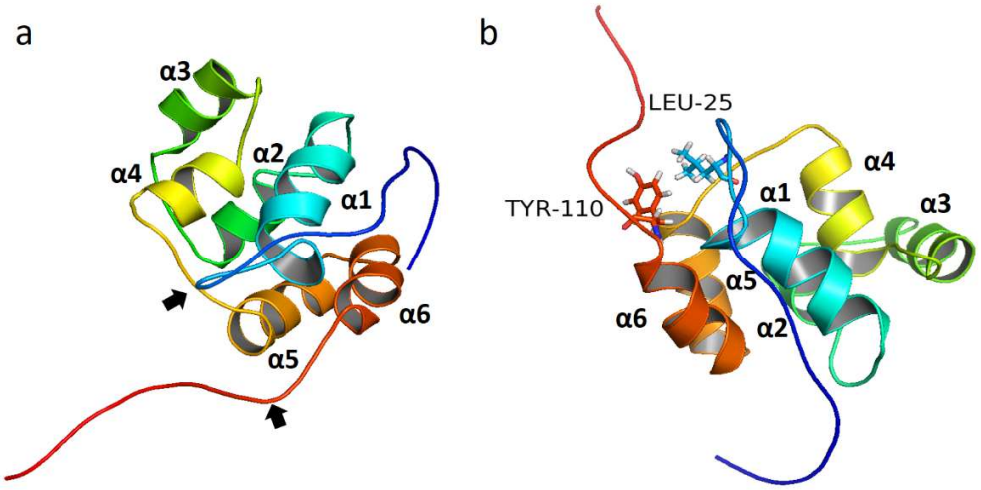

Figure 4.8. a. Ribbon diagram of IRAKM[1-119:R56D,Y61E] NMR structure (pdb ID - 5UKE), including include N-terminal and C-terminal tails. Black arrows indicate the positions of the N-terminal and C-terminal tails removing. The model of the IRAKM death domain without N-terminal and C-terminal tails is used for the docking simulation prediction. IRAKM[18-113:R56D,Y61E] b. The N-terminal L25 and C-terminal Y110 interaction to hold whole

structure. Figure was generated using Pymol (28) and PowerPoint.

In addition to the α-helical core, tail regions contribute to the teriary structure of the IRAKM DD. Specifically, although the N- and C-terminal regions (M6 – P26 and Y110 – G129, respectively) do not adopt regular secondary structure, residues A15 to P26 form a loop that packs against residues in α1, α6, the α4-α5 loop, and Y110 at the beginning of the C-terminal tail (Figure 4.8b). Residue Y110 is central to this N- to C-terminal tail stabilization, with its aromatic ring closely associating with L25 and P26 sidechains that are located right before α-helix 1. Interestingly, the IRAK2 subunit in the Myddosome structure also displays this N-to-C tail interaction, which in this case is mediated by IRAK2 residue W93 [10]. Moreover, Trp in this position is conserved in the IRAK1 sequence but not in IRAK4, suggesting that this N-to-C tail interaction is a common feature among the three IRAK family members that are directly involved in downstream signaling. Notably, in this IRAKM DD structure, the nearby S115-P116 motif recognized by Pin1 is solvent-exposed in the downstream unstructured part of the C-terminal tail, suggesting accessibility for interactions with kinase(s), phosphatase(s), and Pin1.

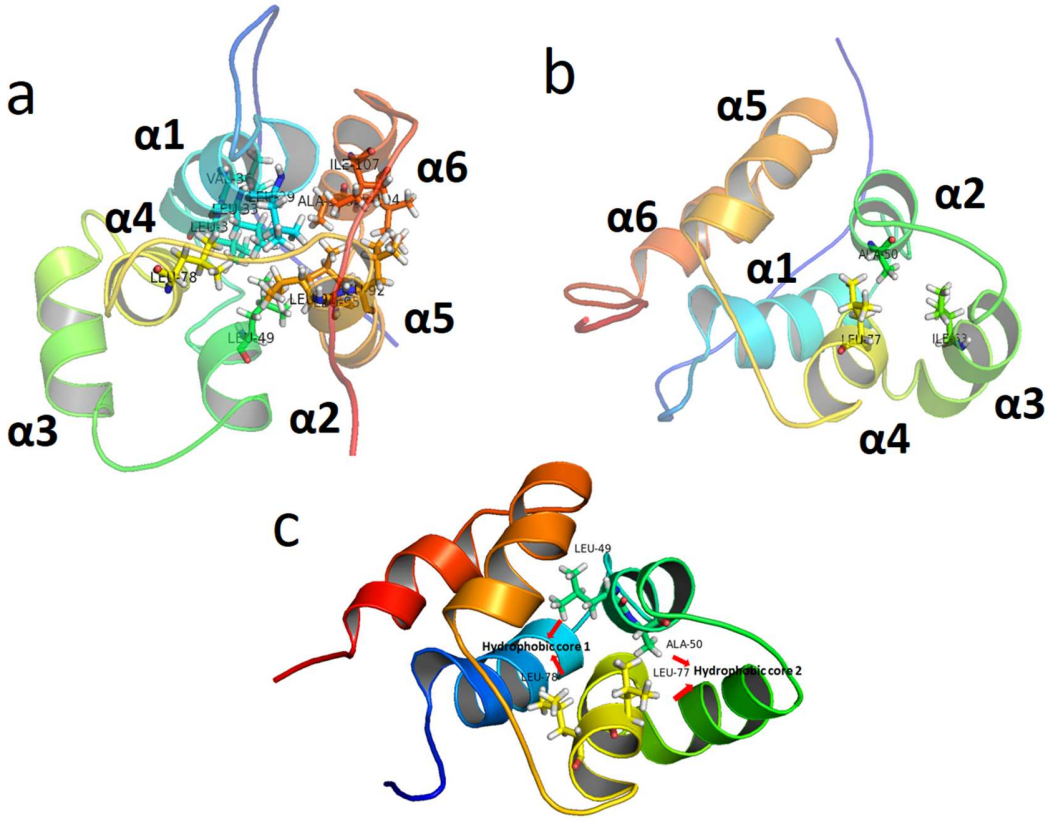

Figure 4.9. a. Hydrophobic core 1 involving alpha-helices 1, 2, 4, 5 and 6. b. The hydrophobic core 2 involving alpha-helix 2, 3, and 4. c. Sequential residues L49-A50 and L77-L78 that belong to different hydrophobic cores. Figure was generated using Pymol [28] and PowerPoint.

The IRAKM death domain tertiary structure is stabilized by two major hydrophobic cores. Hydrophobic core 1 primarily involves alpha-helices 1, 5 and 6, but also includes residues from alpha-helices 2 and 4 (Figure 4.9a). The residues that are in hydrophobic core 1 are L29, L33, V36, L37, L91, L92, L95, A103, I104, I107, L49, and L78. Alpha-helices 2 and 4 contribute only 1 residue each to hydrophobic core 1 (L49 and L78, respectively). Notably, eight out of the twelve residues of hydrophobic core 1 are Leucine. A smaller, distinct hydrophobic core (hydrophobic core 2) involves alpha-helices 2, 3, and 4. The alpha-helices 2, 3, and 4 have

fewer residues than alpha-helices 1, 5, and 6, and form a three-helix bundle that is stabilized by residues A50, I63, and L77 that form hydrophobic core 2 (Figure 4.9b).

The two hydrophobic cores are connected by two pairs of sequential residues in which the sequential residues belong to different hydrophobic cores (Figure 4.9c). Even though the residues L49 and A50 are right next to each other, L49 is directed towards to hydrophobic core 1, and A50 towards to hydrophobic core 2. Similarly, residues L77 and L78 belong to different hydrophobic cores. L77 is part of hydrophobic core 2, and L78 contributes to hydrophobic core 1. These interesting examples show how the relative orientations of secondary structural elements are important for formation of tertiary structural contacts.

Although the hydrophobic cores 1 and 2 defined above bury the involved hydrophobic sidechains on the interior of the IRAKM death domain shielding them from aqueous buffer, several additional hydrophobic sidechains are not included. Some of these hydrophobic residues are involved in stable interactions (based on observation of NOE cross peaks) between the canonical fold and the N- or C-terminal tail regions, or between loops and other regions of the structure. These include interactions that stabilize the L21, L22 and F23 region of the N-terminal tail, the interactions that stabilize Y110 in the C-terminal tail, and the V67:W46:E64 interactions that stabilize association between helices 2 and 3.

Interestingly, while most charged and polar residues are solvent-exposed on the surface of the protein, some charged and polar residues are largely buried. For example, E32 and H100 are both buried in the interface between helices 1 and 6, suggesting a possible mechanism for pH sensitivity of fold stability. Similarly, the carboxylate groups of D59 and E76 make close approach to each other and are mainly buried between helices 3 and 4. The close association of this group of E76 with the indole ring of H62 suggests a hydrogen bond network that would

favor protonation of one or both of these carboxylate groups. Additionally, K71 and K84, which are on loops at opposite ends of helix 4, each have their sidechains nearly fully buried. These residues influence the association of helix 4 with helices 1 and 2 at one end (K71) and with helices 1 and 5 at the opposite end (K84). The NH3+ group of K71 is within 5 angstroms of the carboxylate group of D38, the W46 sidechain, and the backbone carbonyls of D38 and V67, providing rationale for its position in the structure. At the opposite end of the helical bundle, the NH3+ group of K84 closely associates with the backbone carbonyl groups of F23 and K86 but otherwise is surrounded by hydrophobic groups, suggesting compromise in the formation of tertiary structure in this region.

Structural Alignment of IRAK-M DD into the Myddosome complex using Magic Fit in SwissPDBView

IRAK family members interact with themselves, with each other or with MyD88 via their DDs. The structure of IRAK-M DD was not previously determined, so interactions mediated by this domain were not fully studied. It was previously reported that IRAK-M reduces IRAK1 phosphorylation, increases IRAK1 association with MyD88, and inhibits formation of the downstream IRAK1-TRAF signaling complex40. The structural mechanism by which these effects are mediated by IRAK-M are unknown. Since the crystal structure of the MyD88-IRAK4-IRAK2 death domain complex was solved, the implications of this structure on Toll-like receptor signaling cascades was focused on IRAK2-mediated signaling, although it was hypothesized that IRAK1 DD could substitute for IRAK2 in this structure [8]. However, no structures of the IRAK-1 or IRAK-M death domains had yet been solved experimentally, so studies of the IRAK-M interaction with the Myddosome complex were highly speculative [12].

Still missing are the IRAK-1 and IRAK-M components and the mechanism by which IRAK-M inhibits TLR-triggered innate immunity signaling. Our newly solved NMR structure of the IRAK-M DD now adds a level of confidence to structural alignments and simulations of the docking between IRAK-M DD and the different forms of the Myddosome complex. As an initial step in examining interactions of IRAK-M DD in the context of the Myddosome, simple structural alignment was used.

To explore the possibility that the IRAK-M DD can substitute for an IRAK-2 or IRAK1 DD subunit in the Myddosome complex, the NMR structure of IRAKM[1-119:R56D,Y61E] was superimposed onto one of the IRAK2 DD subunits in the Myddosome complex using the Magic Fit structural alignment function in SwissPdbView [29], and the contact surfaces formed between IRAK-M DD and the surrounding IRAK-2 DD and IRAK-4 DD subunits were examined. In the resulting structural model, it is immediately apparent that the ordered N-terminal tail region of IRAK-M DD is placed toward the interior of the Myddosome complex, resulting in steric clashing between this N-terminal segment (missing in the IRAK2 DD subunits) and the surrounding subunits. This suggests that the N-terminal tail must be displaced from its anchored position against the IRAK-M surface in order for IRAK-M to adopt the canonical DD subunit orientation observed in the Myddosome complex. This intriguingly implicates the N-terminal tail as a conformational switch, wherein it is folded against the IRAK-M surface in the monomer and is released from this surface upon docking. Other than the N-terminal tail clashing, the contact surfaces between IRAK-M DD and the surrounding IRAK-2 DD and IRAK-4 DD subunits do not show any obvious additional steric clashes or unfavorable electrostatic interactions. This motivated us to perform rigorous docking simulations without inclusion of the N-terminal tail region.

Docking simulations predict selective formation of IRAK-M/IRAK1 heterotetramer in the context of the Myddosome complex

To investigate possible interactions that might facilitate IRAK-M regulation of IRAK1-mediated signaling, docking simulations were performed using a Myddosome-based model containing IRAK1 DD in place of IRAK2 DD subunits using the program ClusPro40-43. Prior to docking simulations, the mutated IRAK-M residues (R56D and Y61E) were restored in silico to their wild type identities using the Mutate tool in SwissPdbView, and IRAK-M residues 1-17 and 114-119 were deleted from the IRAK-M structure file to generate IRAK-M[18-113]. IRAK-M[18-113] was docked with a modified Myddosome composed of six MyD88, four IRAK4, three IRAK1 DD subunits, and an empty IRAK1 DD subunit space. For each of the four scoring schemes applied, the resulting ten models (representing highly populated clusters of low energy complexes) included IRAK-M DD docked into the empty subunit position in the canonical orientation. These docked models revealed favorable IRAK-M DD interactions with both IRAK1 DD and IRAK4 DD (Figure 4.10, Figure 4.11a,b). Docking simulations were also performed for the double-mutant IRAK-M to assess the impact of the R56D and Y61E mutations. The docking score for MyD88-IRAK4-IRAK1 and wt-IRAKM DD was slightly lower energy (-873.8 at center, and -1069.6 at lowest energy, Figure 4.10a) than the docking score for MyD88-IRAK4-IRAK1 and IRAKM DD(R56D, Y61E) (-872 at center, and -949.5 at lowest energy, Figure 4.10b). However, both wild-type and double-mutant forms yielded IRAK-M DD subunits docked in the canonical orientation.

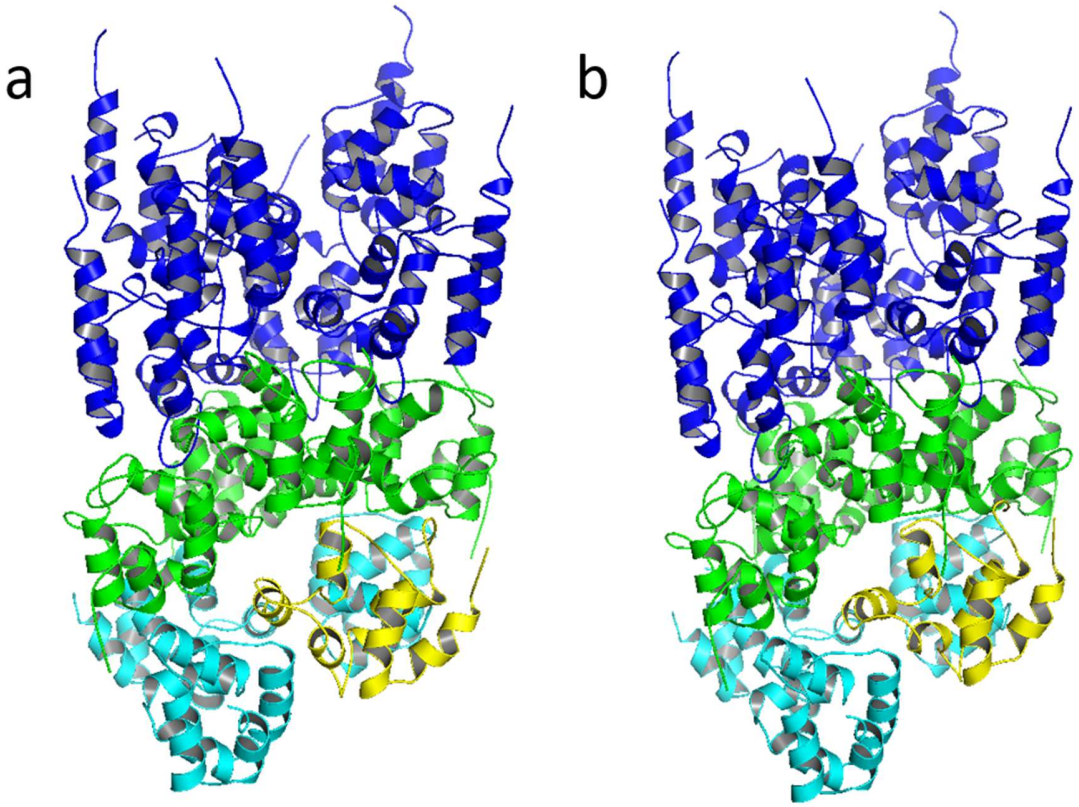

Figure 4.10. A ClusPro generated model of IRAK-M DD docked into a modified Myddosome oligomer containing three IRAK1 DD subunits in the L, M and N positions in the 3MOP structure. Blue: six MyD88 DD subunits, Green: Four IRAK4 DD subunits, Cyan: three IRAK1 DD homology model subunits, Yellow: docked NMR structure of the IRAK-M DD. a. The docking simulation between MyD88-IRAK4-IRAK1 and wt-IRAKM DD by ClusPro. b. The docking simulation between by MyD88-IRAK4-IRAK1 and IRAKM DD: R56D, Y61E by ClusPro.

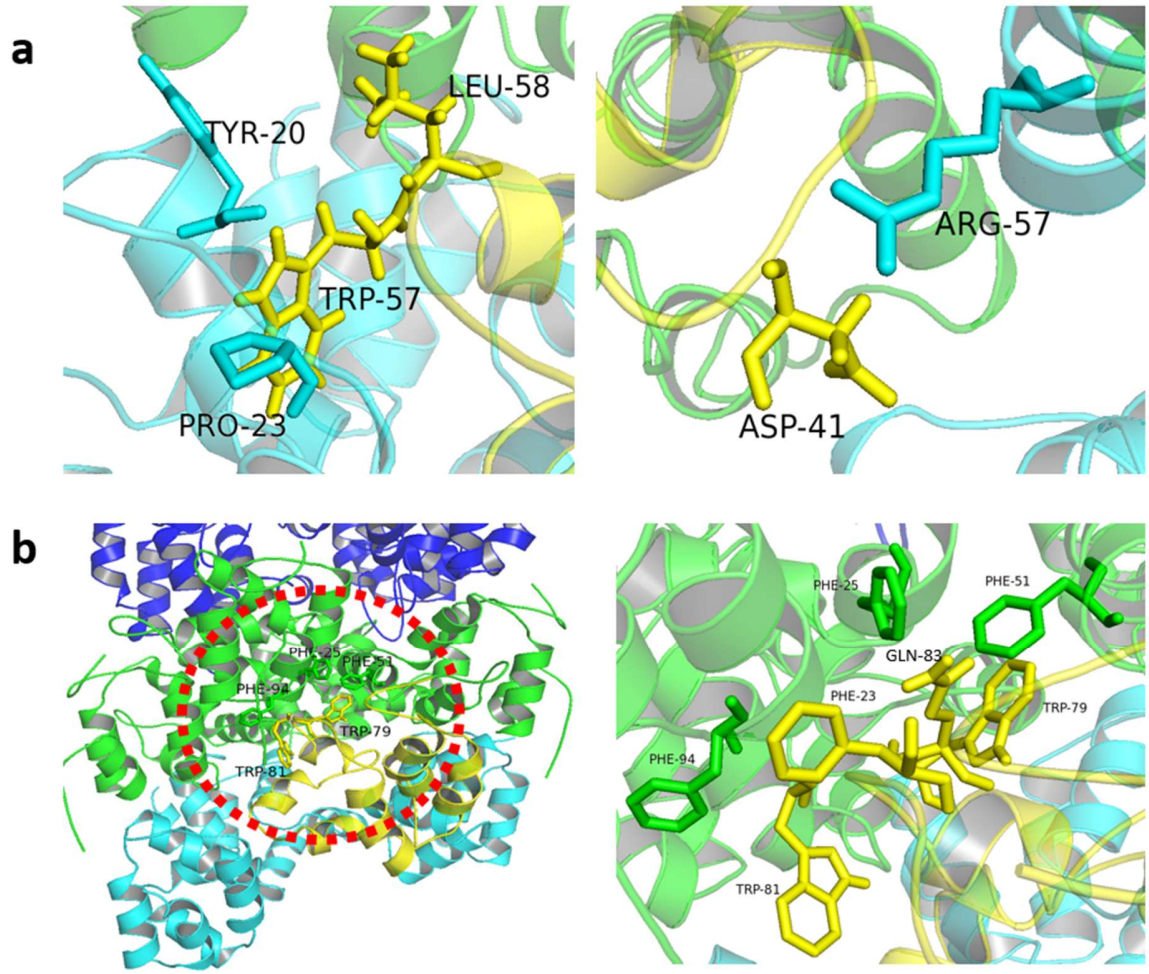

Figure 4.11. a. Interaction between IRAK-M DD and IRAK1 DD from Figure 4.10. Cyan: IRAK1 DDs, Yellow: IRAK-M DD. B. The aromatic residues interaction between IRAK-M DD and IRAK4 DD from Figure 4.10. Green: IRAK4 DDs, Yellow: IRAK-M DD

For comparison, IRAK-M was also docked with a Myddosome complex composed of six MyD88, four IRAK4, three IRAK2 DD subunits and an empty IRAK2 DD subunit space. In contrast to the above findings for IRAK-M docking into an IRAK1-containing Myddosome, these simulations for an IRAK2-containing Myddosome yielded no models with IRAK-M docked into the empty subunit position in the canonical orientation. Repulsion between IRAK-M

E51 and IRAK2 D14 and absence of a favorable IRAK-M D38 interaction with IRAK1 R61 (S47 in IRAK2) could explain this result. Moreover, docking simulations using IRAK-M DD(R56D, Y61E) also yielded no docked models with the canonical orientation. This comparison suggests distinct mechanisms for interaction of IRAK-M with the Myddosome, depending on whether it contains IRAK2 or IRAK1.

For further comparison, we investigated docking of the IRAK-M DD monomer into a Myddosome model containing three IRAK-M DD subunits in place of three IRAK2 DD subunits and leaving an empty subunit space as above. The ClusPro docking simulation provided the best 107 combinations between IRAKM DD and the MyD88-IRAK4-IRAKM complex, but none showed the docked IRAK-M subunit in the canonical orientation. These results further support the prediction that formation of an IRAK-M/IRAK1 heterotetramer is highly selective, and occurs more favorably than and IRAK-M/IRAK2 heterotetramer or an IRAK-M homotetramer.

Simulations show IRAK-M DD tetramer fails to substitute for IRAK2 DD tetramer in the MyD88-IRAK4 complex

Based on the findings that IRAK-M is crucial for NF-κB activation in IRAK1/IRAK2 double knockout mice and that the IRAK-M DD recruits IRAK-M to the TLR-MyD88-IRAK4 complex in response to low dose LPS leading to MEKK3-dependent NFκB activation [12], an additional question of interest is whether an IRAKM DD tetramer can substitute for the IRAK2 tetramer in the Myddosome complex. To address this question, docking of an IRAK-M tetramer to the assembled MyD88-IRAK4 portion of the Myddosome was simulated. The MyD88-IRAK4 complex was generated by deleting the four IRAK2 subunits from the 3MOP pdb structure file, and an IRAK-M DD tetramer model was constructed using Swiss-PbdViewer

and Pymol by superposition with the IRAK2 subunits in the Myddosome structure. These two complexes were submitted for docking simulations to ClusPro. The results showed that the IRAK-M DD tetramer associates in many different ways with the MyD88-IRAK4 assembly, but displays a preference for associating with the MyD88 DD end rather than the IRAK2 DD end of the complex (Figure 4.12). Additional evidence that IRAK-M does not show binding to the IRAK4 platform in the Myddosome was obtained by docking an IRAK-M DD monomer to the MyD88-IRAK4 assembly. In the best 24 balanced models, none show IRAK-M DD monomer bound to the IRAK4 DD surface used for association with the IRAK2 tetramer (Figure 4.13). These results suggest that an IRAK-M tetramer fails to substitute for the IRAK2 DD tetramer. However, its preference for interacting with the MyD88 surface raises the possibility that a putative IRAK-M tetramer might compete with MyD88 association with the TIR (toll-IL-1 receptor) domain of the Toll-like receptor. Together, these simulations suggest that the crucial role of IRAK-M in the IRAK1/IRAK2 double knockout mouse is not mediated by simple tetramer substitution in the Myddosome complex.

As a positive control for tetramer docking to the MyD88-IRAK4 complex, ClusPro docking simulations were also performed for the IRAK2 tetramer obtained from the 3MOP pdb structure file. Indeed, this IRAK2 tetramer docked to the MyD88-IRAK4 assembly in the same orientation as found in the experimentally determined Myddosome structure (3MOP pdb structure file), providing important validation for the use of the ClusPro docking program for predicting tetramer association with the MyD88-IRAK4 assembly.

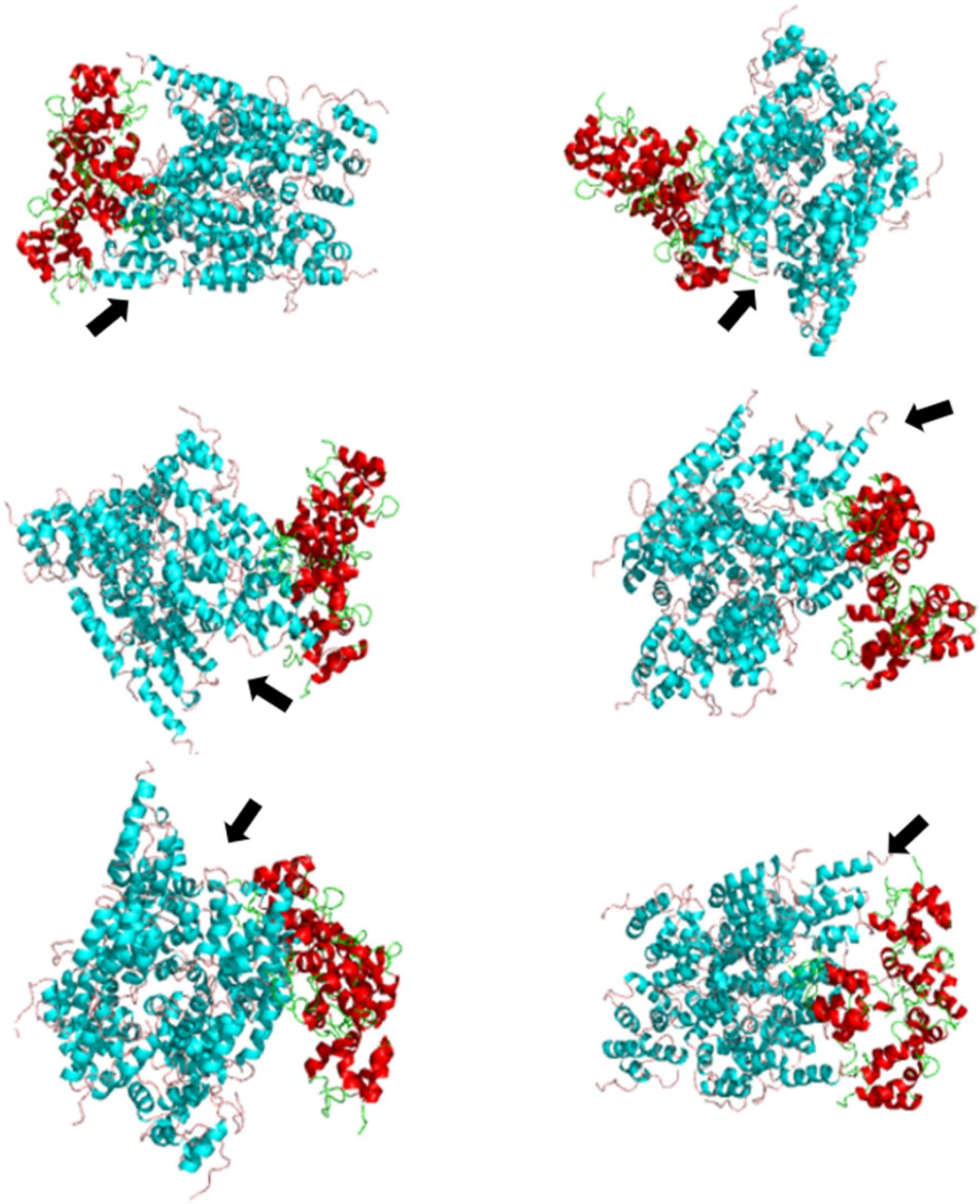

Figure 4.12. IRAKM DD tetramer randomly bound to the surface of the MyD88-IRAK4 complex. The figures are from the Balanced model of the ClusPro results. Cyans: MyD88-IRAK4 complex, Red: IRAKM DD tetramer. Black arrow indicates MyD88 Position

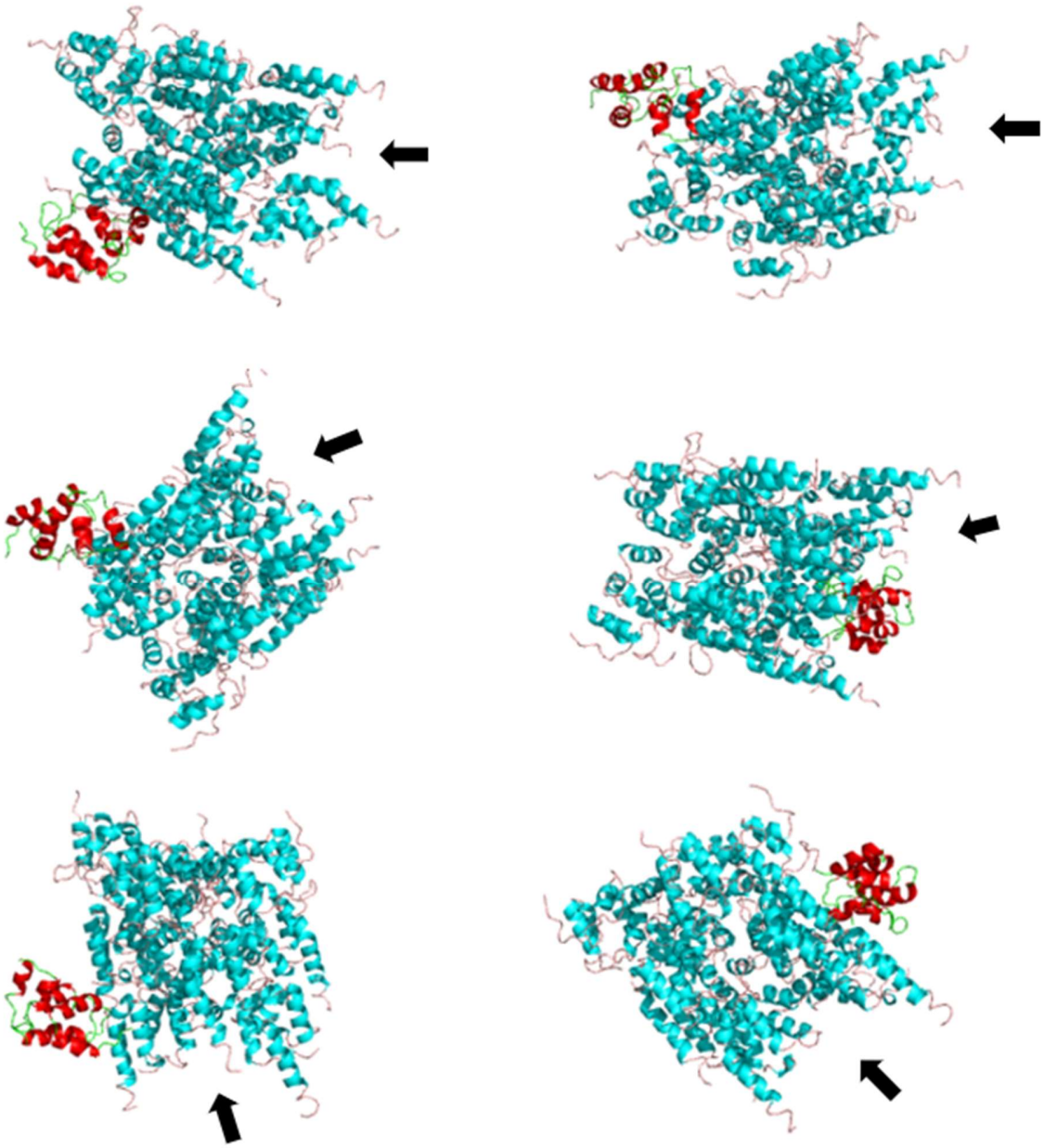

Figure 4.13. IRAKM DD monomer randomly bound to the surface of the MyD88-IRAK4 complex. The figures are from the Balanced model of the ClusPro results. Cyans: MyD88-IRAK4 complex, Red: IRAKM DD: W.T. Black arrow indicates MyD88 Position.

Docking simulations predict specific IRAK-M DD interactions with IRAK2 DD subunits in the Myddosome complex

To further investigate potential mechanisms by which IRAK-M might impart the known effects on IRAK2-mediated NFkB signaling [12], we investigated IRAK-M DD interactions with IRAK2 DD subunits in the context of the full Myddosome complex (MyD88-IRAK4-IRAK2 DDs). The IRAK-M[18-113] monomer and tetramer forms were separately docked with the Myddosome complex using ClusPro.

The resulting docked complexes of the IRAK-M monomer with the Myddosome shows preferred interaction with the IRAK2 bottom surface (Figure 4.14). IRAK-M residues W79 and W81 are consistently involved in the observed interactions with the IRAK2 subunits. The docking score for each resulting complex is very similar (Figure 4.14 A, B, C). The docking scores for A are -965 at the center and -1093.4 at the lowest energy. The docking scores for B are -952.5 at the center and -1103.9 at the lowest energy. The docking scores for C are -927.9 at the center and -1175.2 at the lowest energy. All of three of positions of docking formation have similar energy favorability.

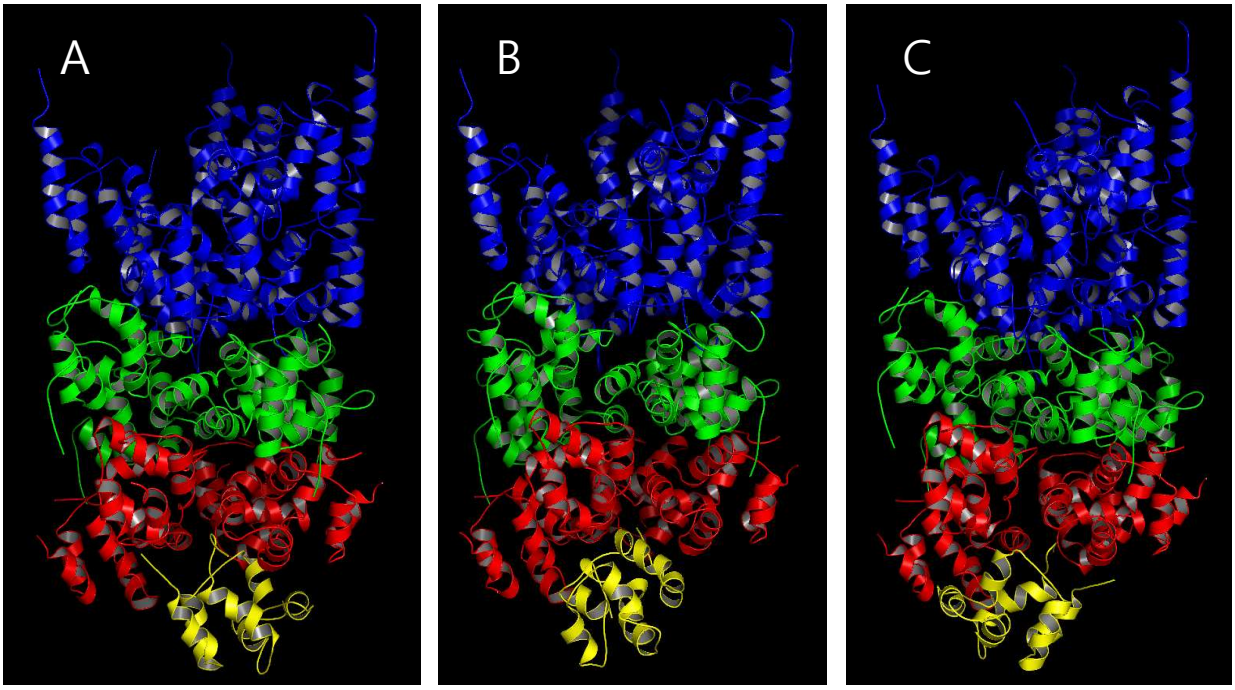

Figure 4.14. The docking simulation of the IRAKM DD monomer to the Myddosome complex. Blue: six of MyD88 DD, Green: four of IRAK4 DD, Red: four of IRAK2 DD, Yellow: IRAKM DD: W.T. A, B, C. The IRAKM DD dock under the MyD88-IRAK4-IRAK2 DD Complex in different positions.

Docking simulations for association of the IRAK-M tetramer with the Myddosome yield three major classes of assembly, two of which show IRAK-M DD subunits interacting similarly with IRAK2 as elucidated in the monomer IRAK-M docking simulations. Specifically, the IRAK-M tetramer utilizes either two (Figure 4.15A) or one (Figure 4.15B) of its IRAK-M DD subunits to dock with the IRAK2 bottom surface. In both of these classes, the orientation of the interacting IRAK-M DD subunit(s) is the same as that of the IRAK-M DD monomer docked to the Myddosome. In contrast, the third class is non-specific interaction of IRAKM DD tetramer in various orientations with the side of IRAK2 or IRAK4 DDs.

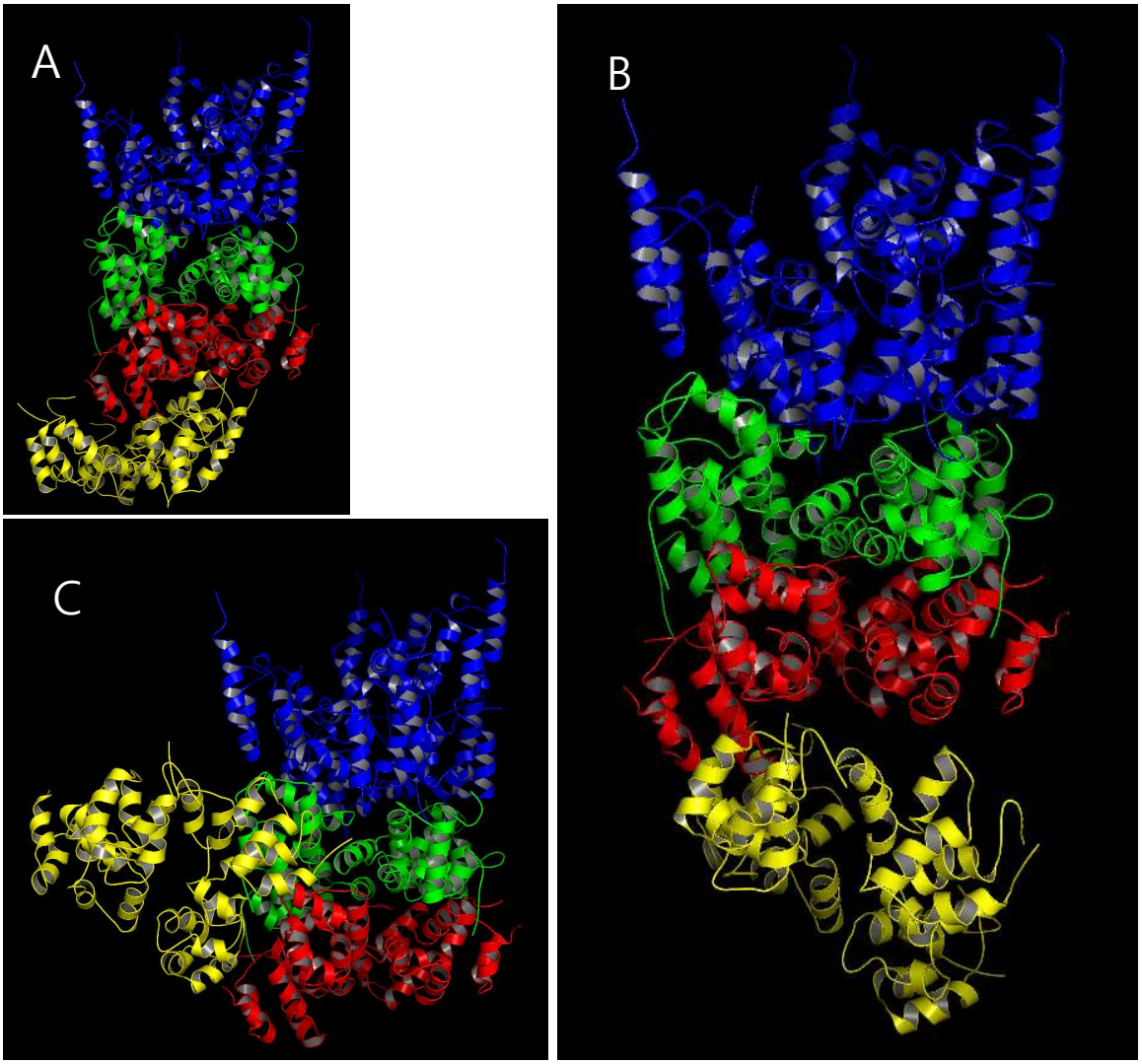

Figure 4.15. The docking simulation of the IRAKM DD tetramer to the Myddosome complex. Blue: six of MyD88 DD, Green: four of IRAK4 DD, Red: four of IRAK2 DD, Yellow: four of IRAKM DD: W.T. A, B, C. The IRAKM DD tetramer dock to the MyD88-IRAK4-IRAK2 DD Complex in different positions.

These docking simulations show that an individual IRAK-M DD subunit does favorably interact with the IRAK2 DD surface displayed in the Myddosome structure. This is in contrast to the docking simulations of the IRAK-M monomer to the IRAK4 DD surface presented above,

where no preferred interactions were observed with the comparable IRAK4 surface. Together, these results suggest that a possible mechanism for IRAK-M regulation of IRAK2-mediated signaling might be through direct binding of IRAK-M to IRAK2 DD subunits assembled in the Myddosome.

Assessment of the impact of IRAK-M DD structural variation on the docking results

The NMR structure determination of IRAK-M[1-119:R56D,Y61E] consists of 20 lowest energy models that are consistent with the NMR constraints, where model 13 is the overall representative, medioid model. Across this ensemble of models, the backbone root mean square deviation (RMSD) is 0.19 Å, indicating excellent agreement of backbone fold across the 20 models. The sidechains, especially those that are surface-exposed, are much less constrained so the ensemble of structures represents a wide range of surface sidechain conformations. Although the ClusPro docking process includes sidechain rearrangements and minor backbone adjustments, an important question is whether different models from the NMR determined ensemble will yield significantly different docked structures.

To address the impact of sidechain conformational variability on the resulting docked structures, three different models from the NMR ensemble (model 1, model 13, and model 20), with an average all-atom RMSD among them of 0.95 Å, were chosen for comparative docking studies. Again, prior to docking simulations, the mutated IRAK-M residues (R56D and Y61E) were restored in silico to their wild type identities and IRAK-M residues 1-17 and 114-119 were deleted to generate IRAKM[18-113] for each model. These substitutions did not change the all-atom RMSD among the three models (0.95 Å). From the docking studies presented above, the most specific docking result was the case where the IRAKM[18-113] monomer was docked with

with a modified Myddosome composed of six MyD88, four IRAK4, three IRAK1 DD subunits, and an empty IRAK1 DD subunit space. Therefore, this case was chosen to evaluate the variation of docked models resulting from variation of IRAK-M DD models used for docking.

Each of the three IRAK-M DD models was docked to the MyD88-IRAK4-IRAK1 DD complex for examination of the effect of side chain orientation. Notably, all three cases yielded IRAK-M DD docked in the canonical DD orientation into the empty subunit position. To evaluate structural differences between these docked IRAK-M DD structures resulting for models 1, 13, and 20, a representative docked complex for each case was selected, and these three docked models were structurally aligned using Magic Fit in SwissPdbView. This structural alignment is dominated by the invariant regions across the three docked models, namely the MyD88-IRAK4-IRAK1 DD portion of the Myddosome. From these aligned complexes, the IRAKM[18-113] residues were selected and saved as separate PDB files while preserving their positions relative to the Myddosome assembly. The RMSD of each combination, {1,13}, {1,20}, {13,20}, {13,1}, {20,1}, {20,13}, was then calculated, along with the mean RMSD across these combinations (Table 4.2). The mean all-atom RMSD is 2.78 Å.

To evaluate how much the IRAK-M DD structure was adjusted during the docking process, the extracted IRAK-M DD structures (post docking) were structurally aligned using Magic Fit. The resulting RMSD (1.74 Å) is larger than the pre-docking RMSD of models 1, 13 and 20 (0.95 Å), indicating that the docking process adjusted the structural models somewhat.

These results indicate that the RMSD between the docked structures (2.78 Å) arises from both orientational differences relative to the Myddosome complex as well as adjustments to the IRAK-M DD structure during the docking process. However, the three models from the NMR ensemble yielded qualitatively the same results, with similarly docked IRAK-M DD in the

canonical orientation in the IRAK1-containing Myddosome. These comparisons provide confidence in the predicted formation of an IRAK-M/IRAK1 heterotetramer in the Myddosome complex that is mediated by their DDs.

Table 4.2. All-atom RMSD of Myddosome-docked IRAK-M DD models 1, 13 and 20

	Avg_RMSD	1st_WT	13th_WT	20th_WT
1st_WT	2.98		2.95	3.01
13th_WT	2.66	2.95		2.37
20th_WT	2.69	3.01	2.37	
Mean global RMSD	**2.77666667**			

Table 4.3. RMSD of IRAKM DD models 1, 13 and 20 before docking to the Myddosome

	Avg_RMSD	1st_WT	13th_WT	20th_WT
1st_WT	0.81		0.80	0.81
13th_WT	1.02	0.80		1.24
20th_WT	1.03	0.81	1.24	
Mean global RMSD	**0.95**			

Table 4.4. RMSD of the extracted and Magic Fit aligned IRAKM DD after docking to the Myddosome

	Avg_RMSD	1st_WT	13th_WT	20th_WT
1st_WT	1.65		1.75	1.55
13th_WT	1.84	1.75		1.93
20th_WT	1.74	1.55	1.93	
Mean global RMSD	**1.74**			

Discussion

The NMR structure of IRAK-M DD represents the first solution NMR structure of a human IRAK family member death domain. This structure was made possible by site-directed mutation of two surface-exposed amino acid residues that successfully inhibited aggregation while preserving the folded state. The domain structure is stabilized by hydrophobic packing that can be parsed into two hydrophobic cores that mediate the association of six alpha helices. Additionally, the N-terminal and C-terminal regions of IRAKM-DD participate in hydrophobic interactions with each other and with the alpha helical fold, which is a feature that is also observed in IRAK2 and is sequence-wise conserved in IRAK1 but not in IRAK4. Extensive interactions anchor the N-terminal tail region to the surface of the helical fold, imparting order to residues A15 – P26. Just downstream of the ordered C-terminal region, the S115-P116 motif recognized by Pin1 is solvent-exposed in the NMR structure of IRAK-M DD, suggesting accessibility for protein-protein interactions. Although this solution NMR-determined structure indeed adopts the expected canonical death domain fold, the details of this structure, including the elucidation of interactions involving the N- and C-termianal tail regions, have enabled docking simulation studies that provide important insights regarding the varied roles of IRAK-M in innate immunity signaling.

Overall, the docking simulations that were performed using the newly determined NMR structure of the IRAK-M DD indicate that the IRAK-M DD interacts favorably with the MyD88-IRAK4-IRAK1 Myddosome complex, where the IRAK-M DD can replace an IRAK-1 DD subunit and form favorable interaction interfaces with both neighboring IRAK-1 DD subunits and with the juxtaposed IRAK-4 DD surface. Importantly, formation of this IRAK1/IRAK-M heterotetramer requires the release of the IRAK-M N-terminal tail region from the domain

surface, suggesting that the IRAK-M N-terminal tail region functions as a conformational switch. In contrast, unfavorable interactions prevent the comparable insertion of the IRAK-M DD into the MyD88-IRAK4-IRAK2 Myddosome complex, and formation of an IRAK-M DD tetramer is not favored. However, an individual IRAK-M DD subunit does favorably interact with the IRAK-2 DD surface displayed in the Myddosome structure. What insights do these docking simulations provide regarding the mechanisms by which IRAK-M facilitates its various and sometimes opposite effects in innate immunity signaling?

IRAK-M is known to inhibit IRAK1-mediated NF-kB signaling, and has been shown to reduce IRAK1 phosphorylation, increase IRAK1 association with MyD88, and inhibit formation of the downstream IRAK1-TRAF signaling complex40. Our docking simulations performed using the NMR structure of IRAK-M DD suggest that the Myddosome framework allows formation of an IRAK1-IRAK-M hetero-tetramer and suggest a model by which IRAK1 can phosphorylate IRAK-M S115-P upon stimulation (Figure 4.16 a-d). In this proposed model, a single IRAK1 molecule cannot hyper-phosphorylate its own UD, rather the IRAK1 UD can only be hyper-phosphorylated by its next-neighbor IRAK1 KD due to spatial constraints (Figure 4.16a). Our docking simulations suggest that the IRAK-M DD might replace every other IRAK-1 DD subunit in the Myddosome complex, thereby forming a heterotetramer with IRAK1 (Figure 4.16b). This alternating IRAK1/IRAK-M structure might prevent the IRAK1 kinase domain (KD) from hyper-phosphorylating the next-neighbor IRAK1 UD, prevent IRAK1 release from the Myddosome, and suppress IRAK1-mediated inflammation (Figure 4.16c).

Through our own collaborative work, we have shown that when cells and mice are stimulated with asthma-inducing IL-33, IRAK-M and Pin1 play essential roles in the induction of inflammation. Specifically, upon IL-33 stimulation, IRAK-M is phosphorylated by IRAK1

at S115, Pin1 is activated, and Pin1 binding and isomerization of the pS115-P motif increases IRAK-M nuclear translocation and protein stability that correlates with increased expression of a set of pro-inflammatroy cytokines [15]. In our proposed IRAK1-IRAK-M hetero-tetramer containing Myddosome model, Pin1 binding to the solvent exposed IRAK-M pS115P motif and subsequent isomerization of this motif could displace the C-terminal region of IRAK-M DD, thereby disrupting the Y105-mediated N-to-C interaction and inducing IRAK-M dissociation from the Myddosome (Figure 4.16d) for downstream IRAK-M dependent signaling.

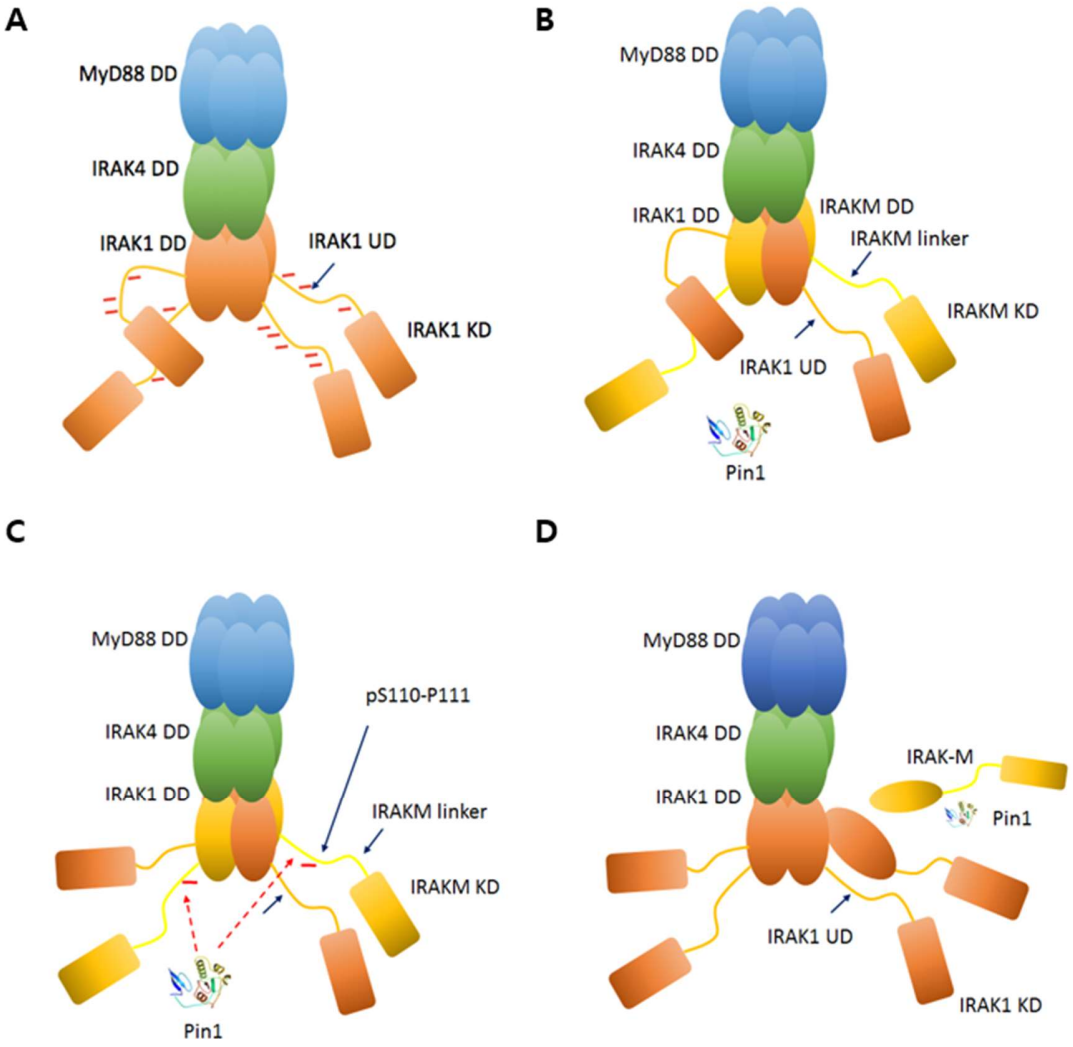

Figure 4.16. Proposed model for IRAK-M and PIN1 regulation of IRAK1 mediated immunity signaling. a. IRAK1 homotetramer assembled on the Myddosome is able to achieve full hyperphosphorylation through each IRAK1 undefined domain (UD) being phosphorylated by neighboring IRAK1 kinase domains (KDs). b. In the presence of IRAK-M, heterotetrameric IRAK-M/IRAK1 assembles on the Myddosome where IRAK-M DD replaces every-other IRAK1 DD subunit, preventing further IRAK1 hyper-phosphorylation and inhibiting IRAK1 release from the Myddosome thereby suppressing IRAK1-mediated inflammation. c. IRAK1 KD

phosphorylates S110 in next-neighbor IRAK-M. d. Binding of PIN1 to IRAK-M pS110P (IRAK-M phosphorylated at residue S110) and subsequent isomerization induces release of IRAK-M from the Myddosome for downstream PIN1- and IRAK-M dependent signaling.

This proposed model, based on our NMR structure and subsequent docking simulations, suggests how formation of an IRAK1-IRAK-M heterotetramer on the Myddosome could prevent IRAK1 activation, possibly explaining the known effects of IRAK-M on IRAK1 phosphorylation, signaling and association with MyD8840. This model also provides a mechanism by which IRAK1 could phoshorylate IRAK-M on S115P to generate a Pin1 recognition site, and that Pin1 binding and isomerization of the pS115-P motif in IRAK-M could promote IRAK-M release from Myddosome complex, leading to IRAK-M dependent signaling [15].

IRAK-M is also known to play an inhibitory role in TLR-induced IRAK2 mediated signaling, and was predicted to do so through formation of an IRAK-M DD tetramer that binds to the IRAK2 tetramer platform in the full Myddosome complex [12]. This prediction was made using an IRAK-M DD homology model. Our ClusPro-generated simulation of docking between the Myddosome (MyD88-IRAK4-IRAK2 DD) complex and our NMR structure of IRAK-M DD is interesting, because it suggests an alternative mode of interaction between IRAK-M DD and the Myddosome whereby one or two IRAK-M DD bind to the IRAK2 DD platform. In fact, our docking simulations showed no resulting docked models as proposed by Zhou et al. [12]. Base on our docking results, IRAK-M DD might bind to the Myddosme complex at the IRAK2 surface as a monomer or dimer rather than as a tetramer. In this manner, IRAK-M DD could suppress IRAK2-mediated signaling by preventing IRAK2 from participating in downstream

interactions.

In conclusion, the solution NMR structure of IRAK-M DD has yielded several important insights regarding the structural mechanisms by which IRAK-M carries out its varied functions in innate immunity signaling pathways. While the IRAK-M N-terminal tail region is ordered and packs against the domain surface in the monomer state, this extended interface must be disrupted in order for IRAK-M to form a heterotetramer with IRAK1 in the context of the Myddosome complex. This implicates the N-terminal tail of IRAK-M as a conformational switch that regulates IRAK-M interactions with the Myddosome. Formation of the IRAK1/IRAK-M heterotetramer is specific, and provides a distinct mechanism by which IRAK-M might facilitate its suppression of IRAK1-mediated signaling. On the other hand, IRAK-M suppression of IRAK2-mediated signaling appears to utilize a very different mechanism, whereby IRAK-M binds to the solvent-exposed IRAK2 teteramer surface. These predictions generated by simulated docking using our NMR-determined IRAK-M DD structure offer models that motivate further cell and molecular biology investigations to more completely understand the structural mechanisms of IRAK-M in the regulation of innate immunity signaling.

Reference

1. Delneste Y, Beauvillain C, Jeannin P. Innate immunity: structure and function of TLRs. Med Sci (Paris). 23 (1): 67–73 (2007)

2. Gay NJ, Keith FJ; Keith. Drosophila Toll and IL-1 receptor. Nature. 351 (6325): 355–6 (1991)

3. Akira ,Shizuo., & Takda, Kiyoshi., Toll-Like receptor Signalling. Nat Rev Immunol 4, 499-510 (2004)

4. Kobayashi K, Hernadez LD, Galan JE et al. IRAK-M is a negative regulator of Toll-like receptor signaling. Cell, 191-202 (2002)

5. Wang J, Hu Y, Deng WW, Sun B. Negative regulation of Toll-like receptor signaling pathway. Microbes infect 321-7 (2009)

6. Fukao T, Koyasu S. PI3K and negative regulation of TLR signaling. Trends Immunol, 24, 358-63 (2003)

7. Vijayyakumar Gosu, Shaherin Basith, et al. Molecular evolution and structural features of IRAK family members, PLOS ONE, e49771(2012)

8. Lin SC, Lo YC, Wu H. Helical assembly in the MyD88-IRAK-4IRAK-2 complex in TLR/IL-1R signalling. Nature 465: 885–890 (2010)

9. Kobayashi K, Hernadez LD, Galan JE et al. IRAK-M is a negative regulator of Toll-like receptor signaling. Cell, 191-202 (2002)

10. Wang J, Hu Y, Deng WW, Sun B. Negative regulation of Toll-like receptor signaling pathway. Microbes infect 321-7 (2009)

11. Fukao T, Koyasu S. PI3K and negative regulation of TLR signaling. Trends Immunol, 24, 358-63 (2003)

12. Zhou H, Yu M, Fukuda K, et al. IRAK-M mediates Toll-like receptor/IL-1R-induced NFκB activation and cytokine production. EMBO J. Feb 20;32(4):583-96 (2013)

13. Balaci L. Spada MC, Olla N et al. IRAK-M is involved in the pathogenesis of early-onset persistent asthma. Am J Hum Genet 1103-14 (2007)

14. Su J, Xie Q, Wilson I, Li L. Differential regulation and role of Interleukin-1 Receptor Associated Kinase-M in innate immunity signaling. Cellular signalling.19(7):1596-1601 (2007)

15. Nechama, M., et al. The IL-33-PIN1-IRAK-M axis is critical for type 2 immunity in IL-33-induced allergic airway inflammation. Nat Commun 9(1): 1603 (2018)

16. Bahrami, A., Assadi, A., Markley, J. L. & Eghbalnia, H., Probabilistic Interaction Network of Evidence Algorithm and its Application to Complete Labeling of Peak lists from Protein NMR Spectroscopy, PLoS Comput Biol. 5(3):e1000307 (2009)

17. Lee, W., Westler, W. M., Bahrami, A., Markley, J. L., PINE-SPARKY: graphical interface for evaluating automated probabilistic peak assignments in protein NMR spectroscopy. Bioinformatics. 25(16):2085-7 (2009)

18. Lee, W., Tonelli, M., Markley, J. L., NMRFAM-SPARKY: enhanced software for biomolecular NMR spectroscopy. Bioinformatics. 31(8):1325-7 (2015)

19. Lee, W., Cornilescu, G., Dashti, H., Eghbalnia, H. R., Tonelli, M., Westler, W. M., Butcher, S. E., Henzler-Wildman, K. A., Markley, J. L., Integrative NMR for biomolecular research.

J Biomol NMR. 64(4):307-32 (2016)

20. Lee W, Petit CM, Cornilescu G, Stark JL, Markley JL. The AUDANA algorithm for automated protein 3D structure determination from NMR NOE data. Journal of Biomolecular NMR. in press (2016)

21. Lee W, Cornilescu G, Dashti H, Eghbalnia HR, Tonelli M, Westler WM, Butcher SE, Wildman-Henzler K, Markley JL. Integrative NMR for biomolecular research. Journal of Biomolecular NMR 64(4):307-332 (2016)

22. Lee W, Stark JL, Markley JL. PONDEROSA-C/S: Client-server based software package for automated protein 3D structure determination. Journal of Biomolecular NMR. 60(2-3):73-5 (2014)

23. Lee W, Kim JH, Westler WM, Markley JL. PONDEROSA, an automated 3D-NOESY peak picking program, enables automated protein structure determination. Bioinformatics 27: 1727–1728 (2011)

24. Kozakov D, Beglov D, Bohnuud T, Mottarella S, Xia B, Hall DR, Vajda, S. How good is automated protein docking? Proteins: Structure, Function, and Bioinformatics. (2013)

25. Kozakov D, Brenke R, Comeau SR, Vajda S. PIPER: An FFT-based protein docking program with pairwise potentials. Proteins. (2006)

26. Comeau SR, Gatchell DW, Vajda S, Camacho CJ. ClusPro: an automated docking and discrimination method for the prediction of protein complexes.Bioinformatics. (2004)

27. Comeau SR, Gatchell DW, Vajda S, Camacho CJ. ClusPro: a fully automated algorithm for protein-protein docking Nucleic Acids Research. (2004)

28. The PyMOL Molecular Graphics System, Version 1.8 Schrödinger, LLC.

29. Guex, N. and Peitsch, M.C. SWISS-MODEL and the Swiss-PdbViewer: An environment for comparative protein modeling. Electrophoresis 18, 2714-2723. (1997)

30. Gwo-Yu Chuang et al, DARS (Decoys As the Reference State) Potentials for Protein-Protein Docking, Biophysical Journal Volume 95 4217–4227. (2008)

31. di Guan, C; Li, P; Riggs, PD; Inouye, H. Vectors that facilitate the expression and purification of foreign peptides in Escherichia coli by fusion to maltose-binding protein. Gene. 67 (1): 21–30. (1988)

32. Wesche, H., et al. IRAK-M is a novel member of the Pelle/interleukin-1 receptor-associated kinase (IRAK) family. J Biol Chem, 274:19403-19410 (1999).

Appendix 1

Plasmid Information

Plasmid Information for pMAL-c2X

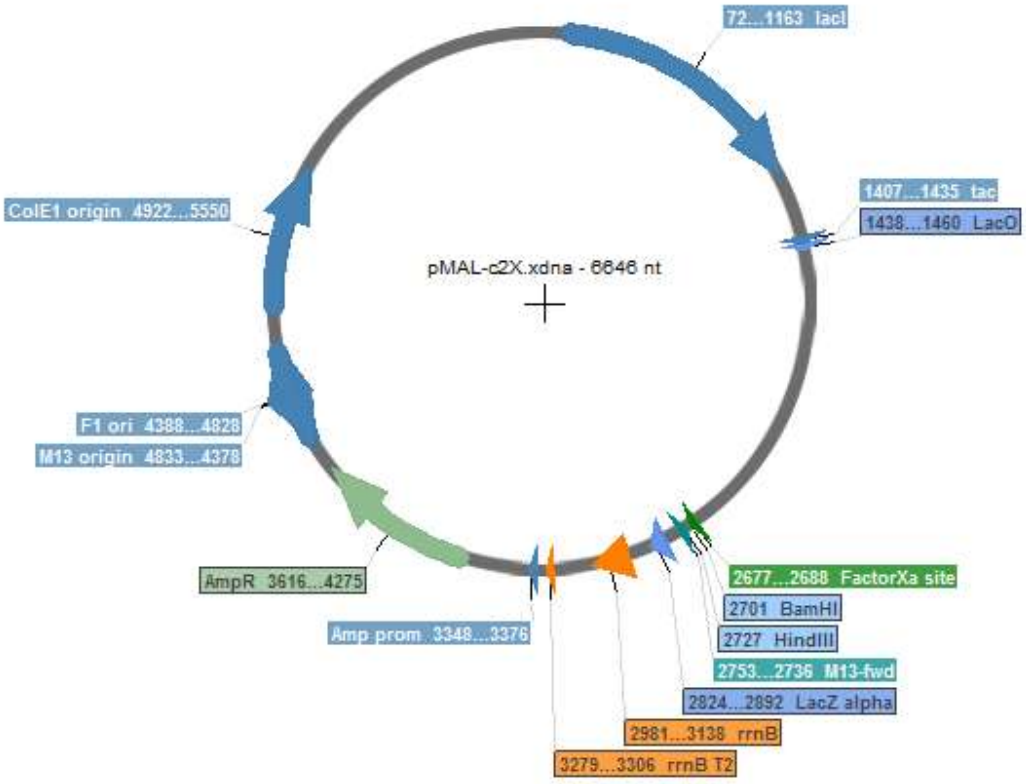

Plasmid Name: pMAL-c2X

Parent Plasmid: pMAL-c2X

Detail of Construction:

pMAL-c2X vector contains tac promoter and lacI, thus protein expression level can be controlled by IPTG concentration. pMAL-c2X vector is Ampicillin resistance. MBP (Maltose Binding Protein) is located at the N-terminal, and inserted DNA will be located at the C-terminal. The restriction site NdeI is at N-terminal of MBP. Restriction sites SacI, EcoRI, **BamHI**, XbaI, SalI, OstI and **HindII** are located at C-terminal of MBP.

Plasmid Information for pMAL-c2X_IRAKM[1-119:R56D,Y61D]

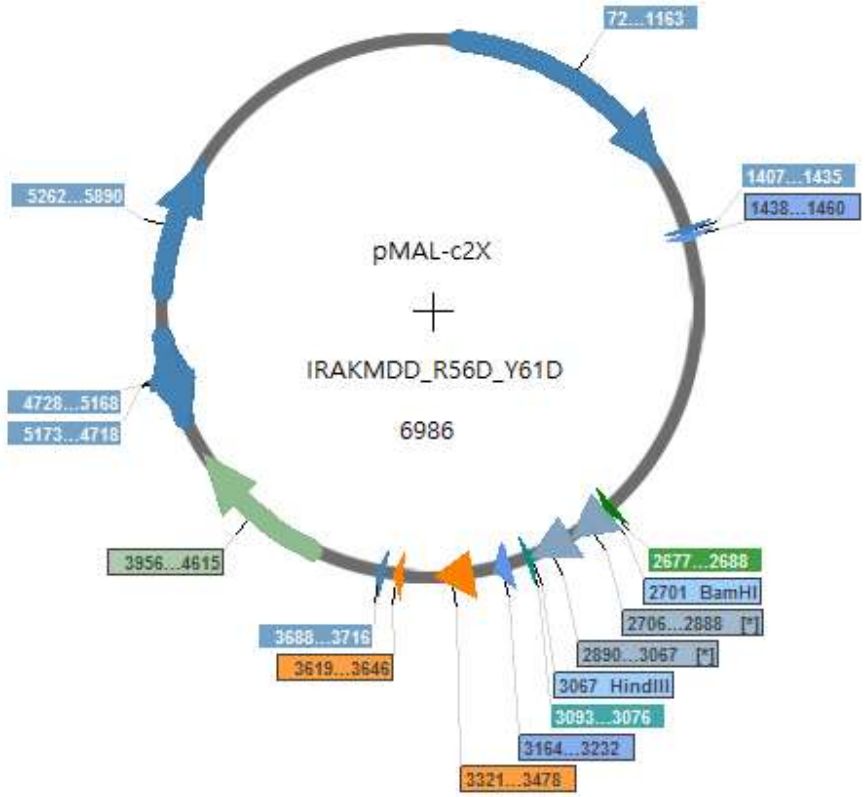

Plasmid Name: pMAL-c2X_IRAKM[1-119:R56D,Y61D]

Parent Plasmid: pMAL-c2X

Detail of Construction:

PCR amplification from clone hIRAKM (IRAK3, NCBI: NM_007199.2) using the primers.

Forward with BamHI: 5’ act gat gga tcc atg gcg ggg aac tgt ggg gcc cgc ggc gcg 3’

Backward with HindIII: 5’ gac agt aag ctt tca acc ttc ctg ata act ctt ctc tga agg 3’

PCR product was ligated into the vector pMAL-c2X using sticky ends. The BamHI and HindIII

restriction sites were used to cut the PCR insert and pMAL-c2X plasmid in order to obtain the pMAL-c2X_IRAKM[1-119]. The R56D and Y61D mutations were achieved using this vector.

Forward : 5’ agc agc tgg ctg gat gtt gat cat att gaa aag gat gta gac caa ggt aaa agt g 3’

Backward : 5’ c act ttt acc ttg gtc tac atc ctt ttc aat atg atc aac atc cag cca gct gct 3’

PCR amplification and mutagenesis were performed by BIO RAD-iProof High-Fidelity DNA Polymerase to generate expression plasmid pMAL-c2X _IRAKM[1-119:R56D,Y61D].

Plasmid Information for pMAL-c2X_IRAKM[1-119:R56D,Y61E]

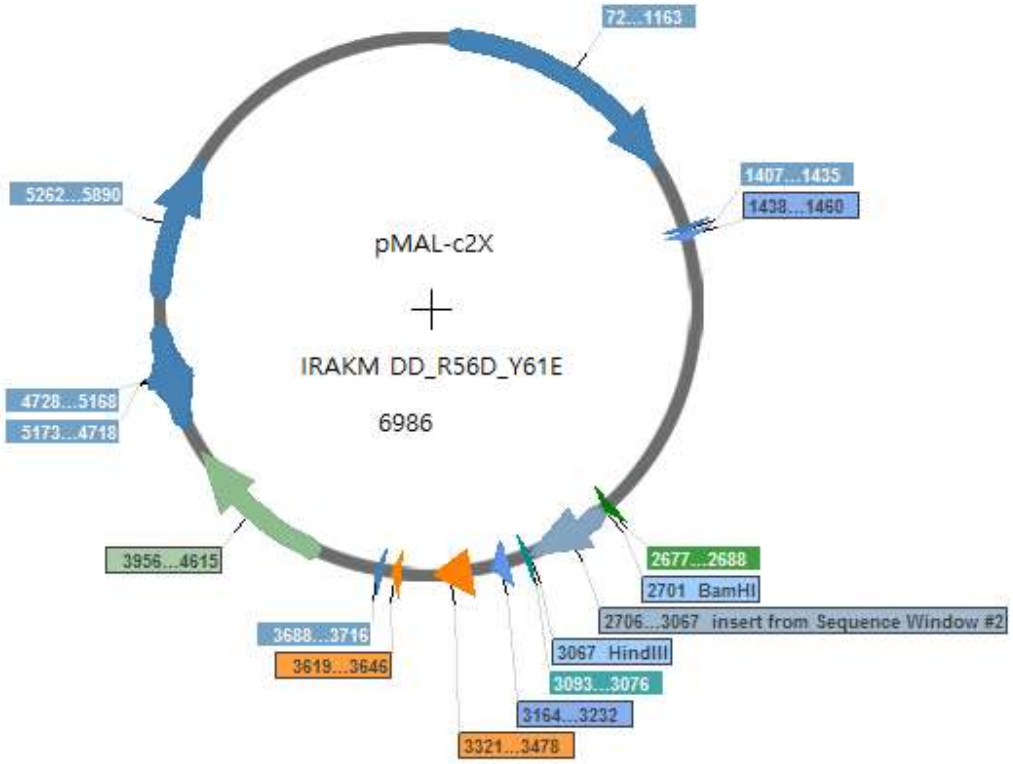

Plasmid Name: pMAL-c2X_IRAKM[1-119:R56D,Y61E]

Parent Plasmid: pMAL-c2X

Detail of Construction:

The R56D and Y61E mutations were achieved using pMAL-c2X_IRAKM[1-119:R56D,Y61D] vector.

Forward : 5’ gtt gat cat att gaa aag gag gta gac caa ggt aaa agt gg 3’

Backward : 5’ cc act ttt acc ttg gtc tac ctc ctt ttc aat atg atc aac 3’

Mutagenesis was performed by BIO-RAD-iProof High-Fidelity DNA Polymerase to generate expression plasmid pMAL-c2X_IRAKM[1-119:R56D,Y61E].